

RICE UNIVERSITY

Wireless Side-Channels in MIMO Full-Duplex Systems

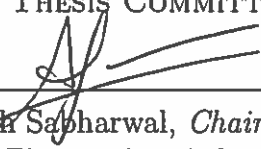
by

Jingwen Bai

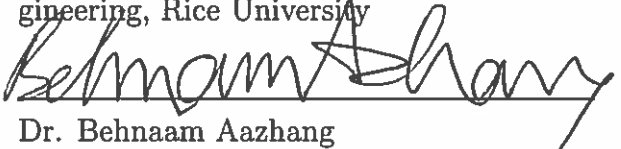
A THESIS SUBMITTED
IN PARTIAL FULFILLMENT OF THE
REQUIREMENTS FOR THE DEGREE

Doctor of Philosophy

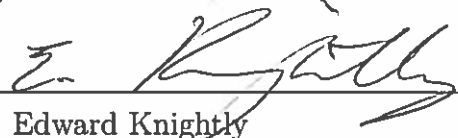
APPROVED, THESIS COMMITTEE:



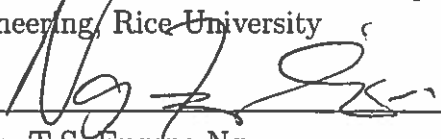
Dr. Ashutosh Sapcharwal, *Chair*
Professor of Electrical and Computer Engineering, Rice University



Dr. Behnaam Aazhang
J.S. Abercrombie Professor of Electrical and Computer Engineering, Rice University



Dr. Edward Knightly
Professor of Electrical and Computer Engineering, Rice University



Dr. T.S. Eugene Ng
Associate Professor of Computer Science and Electrical and Computer Engineering, Rice University

HOUSTON, TEXAS
APRIL 2016

ABSTRACT

Wireless Side-Channels in MIMO Full-Duplex Systems

by

Jingwen Bai

In this thesis, we propose a new approach for enhanced interference management via wireless side-channels in advanced wireless systems such as MIMO full-duplex systems. The rise of multiple radio interfaces, such as WiFi (operating in unlicensed ISM bands) and cellular (operating in licensed bands), with near-default inclusion in smartphones, allows for a new use of the ISM bands to manage interference in cellular bands, by creating wireless “side-channels” between mobile users. In a multi-user MIMO full-duplex system, an in-band full-duplex base station with multiple antennas communicates with multiple up- and downlink users in the same time-frequency slot. We characterize the impact of side-channels in managing interference from uplink users to downlink users in such MIMO full-duplex system.

First, we experimentally quantify the likelihood of establishing ISM side-channels between smartphones in WiFi-free areas such as highways. Next, we study a side-channel assisted two-user MIMO full-duplex system and characterize its generalized degrees-of-freedom and diversity-multiplexing tradeoff. For such a system, we show that the optimal performance is achieved by our proposed vector bin-and-cancel strategy which leverages Han-Kobayashi message splitting.

Then, we study a side-channel assisted multi-user MIMO full-duplex system from a cross-layer protocol design perspective. Our protocol design integrates automatic repeat request (ARQ) at the medium access control (MAC) layer with enhanced interference management via side-channels at the physical layer (PHY). Our proposed joint PHY-MAC protocols exploit the ARQ information offered by the MAC layer to reduce the data retransmission time and improve system goodput.

Finally, we study a multi-cell multi-user MIMO full-duplex system, where new forms of intra- and inter-cell interference appear due to the full-duplex operation. We characterize the up- and downlink ergodic achievable rates for the case of linear precoders and receivers. The rate analysis includes practical constraints such as imperfect full-duplex radio chains, channel estimation error, training overhead and pilot contamination. We show that with large antenna arrays at base stations, the gains from full-duplex are available at the network level despite the increased interference in the full-duplex networks. Moreover, full-duplex networks can use fewer antennas to achieve spectral efficiency gain over the half-duplex counterparts. We also demonstrate that under realistic multi-cell MIMO full-duplex network scenarios, side-channels are effective in significantly improving the spectral efficiency of cell-edge users.

ACKNOWLEDGEMENTS

It has been almost five years since I first landed in Houston. Texas has welcomed me by its uniqueness and warmth. Rice University has attracted me by its breathtaking view and ambience. Most importantly, I met many people who have helped me and accompanied me on the journey of research. I would like to first express my sincere gratitude to my great advisor, Ashutosh Sabharwal, who has led me towards the road of wireless communication research. His dedication towards research and teaching spurs me to be more diligent and efficient in my work. His blunt but genuine advice and criticism always inspire me to become a better researcher. He would not hold back his opinions whenever he sees room for improvement in my work. He would always remind us the importance of having one coherent storyline in every talk we give and every paper we write, which really helps improve my presentation and written skills throughout my Ph.D. study. I would also like to extend my appreciation to my committee members: Prof. Behnaam Aazhang, Prof. Edward Knightly and Prof. Eugene Ng for providing useful comments and suggestions on my thesis. To Prof. Suhas Diggavi from UCLA for his insightful discussions and guidance. To my group members and friends for their help and entertainment. In particular, to my parents for always backing me up in all conditions even though we are thousands of miles apart. Last but not least, to my significant other Achal for always standing by my side and making my life colorful and meaningful.

To my family - mom, dad and Achal

Contents

Abstract	ii
Acknowledgements	iv
1 Introduction	1
1.1 Motivation	1
1.2 Related work	4
1.3 Main Contributions	7
1.4 Organization of the Thesis	10
2 Availability and Potential of Wireless Side-Channels	12
2.1 Introduction	12
2.2 Availability of ISM Side-Channels	15
2.3 Impact on Cellular Capacity of Future Wireless Architectures	20
3 Vector Bin-and-Cancel in Two-User MIMO Full-Duplex System	30
3.1 Introduction	30
3.2 System Model	33
3.3 Approximate Capacity Region and Generalized Degrees-of-Freedom	37
3.4 Diversity and Multiplexing Tradeoff	52
4 ARQ Design in Multi-User MIMO Full-Duplex System	73
4.1 Introduction	73
4.2 System Model	74
4.3 ARQ Protocol Design with Side-Channels	77

4.4	Numerical Results	91
5	Large Antenna Analysis of Multi-Cell Full-Duplex System	97
5.1	Introduction	97
5.2	Multi-Cell Full-Duplex System Model	99
5.3	Achievable Rates in Full-Duplex Networks	103
5.4	Large-Scale full-duplex System Performance	116
5.5	Interference Management via Side-Channels	125
5.6	Numerical Results	126
6	Conclusions	135
6.1	Summary	135
6.2	Future Directions	137
	References	138

List of Figures

1.1	When a multi-antenna full-duplex infrastructure node communicates with multiple half-duplex uplink and downlink users, the uplink users will cause interference to the downlink users.	3
2.1	The proposed use of ISM side-channel, as an additional radio to access ISM bands when available and controlled by cellular providers.	13
2.2	In a MU-MIMO full-duplex system with half-duplex mobiles, there is inter-beam interference among the downlink users (for example, between A and B) and uplink-downlink interference (for example, from C to A and B).	14
2.3	Intra-vehicle and inter-vehicle ISM side-channels among clients.	16
2.4	RSSI versus distance for high-scattering environment which mimics intra-vehicle environment.	18
2.5	RSSI versus distance for inter-car environment.	19
2.6	Estimate on the availability of ISM side-channels based on V2V range distribution.	20
2.7	Cell capacity of downlink traffic as a function of the downlink user density.	24
2.8	Comparison of channel training - data structure between MU-MIMO full-duplex via ISM side-channel and half-duplex MU-MIMO downlink in a given coherence time T_c . The time-slot partition of the ISM band for downlink user-cooperation and uplink-downlink decode-and-cancel is also given.	26

2.9	Cell capacity of asymmetric traffic with a fixed up- and downlink user density.	28
2.10	Expected capacity of asymmetric traffic as a function of SNR.	29
3.1	<i>MIMO full-duplex network: inter-mobile interference becomes an important factor when the full-duplex infrastructure node communicates with uplink and downlink mobile nodes simultaneously.</i>	31
3.2	Channel model: (M_d, N_d, M_u, N_u) side-channel assisted MIMO full-duplex network.	34
3.3	Binning of the common message at uplink transmitter.	41
3.4	Decoding at downlink receiver.	41
3.5	The sum GDoF per antenna for $M_u = N_d$ when BS has an excess of antennas.	47
3.6	The DoF-optimal scheme of two-user side-channel assisted MIMO full-duplex network when $M_u \geq N_d$	47
3.7	Spatial spectral tradeoff in Case A when $\alpha_I = 1$	51
3.8	Spatial spectral tradeoff in Case B when $\alpha_I = 1$	51
3.9	Comparison of the three systems in DoF as a function of the side-channel bandwidth when $\alpha_I = 1$	52
3.10	DMT comparison w/wo side-channel w/wo CSIT when $W = \frac{1}{2M+1}$, $\alpha_S = \frac{M}{2}$	61
3.11	Comparison of the three systems in DMT as a function of the side-channel bandwidth.	68
3.12	DMT of $(M, 1, 1, M)$ w/wo side-channel w/wo CSIT when $\alpha_S \geq \frac{M}{2}$, where $\beta^* = \frac{\alpha_S + \frac{1}{W} - M}{\frac{2}{W} - M}$	69
3.13	The required side-channel bandwidth ratio to compensate for CSIT as a function of the number of antennas at the BS with equal number of antennas at mobiles when $\alpha_S = \frac{M}{2}$	70
3.14	The symmetric DMT of MIMO full-duplex network without side-channel for $\alpha_d = \alpha_u = \alpha_I = 1$	71
3.15	The symmetric DMT with side-channel for $\alpha_d = \alpha_u = \alpha_I = \alpha_S = 1$	71
4.1	(M, K_u, K_d, W) side-channel assisted MU-MIMO full-duplex network, where the side-channels are highlighted in green dash lines.	75
4.2	Proactive protocol process where $K_u = K_d = 2$	86
4.3	Reactive protocol process where $K_u = K_d = 2$	88

4.4	Performance versus transmission rate.	92
4.5	Performance versus number of BS antennas when $R = 3$ bits/s.	94
4.6	Performance versus side-channel bandwidth when $R = 6$ bits/s.	95
4.7	Performance versus interference level when $R = 4$ bits/s.	96
5.1	The full-duplex BS in each cell has M antennas, and the UE has single antenna with either full-duplex or half-duplex radio. Besides the conventional uplink and downlink interference that exist in the half-duplex system, there will be new BS-BS and UE-UE interference highlighted by the red dash lines.	98
5.2	Uplink channel training in full-duplex networks.	109
5.3	Comparisons between lower bounds in Proposition 5 and 6 and numerically evaluated values of the ergodic achievable rates (bits/s/Hz/cell) under both perfect and imperfect CSI assumptions, where $P_{tr} = P_u = 10$ dB and $P_d = 20$ dB.	122
5.4	Full-duplex over half-duplex spectral efficiency ratio in the imperfect CSI system with and without power scaling.	124
5.5	Spectral efficiency gain and antenna reduction tradeoff for various numbers of BS antennas employed in the TDD system under imperfect CSI assumption.	125
5.6	Small cell deployment.	128
5.7	Average full-duplex spectral efficiency gain with BS antenna arrays when $L = 12$ and $\kappa = -60$	128
5.8	Average full-duplex spectral efficiency gain with different dynamic ranges when $M = 100$ and $L = 12$	129
5.9	Average full-duplex spectral efficiency gain with cell density when $M = 100$ and $\kappa = -60$	130
5.10	User spectral efficiency CDF with the size of cooperative user set when $M = 300$, $L = 12$ and $\kappa = -60$ dB.	131
5.11	Full-duplex spectral efficiency gain with the size of cooperative user set when $M = 300$, $L = 12$ and $\kappa = -60$ dB.	132
5.12	Full-duplex spectral efficiency gain with BS antennas arrays when $ \mathcal{S}_{lk} = 5$, $\forall l, k$, $L = 12$ and $\kappa = -60$ dB.	134

List of Tables

2.1	Simulation parameters.	27
5.1	Simulation parameters	127

Introduction

1.1 Motivation

Wireless communications, especially cellular networks, have had an immense societal impact. Each year sees a growing demand, both in the number of users and the data rate per user. As a result, each generation of the cellular networks is designed to support higher peak data rates. The increase in peak rates are achieved by innovations in all network layers, but perhaps the biggest burden of the increase lies with the physical layer in the network. Looking at the evolution of cellular communications, one observes that an increase in peak data rates is a result of both increases in the allocated spectrum and spectral efficiency. That is, networks use more bandwidth and use it better with each cellular generation.

For next generation networks, there are a number of candidate technologies that are under serious consideration. Among those candidate technologies, we will study three candidate technologies in this thesis. The first two, Massive MIMO [1] and full-duplex wireless [2], are already influencing the next-generation standards discussion. The third candidate idea, ISM side-channels, is based on an older idea of cooperative decoding but used in a novel method in this thesis to counter interference in cellular

networks.

In the seminal paper [1], it was demonstrated that as the number of base station antennas grow faster than the number of users, then the processing required at the base stations can be simplified to conjugate beamforming; this regime of operation is referred as Massive MIMO. Thus, complex transmission strategies like zero-forcing are not required to achieve optimal performance. In addition, the base stations do not need to coordinate with each other to manage inter-cell interference. The result has prompted the interest in use of a large number of antennas at base stations to get capacity gains with simple processing. An additional benefit of massive MIMO includes reduced node transmit power for energy savings [3]. The experimental evidence on the benefits of massive MIMO [4, 5, 6] has already sparked strong industry interest and 64-antenna configuration is now being considered for 5G systems.

The second candidate technique is in-band full-duplex communications. In-band full-duplex wireless allows simultaneous transmission and reception using the same frequency band, and thus opens up new design opportunities to increase the spectral efficiency of wireless systems. Full-duplex wireless communication is one of the emerging techniques which can significantly improve the spectral efficiency of wireless networks [2]. The feasibility of a full-duplex radio has been demonstrated by many research groups (see [2, 7, 8, 9, 10] and references therein). Combining MIMO with full-duplex allows new communication patterns. For example, when a multi-antenna infrastructure node is full-duplex capable, multiple uplink *and* downlink users can be served in same time-frequency slot to improve the spectral efficiency many-fold compared with a single-antenna full-duplex system.

A side-effect of the full-duplex operation is that additional interference is introduced because there are more simultaneous active links. Hence, there is a possibility that the full-duplex gain can be offset by the loss due to additional interference. For

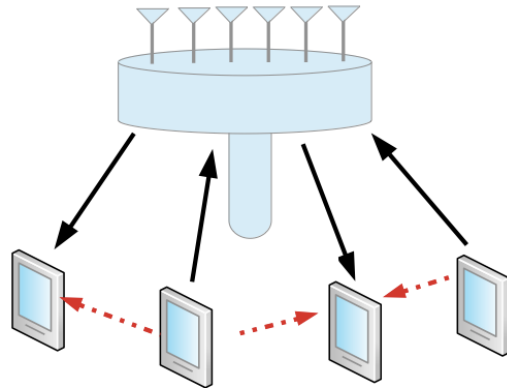


Figure 1.1: When a multi-antenna full-duplex infrastructure node communicates with multiple half-duplex uplink and downlink users, the uplink users will cause interference to the downlink users.

instance, in a single-cell multi-user MIMO full-duplex system (see Figure 1.1), the simultaneous transmission in uplink and downlink will cause interference from the uplink users to the downlink users, which can limit the system performance.

The new challenge of increased interference provides the segue for the third candidate technique, which is the use of ISM bands to create device-to-device side-channels for managing interference. The motivation comes from the fact that the mobile devices are now equipped with multiple radio interfaces that allow them to simultaneously access different parts of the spectrum, e.g. cellular and ISM bands. The ability of simultaneous access to multiple parts of the spectrum provides an opportunity to use multiple bands in new and unique ways. In this thesis, we will consider the use of device-to-device (D2D) wireless channels between mobile devices, to serve as side-channels to *aid* main-channels communication with the infrastructure nodes. For example, the main network could be in a cellular band while the wireless side-channel could be on an unlicensed ISM band. Unlike the conventional use of D2D links, we propose to use the wireless side-channel for enhanced interference management to improve the cellular capacity in advanced systems such as MIMO full-duplex systems.

Since all three ideas increase system capacity, the natural question is whether the

three ideas of massive MIMO, full-duplex and ISM side-channels can be combined to improve overall network capacity. Thus, the main question in this thesis is analyzing the impact of using the three candidate technologies together on both single-cell and multi-cell network capacity, and identifying the different regimes of operation.

1.2 Related work

In this thesis, we have studied a new use of multiple orthogonal bands for enhanced interference management in advanced wireless systems such as MIMO full-duplex systems by creating *wireless side-channels* to aid the main-channel communication. We characterize the impact of side-channels in managing interference from uplink users to downlink users in a multi-user MIMO full-duplex system, where an in-band full-duplex base station (BS) equipped with multiple antennas communicates with multiple up- and downlink users in the same time-frequency slot.

The simultaneous operation of two orthogonal bands has been studied for many purposes. A common method is to use concurrently two radio interfaces, one to access a cellular band and another to access an ISM band network (notably WiFi) at the same time and is now an integral part of cellular provider data strategy to offload cellular traffic to WiFi networks [11]. The simultaneous operation is also used to support wireless tethering, which allows devices to share one cellular link over WiFi. In the conventional D2D communication literature, the use of orthogonal bands involves establishing peer-to-peer communication [12], forming virtual MIMO for cooperative communication [13] (and the references therein). The use of multiple orthogonal bands has also become the core study of the next generation of the wireless systems. Carrier aggregation has been studied in the current LTE standard [14]. LTE-Unlicensed (LTE-U) and Licensed-assisted access (LAA) have been proposed in the 3GPP standardization group [15] to aggregate licensed and unlicensed spectrum so

that LTE system can operate even in the unlicensed band.

Our other major focus in this thesis is the analysis of multi-user multi-cell multiple antenna networks, with full-duplex infrastructure nodes and a mix of half- and full-duplex mobile nodes. Towards that end, there are two lines of work in the area of multi-user MIMO full-duplex networks. The first line of work focuses on information theoretic limits while the other line of work focuses on practical network design at all layers.

Multi-cell analysis of cellular systems is in fact very challenging. As we will discuss in later chapters, the number of parameters increases rapidly with each new cell in the network and more importantly, the network connectivity becomes increasingly complex. Combined with the fact that full-duplex wireless has become popular only recently, there are only a limited number of papers that analyze multi-cell MIMO full-duplex networks. Towards that end, we discuss [16, 17, 18, 19, 20, 21, 22, 23, 24]; note that not all papers are multi-cell studies.

In [16, 17, 18], only a single-cell MIMO full-duplex case is studied. In [17], the degrees-of-freedom of a single cell with a MIMO full duplex BS are studied. Since only a single-cell system is studied, the proposed schemes are a combination of interference alignment and zero-forcing beamforming. Similarly, in [16], degrees-of-freedom of a multi-user MIMO full-duplex network with half-duplex mobile clients are derived, and the regimes where the inter-node interference can be mitigated to yield significant gains over the half-duplex counterpart are identified. The achievability is based on interference alignment and requires full channel-state information at the transmitter (CSIT). The authors also study the case with partial CSIT where only the BS acquires downlink channel values to avoid collecting network-wide CSIT at all transmitters in the system. The authors show that the key to achieving the sum degrees-of-freedom upper bound with only partial CSIT is the ability of the base-station to switch antenna

modes that can be realized via reconfigurable antennas. In [18], the authors study a single cell scenario with a MIMO full duplex BS and full-duplex mobile clients. The exact regress-of-freedom region has been characterized which demonstrate that inter-node interference can be managed to provide significant gain in degrees of freedom over the conventional half-duplex cellular design.

In [19], the authors propose opportunistic scheduling to mitigate inter-node interference in a single-cell MIMO full-duplex network, which is especially useful for the case where there is a large number of single-antenna half-duplex users. The proposed method optimizes the uplink and downlink scheduling jointly and exploits multiuser diversity while treating interference as noise. The key result is that in homogeneous networks, opportunistic scheduling achieves the same sum capacity as would have been achieved if there was no uplink-to-downlink interference, as the number of users grows large. Finally, in [20], a new distributed power control method is presented, again to mitigate inter-node interference in a single-cell MIMO full-duplex network.

Similarly, there are only a limited pieces of work that have studied the network design in MIMO multi-user multi-cell networks. We highlight four such papers in this section, and others are discussed in later chapters. All the papers [21, 22, 23] present practical approaches to mitigate the interference in full-duplex networks. In [21], scheduling and power control algorithms with BS cooperation in the multi-cell SISO full-duplex networks is investigated and [22, 23] studies the MIMO case. The performance analyses are based on extensive simulations, largely because of the challenge of analyzing complex scheduling and power control methods. In [24], the authors study the multi-cell problem when the BSs have full coordination. This converts the problem into a network MIMO problem, and essentially allows one to treat the multi-cell problem as one giant MIMO cell. This, in turn, allows the use of interference alignment to achieve the highest possible degrees of freedom. While this

approach provides insights into the maximum possible degrees of freedom, it relies on full coordination and proposes a very difficult transmission method - both of them extremely challenging to implement in practice. Compared to the above works, we focus on the case when there is no BS coordination and hence we cannot convert the problem to the more tractable single-cell problem. In addition, we allow only simple linear processing at the BSs, namely conjugate beamforming, and hence complex schemes like zero-forcing or interference-alignment cannot be employed.

1.3 Main Contributions

Our main contributions are summarized below.

1.3.1 Side-channels opportunity and potential capacity gains

We experimentally quantify the opportunities of using ISM side-channels between smartphones in WiFi-free areas such as highways. With our designed Android applications for link measurement and California rush hour traffic data, we show that there is a high probability for an ISM side-channel to exist on highways with reliable link quality during the rush hour.

We demonstrate a potential use of ISM side-channels to significantly reduce interference in a MIMO wireless system and increase the overall cellular network capacity, by flexibly accommodating both multi-user beamforming and full-duplex operation. With ISM side-channels, we can leverage techniques like decode-and-cancel [25] and user-cooperation [26] to manage intra-cell interference in a single-cell MIMO system. The capacity loss due to intra-cell interference can be completely recovered by exploiting the ISM side-channels among users. The simulation results based on our WiFi side-channel measurements show that a multi-user MIMO full-duplex network

with 20 antennas at BS using ISM side-channels can achieve 6-fold capacity gain compared with a multi-user MIMO half-duplex system, and 12-fold gain compared with a TDMA system, and recover the full-duplex multiplexing gain which previous schemes without ISM side-channels fail to achieve.

1.3.2 Single-cell multi-user MIMO full-duplex system

We study a side-channel assisted single-cell multi-user MIMO full-duplex system. We show that its capacity region is achievable within a constant bit by a vector-bin-and-cancel scheme. Further, we characterize its generalized degrees-of-freedom (GDoF) for time-invariant channels and diversity-multiplexing tradeoff (DMT) for slow-fading channels with different levels of channel uncertainty at the transmitter. We quantify how the side-channel improves the GDoF and DMT compared to a system without the extra orthogonal spectrum. The insights gained from our analysis reveal: i) the trade-off between spatial resources from multiple antennas at different nodes and spectral resources of the side-channel, and ii) the interplay between the channel uncertainty at the transmitter and use of the side-channel.

Next, we develop a protocol for assistance via side-channels for a side-channel assisted multi-user MIMO full-duplex system from a cross-layer design perspective. Our side-channel protocol integrates automatic repeat request (ARQ) for retransmitting erroneous packets at the medium access control (MAC) layer with an enhanced physical layer (PHY) interference management scheme via side-channels. We propose two different joint PHY-MAC protocols which exploit the ARQ information offered by the MAC layer to reduce the data retransmission time and improve system good-put. The first protocol is a proactive side-channel assisted ARQ protocol which uses the side-channels proactively irrespective of the downlink feedback and is based only on conventional uplink ARQ feedback. The second side-channel protocol is a reac-

tive protocol which triggers the use of side-channels based on the conventional uplink ARQ feedback and our designed downlink ARQ feedback mechanisms. We analytically evaluate system goodput of both protocols and show that the proactive protocol provides higher goodput compared to reactive protocol at the cost of higher energy consumption for the use of side-channels.

1.3.3 Multi-cell multi-user MIMO full-duplex system

We analyze a multi-cell multi-user MIMO full duplex system and characterize its uplink and downlink ergodic achievable rates when low-complexity linear receivers and precoders are used. We consider the case where each BS has multiple antennas with full-duplex capability while each user has a single antenna with either full-duplex or half-duplex radio. Practical constraints such as imperfect self-interference cancellation, channel estimation error, training overhead and pilot contamination are considered in our analysis.

We further analyze the system performance in the asymptotic regime where the number of BS antennas grows infinitely large. We show that the transmit power of BSs and users can be scaled down proportionally with an increasing number of BS antennas to maintain a fixed asymptotic rate. Our analysis reveals that the impact of imperfect self-interference cancellation, intra-cell and inter-cell interference in the multi-cell multi-user MIMO full-duplex networks disappear as the number of BS antennas becomes infinitely large. Further, under the assumption of perfect channel knowledge, the full-duplex system asymptotically achieves $2\times$ spectral efficiency gain over the half-duplex system. We also show that when channel estimation error and channel training overhead are considered, the $2\times$ asymptotic full-duplex gain is achievable if all users being served are full-duplex capable.

Lastly, we numerically evaluate the system performance at finite SNR and with a

finite number of BS antennas. Our numerical results reveal that to achieve the same spectral efficiency, significantly fewer BS antennas are needed in a MIMO full-duplex network compared with that in a MIMO half-duplex network. Also, under realistic 3GPP multi-cell network scenarios [27], the overall full-duplex gains can be achieved despite the increased interference introduced in the full-duplex networks. Finally, we demonstrate that the use of side-channels can significantly improve the spectral efficiency achieved by the cell-edge users.

1.4 Organization of the Thesis

The rest of the thesis is organized as follows. In Chapter 2, we study the likelihood of establishing a reliable wireless side-channel link between users and the potential of using the side-channels to increase the overall cellular network capacity via enhanced interference management. The results in Chapter 2 were originally presented in [28]. In Chapter 3, we derive the capacity region of a side-channel assisted two-user MIMO full-duplex system to within a constant bit, achieved by a vector bin-and-cancel scheme. We also characterize its generalized degrees-of-freedom and diversity-multiplexing tradeoff. The results presented in Chapter 3 were originally published in [29]. In Chapter 4, we propose two different ARQ protocol designs with side-channels in a single-cell multi-user MIMO full-duplex system, which enable an enhanced PHY scheme with side-channels by exploiting the ARQ information offered by the MAC layer. In Chapter 5, we provide a large antenna analysis for a multi-cell multi-user MIMO full-duplex system when simple linear precoders and receivers are used. Our analysis incorporates practical constraints such as imperfect self-interference cancellation, channel estimation error, training overhead and pilot contamination. We numerically evaluate our system performance under realistic 3GPP multi-cell network settings. The results in Chapter 5 are also reported

in [30]. Chapter 6 concludes the thesis.

Availability and Potential of Wireless Side-Channels

2.1 Introduction

Almost all smartphones today can *simultaneously* operate in two orthogonal frequency bands, i.e., ISM and cellular bands. The ISM bands are commonly used by WiFi and Bluetooth, and the cellular bands for cellular voice and data. While WiFi infrastructure is considered “ubiquitous” in metropolitan areas, the truth is that its deployment is limited to very low mobility environments; most common WiFi covered zones include homes, offices, malls and restaurants. Due to its short-range and limited support for handoffs in high mobility scenarios, large outdoor swaths of cities may have limited, very weak or no WiFi coverage. We focus on the areas where WiFi coverage is practically unavailable such as highways.

In this chapter, we propose and study the potential for an additional use of ISM bands to create *side-channels* for interference management to increase the overall cellular network capacity. The proposed use is neither data-offloading nor data-forwarding. The side-channels are established between mobile clients and *controlled*

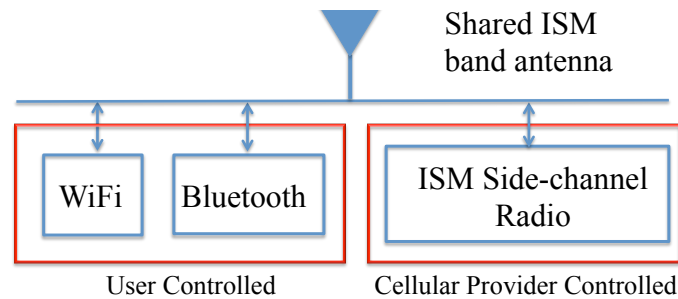


Figure 2.1: The proposed use of ISM side-channel, as an additional radio to access ISM bands when available and controlled by cellular providers.

by the cellular provider in only WiFi-free zones, and used to manage intra-cell interference in advanced MU-MIMO techniques; see Figure 2.1. We understand that our model of cellular controlled ISM bands appears to be problematic at first, since ISM channel use has always been under the control of end-users. We expect that users will still have the highest priority to control ISM band (e.g. for WiFi or tethering). Our proposed solution will only be active when the user has no use of the ISM band and opts in to allow cellular providers to manage the use of the ISM side-channels for improved capacity for the client.*

We will leverage the ISM side-channels among mobile clients to boost data rate of cellular transmissions by *enhanced intra-cell interference management*. We will consider the advanced upcoming techniques like multi-user MIMO (MU-MIMO) and full-duplex communication as our examples for the use of ISM side-channels. In both MU-MIMO and full-duplex, multiple flows are active in the *same* cell, which leads to intra-cell interference as shown in Figure 2.2.

In Section 2.2, we quantify the opportunities of using ISM side-channels among smartphones in WiFi-free area such as highways. Using our designed Android applications, we measure WiFi link quality between two smartphones either placed within one vehicle, or in separate vehicles. The measurements provide an estimate on the

*Our focus is only on capacity improvement in this chapter, and many important issues like energy efficiency and security will be addressed in future work.

range of ISM band links between smartphones. We find that up to a distance of 50 meters, we can obtain an average received power greater than -80 dBm.* Combining with highway traffic data accessible in California, we derive an estimate on the probability of establishing ISM side-channels on highways during rush hour. We find that during rush hour, there is a 69% chance for an ISM side-channel to exist within 50 meters on highways with reliable link quality.

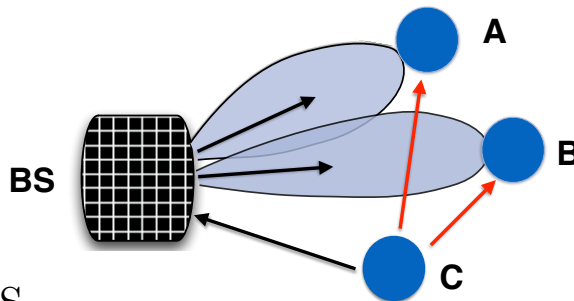


Figure 2.2: In a MU-MIMO full-duplex system with half-duplex mobiles, there is inter-beam interference among the downlink users (for example, between A and B) and uplink-downlink interference (for example, from C to A and B).

In Section 2.3, we compute the potential increase in capacity due to ISM side-channels. We analyze information-theoretic cellular capacity increase with ISM side-channels in the future advanced wireless systems. Recent results on experimental evaluation of MU-MIMO [31] and full-duplex infrastructure for short to medium range communication [7, 8] demonstrate the potential significant improvement on spectral efficiencies over all previous existing wireless architecture. However, one detrimental factor which limits the performance of such architecture is the intra-cell interference among the users in the same cell. For instance, in the MU-MIMO downlink, serving multiple downlink users simultaneously via transmit beamforming techniques [32] will incur inter-beam interference owing to the imperfect channel state information at the transmitter. On full-duplex base stations, there is a potential to schedule the up- and downlink pairs in the same resource block, hence the uplink stream may interfere

*WiFi radio noise floor is typically -95 dBm, so -80 dBm indicates an SNR of 15 dB.

with the downlink stream especially in a dense environment. In a MU-MIMO full-duplex system shown in Figure 2.2, there is inter-beam interference between downlink user A and B, and uplink-downlink interference from uplink user C to downlink users A and B. We demonstrate that with ISM side-channels, we can leverage techniques like decode-and-cancel [25] and user-cooperation [26] to manage intra-cell interference. The capacity loss due to intra-cell interference can be completely recovered by exploiting the ISM side-channels among users. The simulation results based on our WiFi channel measurements show that a multi-user MIMO full-duplex network with 20 antennas at BS using ISM side-channels can achieve 6-fold capacity gain compared with a MU-MIMO half-duplex system, 12-fold gain compared with a TDMA system, and recover the full-duplex multiplexing gain which previous schemes without ISM side-channels fail to achieve.

2.2 Availability of ISM Side-Channels

In this section, we estimate the likelihood of establishing ISM side-channels between smartphone users, in places where there is no WiFi coverage such as highways. In highways, as shown in Figure 2.3, there are two different types of opportunities to establish ISM side-channels: intra-vehicle where the smartphones are in the same vehicle and inter-vehicle where the smartphones are placed in separate vehicles.

We first measure the channel strength of WiFi links between smartphones in both intra- and inter-vehicle environments. We use WiFi as a proxy for this future ISM side-channel only for link quality measurements, since it is the only easily accessible radio available in ISM band embedded in the form-factor device of the envisioned use. * The measurement data provides us with estimates on the range of WiFi links

*An actual implementation of ISM side-channel may re-use parts of WiFi PHY and/or MAC, but our emphasis is only to characterize the theoretical benefit of using the ISM band.

between smartphones possible in highways. Then we use the highway traffic data, combined with our range tests, to estimate the number of times two smartphones can be within each other’s ISM band communication range.

We note that several experiments have been reported for vehicle-to-vehicle dedicated short-range communication (DSRC) in [33]. However, DSRC measurements are often performed to mimic vehicle mounted transceivers and antennas, which are potentially more capable than smartphone radios and antennas. To get a more realistic smartphone-to-smartphone link range estimate, we chose to perform our own independent tests using current WiFi hardware in smartphones.

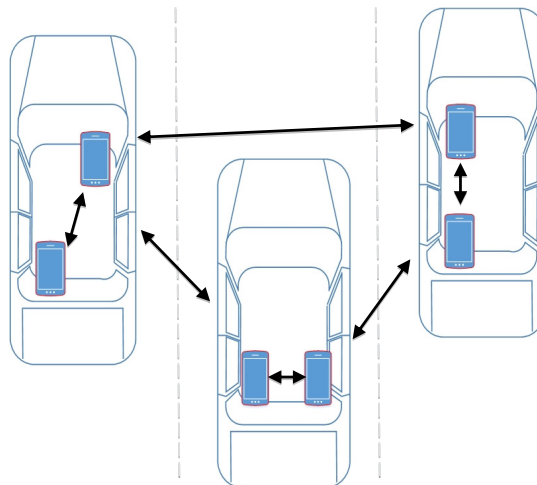


Figure 2.3: Intra-vehicle and inter-vehicle ISM side-channels among clients.

2.2.1 Methodology

Two Android smartphones (HTC One M7 and Nexus 4) were used in all our experiments to set up the WiFi connection for measurement. We let one smartphone (i.e., “server”) initiate a WiFi Hotspot and the other device (i.e., “client”) can request to join this network. After the connection is complete, the channel strength can be measured from the client side.

We developed two Android apps, one for server and one for client. The two apps

were developed on a Windows 64-bit platform: JDK 1.6.0_37, Eclipse Helios Service Release 2 as the development IDE and Android SDK 4.3 (API 18). The client app records the WiFi received signal strength indicator (RSSI) and SSID, along with the timestamp of each measurement, GPS location of the device.

2.2.2 Channel measurement results

We conducted measurement campaigns to measure the WiFi channel strength for both intra-vehicle and inter-vehicle environments. In our experiments, we collected 1000 samples for each measurement recording.

For the intra-vehicle experiment, one smartphone was placed at the front seat of a compact car, and the other smartphone was positioned at the back seat of the car with a separation of 1.5 meters. The resulting average RSSI is -34.5 dBm with a standard deviation of 5.5 dBm. Due to size limit of the vehicle we had for the experiment, we also conducted a high-scattering indoor experiment to mimic the intra-vehicle environment such as van or limousine. This campaign was conducted inside the engineering building at Rice University where a cluttered room was filled with chairs, desks, and people walking around. We placed the two smartphones at different distances, and measured the corresponding WiFi channel strength. Figure 2.4 illustrates the empirical WiFi link quality between smartphones in a high-scattering environment which mimics the intra-vehicle environment. Within 10 meters range test, the RSSI varies from -41 dBm to -63 dBm which corresponds to an SNR of 32 to 54 dB (assuming the WiFi noise floor is -95 dBm). The result shows that we can expect a reliable ISM side-channel to exist between smartphones in the same vehicle within 10 meters range.

Another measurement campaign was performed to characterize inter-vehicle environment. We conducted the experiment in a parking lot at Rice University. Two

vehicles each of which has a smartphone inside were parked at different distance separation. In Figure 2.5, over the range up to 50 meters we tested, the average RSSI is always above -80 dBm which indicates an SNR of 15 dB. Thus we can expect a reliable side-channel to exist between inter-vehicle smartphone users within 50 meters range. We expect that as device-to-device communication gains more traction, the link quality and range may improve over time.

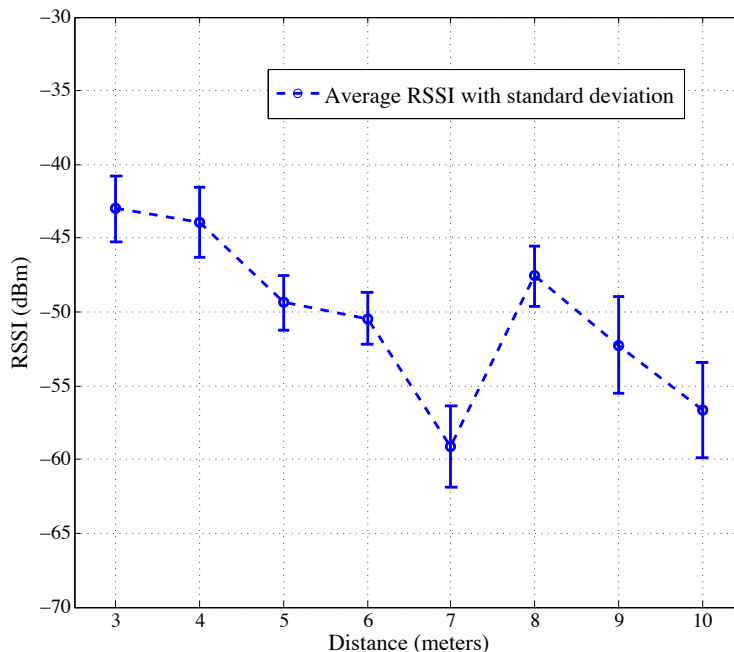


Figure 2.4: RSSI versus distance for high-scattering environment which mimics intra-vehicle environment.

2.2.3 Analysis with highway traffic data

We used the rush hour traffic counts from annual traffic data provided by California department of transportation [34]. During the rush hour, the physical traffic is very congested. More physical congestion will likely result in higher network congestion since more users will be served in the cell. It is also a more relevant use case of ISM side-channels since this is exactly when cellular systems may need to invoke more complicated methods to increase system capacity. From rush hour traffic

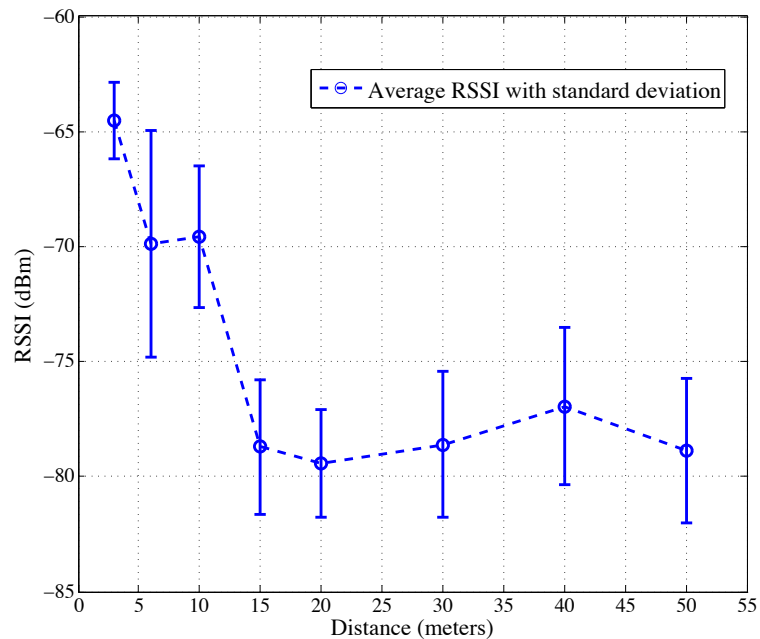


Figure 2.5: RSSI versus distance for inter-car environment.

counts at all count locations on 900 California highways including Interstate, California State Route, and United States Route, we first compute an approximate vehicle-to-vehicle (V2V) range which is defined as

$$\text{V2V range(meter)} = \frac{\text{Avg Rush Hour Speed(meters/hour)}}{\text{Rush Hour Traffic Counts(vehicles/hour)}}.*$$

Figure 2.6 shows the histogram of V2V range. We see that 69% of the time, one can expect another vehicle within 50 meters range. Given that our previous experiments showed that the inter-vehicle WiFi link exists for ranges less than 50 meters, and assuming at least one smartphone per vehicle, *we conclude that during rush hour, one can expect 69% of the time we will have at least one inter-vehicle ISM side-channel.* Of course, if there are multiple smartphones in one vehicle, then the probability of establishing an intra-vehicle ISM side-channel with reliable link quality is almost one, since most vehicles are less than 50 meters in length.

*We used 40 miles/hour as an average highway rush hour speed.

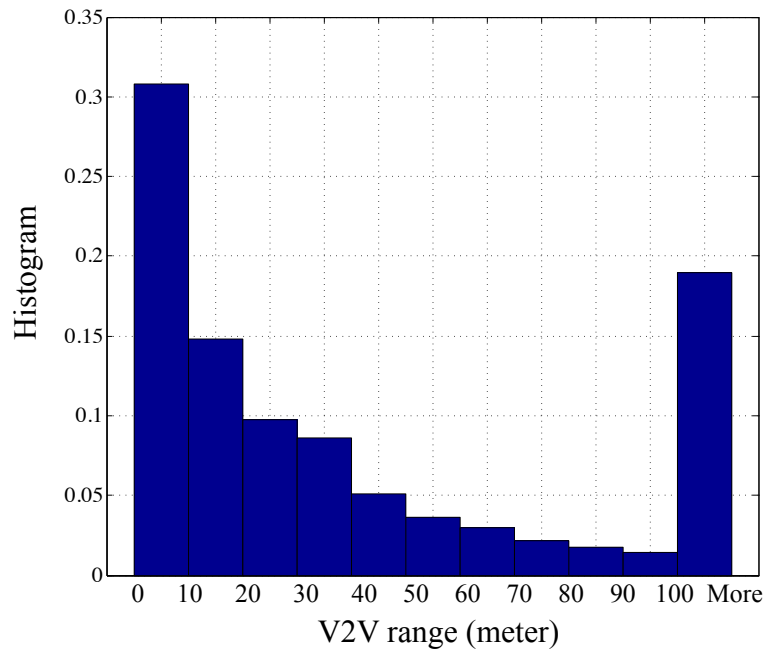


Figure 2.6: Estimate on the availability of ISM side-channels based on V2V range distribution.

2.3 Impact on Cellular Capacity of Future Wireless Architectures

MU-MIMO and full-duplex communication are two promising techniques which can substantially improve the spectral efficiency over the traditional wireless system such as TDMA. However, as we will discuss in the following sections, the intra-cell interference originated in the new wireless systems can lead to substantial performance degradation. We will show the significant capacity gains with ISM side-channels for improved interference management. We assume a base station is equipped with M antennas, serving K downlink and L uplink users in the cell, and $M \geq K, L$.

2.3.1 Half-duplex MU-MIMO downlink

2.3.1.1 Inter-beam interference

One common approach used in MU-MIMO downlink is zero-forcing beamforming (ZFBB) [32]. The ZFBB system can achieve the full multiplexing gain (i.e., $\min\{M, K\} = K$) for MU-MIMO downlink. When the transmitter has perfect channel state information (CSIT), ZFBB can completely eliminate multi-user interference, which creates a parallel, non-interfering channel to each user.

However, in a practical MU-MIMO system, a base station with large number of antennas faces the challenge of acquiring large number of channel coefficients, which need to be estimated and fed back to the base station within a small fraction of the coherence time. The situation is further complicated by the fact that the channel coefficients will incur pilot contamination [35] if the pilots for channel estimation are sent at the same time as the pilots of neighboring base-stations. Thus the channel knowledge acquired by the base station is not perfect. The ZFBB system is extremely sensitive to the accuracy in CSIT. The imperfect CSIT not only leads to a decrease in the desired signal power but more importantly, makes it impossible to form a very sharp beam toward each user without causing interference to others. Therefore unavoidably there exists *inter-beam interference* among the users in a practical ZFBB system.

To capture the imperfection of CSIT, a finite rate feedback model was introduced in [36], in which each user quantizes its channel instantiation to a finite number of bits that are fed back to the transmitter at the beginning of each block in block fading channels. Then the base station computes the beam weight vector according to the quantized channel. Because of the quantization error, the inter-beam interference can not be completely eliminated. From [36], we can find out the upper bound to the rate of ZFBB system with a finite-rate feedback where the feedback quality is fixed

at high signal-to-noise ratio (SNR):

$$R_{\text{FB}}(\text{SNR}) \leq K \left(1 + \frac{B + \log_2 e}{K - 1} + \log_2 e + \log_2(K - 2) \right), \quad (2.1)$$

where B is the number of feedback bits per user. From (2.1), we can see that the full multiplexing gain vanishes due to inter-beam interference if the feedback quality is fixed, namely, B does not scale with increasing SNR. Thus R_{FB} does not scale with respect to SNR.

2.3.1.2 Capacity Improvement

In this section, we first analytically show the capacity benefits of leveraging ISM side-channels to manage the inter-beam interference in ZFBF system. In a dense environment, via ISM side-channels, we can perform user-cooperation [26] among the mobile users. In the user-cooperation scheme, the base station does not acquire any CSIT, thus it will blindly transmit signals to the downlink users using only K antennas. Each user will first amplify-and-forward the received signal to other users via the ISM side-channels. Then each user can perform receive beamforming based on the its own channel knowledge and the transferred channel knowledge from other users to null out the interference. The partition of time slots of the user-cooperation scheme is shown in Figure 2.8 as compared with ZFBF with feedback.

At high SNR, the rate of user-cooperation via ISM side-channels [26] can be approximated as

$$R_{\text{ISM}}(\text{SNR}) \approx K \log_2(\text{SNR}). \quad (2.2)$$

Thus with ISM side-channels, the full multiplexing gain can be recovered even without CSIT, which significantly improves upon ZFBF with a fixed feedback quality. Also note that without CSIT, the multiplexing gain in the MU-MIMO downlink is only

one [37].

Now we will verify our analysis with simulation results based on our measurements. The simulation parameters are listed in Table 2.1. We assume as the number of user density increases, the inter-user distance reduces. Figure 2.7 depicts the downlink cell capacity as a function of the downlink user density. We can see that the user-cooperation significantly improves upon ZFBF with finite feedback where the number of feedback bits per user is 10. As the density of the downlink users increases, the inter-beam interference due to finite feedback in ZFBF system become severe, thus limiting the cell capacity and number of users which can be served in the area. Also, the capacity of ZFBF even with perfect CSIT will start to decrease as the number of downlink users become larger. This is because some portion of the total transmit power is dispersed to create more nulls per user, which leads to a decrease in the desired signal power.

We note that the ZFBF with perfect CSIT will perform better than user-cooperation due to the fact that ZFBF with perfect CSIT uses all base station antennas to provide higher power gain, while for user-cooperation, since we eliminate the acquisition of CSIT, we only use a subset of the antennas for downlink transmission. However, when we have asymmetric traffic demand (i.e., both uplink and downlink traffic), we can exploit the remaining antennas to support uplink streams which allows full-duplex operation, as described in the next section.

2.3.2 MU-MIMO full-duplex with half-duplex clients

In this section, we will demonstrate how ISM side-channels will enable a flexible wireless system design, a new wireless architecture of MU-MIMO full-duplex which would not be feasible due to the intra-cell interference (i.e., both inter-beam interference and uplink-downlink interference). Then we will show the significant capacity

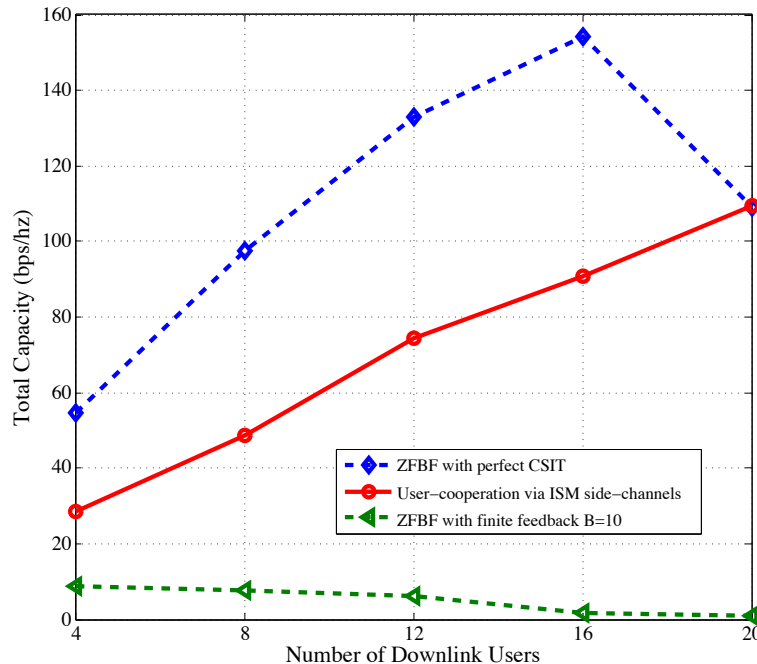


Figure 2.7: Cell capacity of downlink traffic as a function of the downlink user density.

improvement of our MU-MIMO full-duplex system via ISM side-channels.

2.3.2.1 Uplink-downlink interference

With ISM side-channels, only K out of M antennas at the base station are needed to achieve the full multiplexing gain in MU-MIMO downlink. When we have asymmetric traffic demand of both up- and downlink flows, we can employ the remaining $M - K$ antennas to enable full-duplex operation at the base station [8] by adopting different kinds of spatial isolation techniques such as polarization, directionality and absorption. With full-duplex capability at the base station, ideally up to $M - K$ uplink streams can also be supported simultaneously in addition to the K downlink streams using receive beamforming techniques. However, in a dense environment where all users are within the communication ranges of each other, it is inevitable that the uplink streams will interfere with all downlink streams since both the up- and downlink streams are in the same resource block as shown in Figure 2.2. Not only we can

not harvest the benefits of having full-duplex operation, but also we will harm the downlink users. The gain of full-duplex will vanish because of such *uplink-downlink interference* [38] especially in a clustered environment.

In [25], we show that one simple scheme called decode-and-cancel via ISM side-channels can completely recover the full-duplex multiplexing gain. In decode-and-cancel, the uplink user will encode its main-channel (cellular band) message using an independent codebook and send the coded messages to the downlink user through the ISM side-channel. The downlink user then will decode the uplink message from the side-channel, form the main-channel interfering signal locally, and subtract out the interference from the main-channel. The decode-and-cancel scheme involves only single-user decoders, and allows the uplink user to encode the message using different modulation and coding schemes which can be adapted to the ISM side-channel condition.

2.3.2.2 Channelization of ISM side-channels

In this section, we will illustrate how cellular providers can provide a more flexible and structured way for intra-cell interference management via ISM side-channels; this is one of the main reasons to let cellular providers handle the use of ISM bands without user intervention. First, the base station will orthogonalize the downlink and uplink transmission of pilots for channel estimation as shown in Figure 2.8. During the training period of uplink channels, the downlink users can overhear the uplink pilots to estimate the interference channel between the up- and downlink users. Then the base station will start the data transmission for downlink and reception for uplink simultaneously. Since usually the ISM band has much larger bandwidth than that of the licensed band, we can divide the whole bandwidth of ISM band into two parts, one (BW_1) is for downlink user-cooperation to resolve inter-beam interference. The

other part (BW_2) is used to manage the uplink-downlink interference.

In each sub-band of ISM band, we will partition the time slots for the corresponding participating users. As illustrated in Figure 2.8, the k th downlink user amplifies-and-forwards its received signal to other participating downlink users in time-slot T_{D_k} in ISM band BW_1 . The i th uplink user will use decode-and-cancel scheme to broadcast the coded copy of its message in time-slot T_{U_i} in ISM band BW_2 . The downlink receivers will then decode the uplink message in ISM band BW_2 , and subtract out the interference from the main-channel using the channel knowledge of the interference channel. Finally, downlink users can perform receive beamforming with the help of user-cooperation.

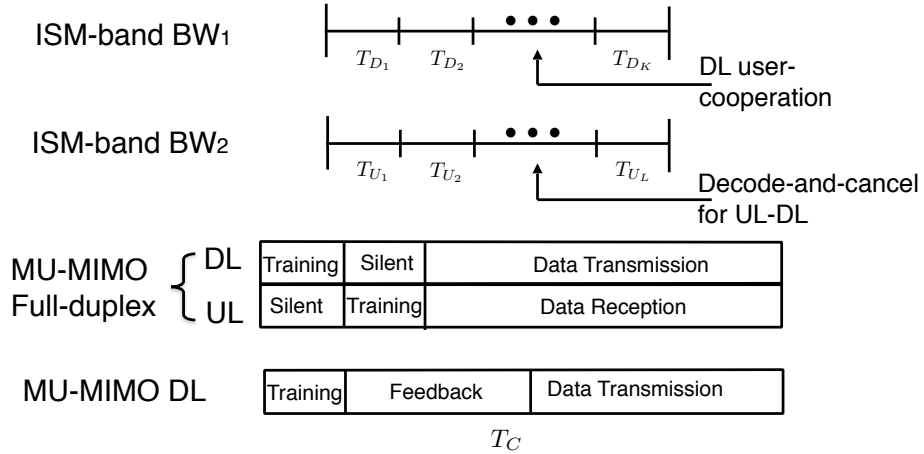


Figure 2.8: Comparison of channel training - data structure between MU-MIMO full-duplex via ISM side-channel and half-duplex MU-MIMO downlink in a given coherence time T_c . The time-slot partitioning of the ISM band for downlink user-cooperation and uplink-downlink decode-and-cancel is also given.

In comparison, in the MU-MIMO downlink, the base station first sends pilots for channel estimation, and then each user will feedback the estimates to the base station which requires $O(M \times K)$ time slots since there are K users and M antennas at the base station. We can see that the overhead of obtaining CSIT is prohibitive especially in large antennas regime, which considerably limits the rate of data transmission given the coherence time T_c .

Area	50×50 square meters
Base station antennas	$M = 20$
Maximum number of users	$K + L = 20$
Uplink and Downlink SNR	35 dB
ISM Side-channel RSSI	Refer to our measurement in Figure 2.5
Main-channel	QPSK uncoded system under Rayleigh fading

Table 2.1: Simulation parameters.

2.3.2.3 Capacity improvement

Based on our analytical calculation [38], we can achieve a maximum multiplexing gain of M with ISM side-channels for improved intra-cell interference management,* while the multiplexing gain of MU-MIMO downlink system is K , and for TDMA system, the multiplexing gain is only one. Hence theoretically our system with ISM side-channels can at most improve the capacity of MU-MIMO downlink by $\frac{M}{K}$ -fold and traditional TDMA by M -fold.

We now illustrate the capacity gains by simulation; the details are listed in Table 2.1. Figure 2.9 compares the cell capacity of four systems: 1) TDMA where all the antennas are used to serve one flow at a time; 2) half-duplex ZFBF downlink with perfect CSIT where all the antennas are used for downlink transmission; 3) full-duplex ZFBF with perfect CSIT where a subset of antennas are used for downlink and the rest are used for uplink; 4) MU-MIMO full-duplex via ISM side-channels where no CSIT is required for the downlink and the uplink streams are decoded via receive ZFBF. We have a fixed up- and downlink user density. We find out our MU-MIMO full-duplex system via ISM side-channels achieves the highest capacity among the four. The capacity gain over ZFBF with perfect CSIT half-duplex downlink can be

*Under the condition that the ISM side-channel strength is above certain SNR dependent threshold.

as high as $6\times$ in this particular case and is proportional to $\frac{M}{K}$ -fold which agrees with our theoretical analysis. The gain over TDMA is as high as $12\times$. Further, we can see that without ISM side-channels, even with perfect CSIT the full-duplex gain vanishes as the number of downlink users increases. In contrast, leveraging the ISM side-channels of mobile users can substantially alleviate the uplink-downlink interference thus recovering the $2\times$ full-duplex gain.

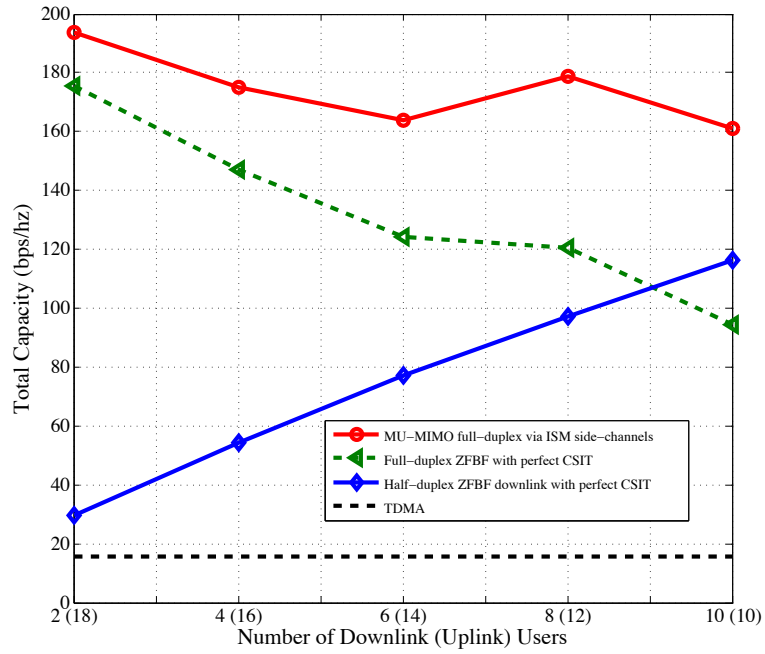


Figure 2.9: Cell capacity of asymmetric traffic with a fixed up- and downlink user density.

We also present the capacity benefit of ISM side-channels with respect to availability range distribution of ISM side-channels. In an area of 50 meters length, we can compute the conditional probability distribution based on our empirical results in Section 2.2.3.* In Figure 2.10, we show the expected capacity, i.e., $\mathbb{E}_d[\text{Capacity}(d)]$, where the capacity is a function of the inter-user distance d . The expectation is taken over the conditional probability distribution. We can see that the expected capacity

*The conditional probability for a given distance range $(x,y]$ can be computed as $\text{Prob}((x,y] - \text{distance} \leq 50)$.

of our ISM side-channels system performs the best among the four, and the gains scale with increasing SNR.

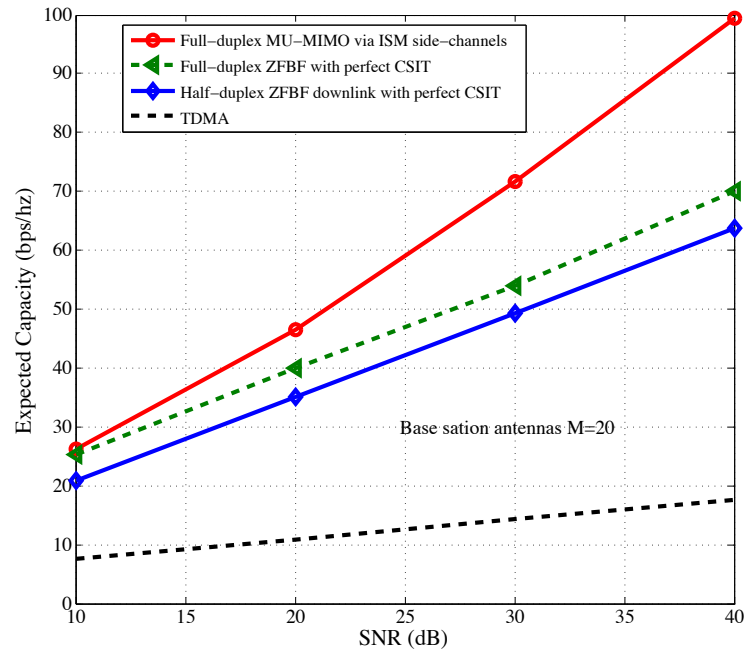


Figure 2.10: Expected capacity of asymmetric traffic as a function of SNR.

Vector Bin-and-Cancel in Two-User MIMO Full-Duplex System

3.1 Introduction

In this chapter, we will study how the side-channel will impact the system performance in a two-user MIMO full-duplex system. In Figure 3.1, a full-duplex capable BS communicates with two half-duplex mobiles simultaneously to support one uplink (UL) and one downlink (DL) flow. A major bottleneck in this network is the inter-mobile interference from uplink mobile (node M1) to downlink mobile node (node M2), because of which the degrees-of-freedom of the network collapse to one when all nodes are equipped with single antenna (SISO) [38]. As a result, we proposed a *distributed full-duplex architecture* [38] to leverage the wireless side-channel to mitigate inter-mobile interference. In the case of MIMO scenario, one driving question is if and how the spatial degree-of-freedom, i.e., number of antennas at the base station and mobiles, will be correlated to the spectral degrees-of-freedom offered by the side-channel.

In our setup, we assume that uplink node M1 has M_u transmit antennas, the

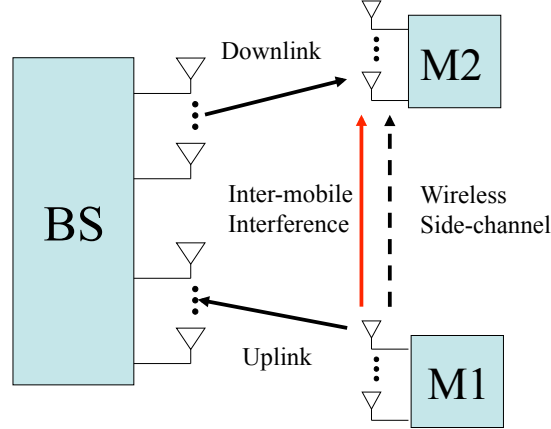


Figure 3.1: *MIMO full-duplex network: inter-mobile interference becomes an important factor when the full-duplex infrastructure node communicates with uplink and downlink mobile nodes simultaneously.*

downlink node M2 has N_d receive antennas, the full-duplex BS has M_d and N_u transmit and receive antennas, respectively. The bandwidth of the side-channel between the mobiles is W -fold compared to the main-channel. We summarize the main results in this chapter as follows.

1. In the time-invariant channels, we obtain the capacity region to within a constant bit achieved by a vector bin-and-cancel scheme. We also analyze the role of channel uncertainty at the transmitter and characterize the GDoF as a function of antenna numbers and side-channel bandwidth under different assumptions of CSIT. The insights gained from GDoF reveal the tradeoff between spatial resources from multiple antennas and spectral resources of the side-channels as well as the interplay between the channel uncertainty at the transmitter and the use of side-channel. In the case when BS has more antennas than mobiles, if there are more downlink receive antennas than uplink transmit antennas, i.e., $N_d \geq M_u$, there is no benefit to obtain CSIT since with and without CSIT achieve the same degrees-of-freedom. On the other hand, if $M_u > N_d$, having CSIT require less side-channel bandwidth to achieve no-interference per-

formance. Thus we conclude that having more spatial degree-of-freedom at the interfered downlink receiver or larger side-channel bandwidth can simplify transceiver design by ruling out the necessity to obtain CSIT.

2. In slow-fading channels, we derive the general DMT under different assumptions of CSIT. Specifically, we quantify the bandwidth of the side-channel required to compensate for *lack of CSIT* such that the DMT without CSIT achieves the optimal DMT with CSIT. Interestingly, in the case when $M_d = N_u = M \geq M_u, N_d$, the required bandwidth is inversely proportional to the number of antennas at the BS, i.e., $W \propto \frac{1}{M}$. The caveat is that the side-channel channel SNR, in the meantime, has to grow with the number of antennas at BS. The result provides guidance towards system design: larger number of BS antennas, e.g. recent discussions on massive MIMO [5], can help reduce the required side-channel bandwidth to combat inter-mobile interference.

We also observe the dependency of CSIT and the antenna number ratio between the mobiles. For the symmetric DMT, when $M_u > N_d$, without side-channel, the lack of CSIT will result in performance loss. However, larger side-channel bandwidth will help bridge the performance gap. On the other hand, when $N_d \geq M_u$, there is no benefit to obtain CSIT to achieve no-interference DMT since, with and without CSIT, one requires the same amount of side-channel bandwidth to completely eliminate the effect of interference. Hence in the protocol design, the scheduler could possibly group downlink user with more receive antennas to eliminate the overhead of acquiring CSIT.

3. We evaluate the required side-channel bandwidth to achieve the no-interference GDoF and DMT under different channel models such that the effect of inter-mobile interference can be completely eliminated via side-channel. The key difference in the findings between the two channel scenarios, for instance, when

$M_d = N_u = M \geq M_u, N_d$, is that in GDoF analysis under time-invariant channels, the required W does not depend on the antenna number ratio between the mobiles; while in DMT analysis under slow-fading channels, required W is a function of the antennas number ratio $A = \frac{\max(M_u, N_d)}{\min(M_u, N_d)}$ and $W \propto \frac{1}{A}$. The impact on the system design is that we should schedule up- and downlink user pair with higher antenna ratio to cancel out interference with reduced side-channel bandwidth.

Notations: We use A^\dagger to denote Hermitian of A , and $|A|$ to denote the determinant of A . We use $(x)^+$ to denote $\max(x, 0)$. We use $\mathcal{CN}(0, Q)$ to denote a circularly symmetric complex Gaussian distribution with zero mean and covariance matrix Q . We use I_N to denote identity matrix of rank N . We use $f(\rho) \doteq g(\rho)$ to denote that $\lim_{\rho \rightarrow \infty} \frac{\log f(\rho)}{\log g(\rho)} = 1$. We use $A \preceq B$ to denote that matrix $B - A$ is a positive-semidefinite positive (p.s.d) matrix.

3.2 System Model

In this section, we describe the system model to be used for the rest of the chapter. We assume the full-duplex BS is equipped with M_d transmit antennas for the downlink and N_u receive antennas for the uplink. The uplink mobile M1 is equipped with M_u transmit antennas and downlink mobile M2 is equipped with N_d receive antennas. Besides the main-channel which includes uplink, downlink and interference link, there also exists an out-of-band wireless side-channel between the uplink mobile and downlink mobile. We refer to the channel model shown in Figure 3.2 as (M_d, N_d, M_u, N_u) side-channel assisted MIMO full-duplex network. Let W_m and W_s denote the bandwidth of the main-channel and side-channel, respectively. Parameter $W = \frac{W_s}{W_m}$ represents the bandwidth ratio of the side-channel to that of the

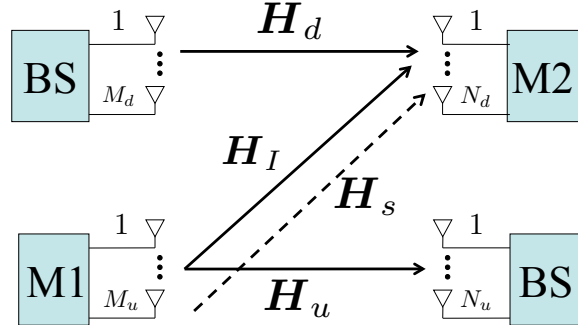


Figure 3.2: Channel model: (M_d, N_d, M_u, N_u) side-channel assisted MIMO full-duplex network.

main-channel.

Since one of the transmitter and receiver is co-located in the same node, the base-station BS, the uplink message received by the BS is causally known to the BS transmitter for downlink transmission. As a result, the side-channel assisted full-duplex network can be viewed as a Z-interference channel with implicit feedback and an out-of-band side-channel.

We assume that the channel parameters in our system model consist of two components: a small-scale fading factor due to multipath and a large-scale fading factor due to path loss. We denote the small-scale fading channels matrix as $\mathcal{H} = \{H_d, H_u, H_I, H_S\}$, where each entry in \mathcal{H} represents the small-scale fading channel matrix for the downlink, uplink, inter-mobile interference channel and the side-channel, as shown in Figure 3.2. We assume that all entries in H_k , where $k \in \{d, u, I, S\}$, are mutually independent and identically distributed (i.i.d.) according to $\mathcal{CN}(0, 1)$ and all channel matrices are full rank with probability one. We will consider two different scenarios for the small-scale fading.

- *Time-invariant channels*: \mathcal{H} is fixed during the entire communication period.
- *Slow-fading channels*: \mathcal{H} remains unchanged during each fade duration or coherence time, and varies i.i.d. between distinct fade periods.

As for the large-scale fading factor, it captures the channel attenuation due to distance. Thus the channel attenuation between the transmitter and receiver is the same for every transmit-receive antenna pair. Hence the channel attenuation for each channel is denoted by a scalar γ_k , where $k \in \{d, u, I, S\}$. The transmitter at BS and uplink node M1 have a maximum power budget P_d and P_u , respectively. To simplify the notation, let $\rho_d = \gamma_d P_d$, $\rho_u = \gamma_u P_u$, $\rho_S = \gamma_S P_u$ and $\rho_I = \gamma_I P_u$, which denotes the average signal-to-noise ratio and interference-to-noise ratio at each receive antenna with additive Gaussian noise of unit variance.

Next, we describe the channel input-output relationships as follows.

3.2.0.4 Uplink

The node M1 will split the transmit power between main-channel and side-channel, i.e., $\bar{\lambda}P_u$ and λP_u for main-channel and side-channel data transmission, respectively. We define $\bar{\lambda} = 1 - \lambda$, $\lambda \in [0, 1]$. Thus the received uplink signal $Y_u \in \mathbb{C}^{N_u \times 1}$ at BS is given by

$$Y_u(t) = \sqrt{\bar{\lambda}\rho_u}H_u X_u(t) + Z_u(t), \quad (3.1)$$

where $X_u(t) \in \mathbb{C}^{M_u \times 1}$ is the uplink vector signal; $H_u \in \mathbb{C}^{N_u \times M_u}$ represents uplink channel and $Z_u(t) \in \mathbb{C}^{N_u \times 1}$ is the receiver additive Gaussian noise which contains i.i.d. $\mathcal{CN}(0, 1)$ entries.

3.2.0.5 Downlink

The received downlink signal $Y_d \in \mathbb{C}^{N_d \times 1}$ at the node M2 is a combination of the downlink signal and the interfering uplink signal, and is given by

$$Y_d(t) = \sqrt{\rho_d}H_d X_d(t) + \sqrt{\bar{\lambda}\rho_I}H_I X_u(t) + Z_d(t), \quad (3.2)$$

where $X_d(t) \in \mathbb{C}^{M_d \times 1}$ is the downlink vector signal; $H_d \in \mathbb{C}^{N_d \times M_d}$ is the downlink channel matrix and $H_I \in \mathbb{C}^{N_d \times M_u}$ is the inter-mobile interference channel matrix; $Z_d(t) \in \mathbb{C}^{N_d \times 1}$ is the receiver additive Gaussian noise which contains i.i.d. $\mathcal{CN}(0, 1)$ entries.

3.2.0.6 Side-channel

We assume that the number of side-channel antennas are same as the main-channel. Thus the received signal $Y_S \in \mathbb{C}^{N_d \times 1}$ at the node M2 is given by

$$Y_S(t) = \sqrt{\lambda \rho_S} H_S X_S(t) + Z_S(t), \quad (3.3)$$

where $X_S(t) \in \mathbb{C}^{M_u \times 1}$ is the side-channel vector signal; $H_S \in \mathbb{C}^{N_d \times M_u}$ is the channel matrix of the side-channel; $Z_d(t) \in \mathbb{C}^{N_d \times 1}$ is the Gaussian noise added to the side-channel which contains i.i.d. $\mathcal{CN}(0, W)$ entries. Note that the noise variance of each entry in the side-channel is W times larger than that in the main-channel.

The power constraint of the input signals is given as:

$$\frac{1}{L} \sum_{t=1+Lk}^{L(k+1)} \text{Trace} \left(\mathbb{E}[X_i(t) X_i(t)^\dagger] \right) \leq 1, \quad k \in \mathbb{N}, i \in \{d, u, S\}, \quad (3.4)$$

where in time-invariant channels, $k = 0$, and L denotes the entire communication duration; in slow-fading channels, L denotes the coherence time.*

We define the strength level of different links with respect to nominal SNR, ρ , in decibels[†]

$$\alpha_i = \frac{\log \rho_i}{\log \rho}, \quad i \in \{d, u, I, S\}. \quad (3.5)$$

*In the rest of the chapter, we omit the time-index t in the expressions.

[†]We can set $\rho = \rho_d$ or ρ_u such that either $\alpha_d = 1$ or $\alpha_u = 1$.

Note that the above normalization allows different links to have disparate strength.

3.3 Approximate Capacity Region and Generalized Degrees-of-Freedom

A full-duplex node can be viewed as “two nodes,” with a co-located transmitter and receiver, that are connected by an *infinite* capacity link. Inspired by this interpretation, in [38], we proposed a *distributed full-duplex* architecture which is enabled by a wireless side-channel of *finite* bandwidth when the transmitter and interfered receiver are not co-located. When channel knowledge is known globally, we showed that a bin-and-cancel scheme achieves the capacity region to within 1 bit/s/Hz of the capacity region for all channel parameters in SISO case [38].

In this section, we will study the capacity region in MIMO case under different assumptions of channel uncertainty at the transmitter. CSIT plays a critical role in MIMO interference channels. With CSIT, the transmitter can design the precoding matrix to steer the direction of the transmit signal to achieve higher rate. However, the cost of obtaining CSIT is also prohibitive since the receiver has to feed back the channel knowledge within the coherence time which incurs operational overhead. Thus it is crucial to explore the role of channel uncertainty at the transmitter in system performance. We assume that the receiver-side channel information is always available as the receiver can track the instantaneous channel from the training pilots. In what follows, we will study the capacity region in time-invariant channels. Next, we will present how CSIT and the use of side-channel is correlated, we also characterize the spatial and spectral tradeoff between multiple antennas at different nodes and spectral resources provided by side-channel.

3.3.1 Capacity region to within a constant gap With CSIT

3.3.1.1 Outer bound

Lemma 1. *Given the channel realization \mathcal{H} , the capacity region $\mathcal{C}(\mathcal{H})$ of the side-channel assisted MIMO full-duplex network is outer bounded by*

$$\begin{aligned}
 R_d &\leq W_m \left(\log \left| I_{N_d} + \rho_d H_d H_d^\dagger \right| \right) \triangleq \bar{C}_d, \\
 R_u &\leq W_m \left(\log \left| I_{N_u} + \bar{\lambda} \rho_u H_u H_u^\dagger \right| \right) \triangleq \bar{C}_u, \\
 R_d + R_u &\leq W_m \left(\log \left| I_{N_d} + \rho_d H_d H_d^\dagger + \bar{\lambda} \rho_I H_I H_I^\dagger \right| + W \log \left| I_{N_d} + \frac{\lambda \rho_S}{W} H_S H_S^\dagger \right| \right. \\
 &\quad \left. + \log \left| I_{N_u} + \bar{\lambda} \rho_u H_u (I_{M_u} + \bar{\lambda} \rho_I H_I^\dagger H_I)^{-1} H_u^\dagger \right| + N_d \right) \triangleq \bar{C}_{\text{sum}},
 \end{aligned} \tag{3.6}$$

Proof. See Appendix A in [29]. Note that if the interference channel (ρ_I) or side-channel quality ($W\rho_S$) exceeds certain threshold such that $C_{\text{sum}} \geq C_d + C_u$, the capacity is just trivially outer bounded by the first two individual constraints in (3.6). \square

3.3.1.2 Achievable rate region

A vector bin-and-cancel scheme based on a simple Han-Kobayashi coding strategy achieves the following rate region when CSIT is available. The scheme will be elucidated later in Section 3.3.2.

Lemma 2. *The achievable rate region $\mathcal{R}_{\text{BC}}(\mathcal{H})$ of the side-channel assisted MIMO three-node full-duplex network for time-invariant channels is*

$$\begin{aligned}
 R_d &\leq \bar{C}_d - W_m c_1, \\
 R_u &\leq \bar{C}_u - W_m c_2, \\
 R_d + R_u &\leq \bar{C}_{\text{sum}} - W_m (c_1 + c_2),
 \end{aligned} \tag{3.7}$$

where

$$\begin{aligned}
c_1 &= \min\{M_d + M_u, N_d\} \log(\max\{M_d, M_u\}) + \hat{m}_I, \\
c_2 &= (m_u + Wm_I) \log M_u + m_X \log(M_u + 1), \hat{m}_I = m_I \log \left(1 + \frac{1}{M_u}\right), \\
m_d &= \min\{M_d, N_d\}, m_u = \min\{M_u, N_u\}, m_X = \max\{M_u, N_d\}, m_I = \min\{M_u, N_d\}.
\end{aligned} \tag{3.8}$$

Proof. See Section 3.3.2 for description of the achievability and Appendix B in [29] for the rate calculation. \square

Based on the lemmas above, we will state the result of constant-bit gap to capacity region under time-invariant channels in the following theorem.

Theorem 1. *For the side-channel assisted two-user MIMO full-duplex network under time-invariant channels, the achievable rate region $\mathcal{R}_{\text{BC}}(\mathcal{H})$ is within $\max\{c_1, c_2\}$ bit/s/Hz of the capacity region $\mathcal{C}(\mathcal{H})$, where c_i , $i = 1, 2$ is given in (3.8).*

Proof. The proof is straightforward. From Lemma 1 and Lemma 2, we can calculate the rate difference and divide it by the total bandwidth $W_m + W_s$ of the system. In other word, for any given rate pair $(R_d, R_u) \in \mathcal{C}(\mathcal{H})$ (bit/s), the rate pair $((R_d - (W_m + W_s)c_1)^+, (R_u - (W_m + W_s)c_2)^+)$ is achievable in $\mathcal{R}_{\text{BC}}(\mathcal{H})$. \square

In the SISO case, we can easily verify that the vector bin-and-cancel achieves the capacity region to within one bit.

3.3.2 Achievability

In this section, we will describe the vector bin-and-cancel scheme used to show the achievability in Lemma 2. In vector bin-and-cancel, we use Han-Kobayashi [39] style

common-private message splitting with a simple power splitting. The common message can be decoded at both receivers while the private message can only be decoded at the intended receiver. The downlink message ω_d only consists of private message for the downlink receiver which is of size 2^{nR_d} , and is encoded into codeword X_d . The uplink message is divided into the common part $\omega_{u,c}$ of size $2^{nR_{u,c}}$ and the private part $\omega_{u,p}$ of size $2^{nR_{u,p}}$. The uplink codeword is then obtained by superposition of the codewords of both $\omega_{u,c}$ and $\omega_{u,p}$,

$$X_u = S_u + U_u,$$

where S_u and U_u are the codewords of uplink common message $\omega_{u,c}$ and private message $\omega_{u,p}$, respectively.

Next, we partition the uplink common message $\omega_{u,c}$: the common message set is divided into 2^{nR_s} equal size bins such that $\mathcal{B}(l) = [(l-1)2^{n(R_{u,c}-R_s)} + 1 : l2^{n(R_{u,c}-R_s)}]$, $l \in [1 : 2^{nR_s}]$. The total number of bin indices 2^{nR_s} is determined by the strength of the side-channel, α_s , and the bandwidth ratio W . The bin index l is then encoded into codeword X_s and sent from the uplink transmit antenna arrays over the side-channel, which is shown in Figure 3.3.

All the codewords are mutually independent complex Gaussian random vectors with covariance matrices given as follows to satisfy the power constraint given in (3.4):

$$\begin{aligned} \mathbb{E}(X_d X_d^\dagger) &= \frac{1}{M_d} I_{M_d}, & \mathbb{E}(U_u U_u^\dagger) &= \frac{1}{M_u} (I_{M_u} + \bar{\lambda} \rho_I H_I^\dagger H_I)^{-1} \\ \mathbb{E}(S_u S_u^\dagger) &= \frac{1}{M_u} I_{M_u} - \mathbb{E}(U_u U_u^\dagger), & \mathbb{E}(X_u^s X_u^{s\dagger}) &= \frac{1}{M_u} I_{M_u}, \end{aligned} \quad (3.9)$$

where $\lambda \in (0, 1)$, $\bar{\lambda} + \lambda = 1$. The parameter λ denotes the fraction of power allocated to the side-channel. For the power splitting between the uplink private and common

message, we set the power of the private message such that its received signal strength is below the noise floor at each unintended receiver's antenna. And we allocate the power of the codewords equally among the transmit antenna array.

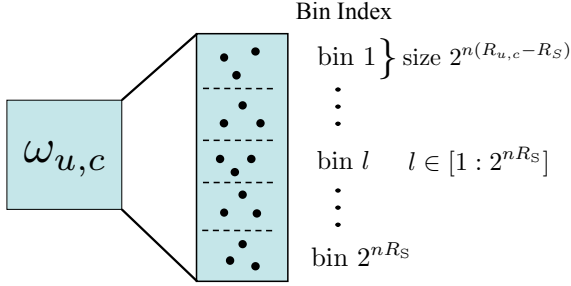


Figure 3.3: Binning of the common message at uplink transmitter.

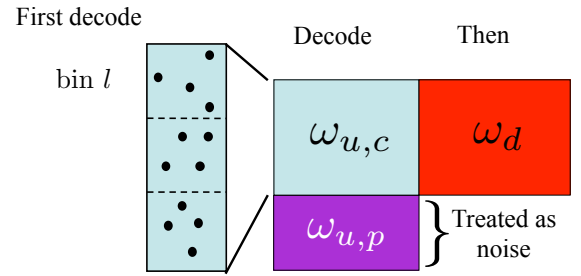


Figure 3.4: Decoding at downlink receiver.

Now we describe the decoding process. The decoding at the BS is straightforward. Upon receiving Y_u , the BS decodes $(\omega_{u,c}, \omega_{u,p})$. The achievable rate region of $(R_{u,c}, R_{u,p})$ is the capacity region of multiple-access channel denoted as \mathcal{C}_1 , where

$$\begin{aligned}
 R_{u,c} &\leq I(S_u; Y_d | X_d) \\
 R_{u,p} &\leq I(U_u; Y_u | S_u) \\
 R_{u,c} + R_{u,p} &\leq I(S_u, U_u; Y_u)
 \end{aligned} \tag{3.10}$$

The decoding at the downlink receiver has two stages as shown in Figure 3.4. In stage one, upon receiving Y_S , the downlink receiver first decodes the bin index l from the side-channel. In stage two, upon receiving Y_d , the downlink receiver decodes $(\omega_d, \omega_{u,c})$ with the help of side-channel information while treating uplink private message $\omega_{u,p}$ as noise.* This is a multiple-access channel (MAC) with side-channel whose

*With the assistance of the bin index, more uplink common message can be decoded which otherwise is restricted by the interference link.

capacity region denoted as \mathcal{C}_2 is given in [38] (see Lemma 1), hence we have

$$\begin{aligned} R_d &\leq I(X_d; Y_d | S_u) \\ R_{u,c} &\leq I(S_u; Y_d | X_d) + I(X_S; Y_S) \\ R_d + R_{u,c} &\leq I(X_d, S_u; Y_d) + I(X_S; Y_S). \end{aligned} \tag{3.11}$$

The achievable rate region of side-channel assisted full-duplex network is the set of all (R_d, R_u) such that $R_d, R_u = R_{u,c} + R_{u,p}$ satisfying that $(R_{u,c}, R_{u,p}) \in \mathcal{C}_1$ and $(R_d, R_{u,c}) \in \mathcal{C}_2$. Using Fourier-Motzkin elimination, the achievable rate pairs (R_d, R_u) are constrained by the following rate region

$$\begin{aligned} R_d &\leq I(X_d; Y_d | S_u) \\ R_u &\leq \min\{I(S_u, U_u; Y_u), I(U_u; Y_u | S_u) + I(S_u; Y_d | X_d) + I(X_S; Y_S)\} \\ R_d + R_u &\leq I(U_u; Y_u | S_u) + I(X_d, S_u; Y_d) + I(X_S; Y_S). \end{aligned} \tag{3.12}$$

The achievable rate region given above is calculated in Appendix B in [29], thus we can obtain the explicit achievable rate expression in Lemma 2.

3.3.3 High SNR approximation

From Theorem 1, vector bin-and-cancel scheme achieves the capacity region to within a constant bit for *all* values of channel parameters under time-invariant channels. In the high SNR limit, a constant number of bits (which do not vary with respect to SNR) are insignificant and can be ignored on the scale of interest. Therefore we can establish the high SNR capacity region approximation to within $\mathcal{O}(1)$ in the following corollary.

Corollary 1. *For a given the channel realization \mathcal{H} , vector bin-and-cancel is asymptotically capacity achieving and the asymptotic capacity approximation $\mathcal{C}(\mathcal{H})$ is given*

by

$$\begin{aligned} \mathcal{C}(\mathcal{H}) \doteq & \left\{ (R_d, R_u) : R_d \leq W_m \log \left| I_{N_d} + \rho_d H_d H_d^\dagger \right| \triangleq C_d, \right. \\ & R_u \leq W_m \log \left| I_{N_u} + \bar{\lambda} \rho_u H_u H_u^\dagger \right| \triangleq C_u, \\ & R_d + R_u \leq W_m \left(\log \left| I_{N_d} + \rho_d H_d H_d^\dagger + \bar{\lambda} \rho_1 H_1 H_1^\dagger \right| + W \log \left| I_{N_d} + \frac{\lambda \rho_S}{W} H_S H_S^\dagger \right| \right. \\ & \left. \left. + \log \left| I_{N_u} + \bar{\lambda} \rho_u H_u (I_{M_u} + \bar{\lambda} \rho_1 H_1^\dagger H_1)^{-1} H_u^\dagger \right| \right) \triangleq C_{\text{sum}} \right\}. \end{aligned} \quad (3.13)$$

The high SNR capacity approximation can be used to derive the generalized degrees of freedom (GDoF). The GDoF captures the asymptotic behavior of the capacity and the corresponding optimal schemes, allowing different links to grow at disparate rates.

The GDoF region is defined as follows *

$$\left\{ (\text{DoF}_d, \text{DoF}_u) : \text{DoF}_i = \lim_{\rho \rightarrow \infty} \frac{R_i(\rho_i)}{W_m \log \rho}, \quad i \in \{d, u\} \text{ and } (R_d, R_u) \in \mathcal{C}(\mathcal{H}) \right\}, \quad (3.14)$$

where $W_m \log \rho$ is the point-to-point main-channel capacity with nominal SNR in bit/s. DoF_d and DoF_u denote the degrees of freedom (DoF) of downlink and uplink, respectively. Using high SNR capacity approximation, we state the GDoF region as follows.

Corollary 2. *Assuming $\alpha_d = \alpha_u = 1$, the GDoF region of (M_d, N_d, M_u, N_u) side-*

*Notice that our definition deviates slightly from the conventional definition of GDoF in that we account for the asymmetric bandwidths of different links and the rate is calculated as bit/s instead of bit/s/Hz.

channel assisted MIMO full-duplex network satisfies the following constraints

$$\begin{aligned} \text{DoF}_d &\leq m_d, \quad \text{DoF}_u \leq m_u, \\ \text{DoF}_d + \text{DoF}_u &\leq f\left(N_u, ((1 - \alpha_I)^+, m_I), (1, (M_u - N_d)^+)\right) \\ &+ f(N_d, (\alpha_I, M_u), (1, M_d)) + Wf(N_d, (\alpha_S, M_u)), \end{aligned} \quad (3.15)$$

where $m_d = \min\{M_d, N_d\}$, $m_u = \min\{M_u, N_u\}$, $m_I = \min\{M_u, N_d\}$ as defined in (3.8); function $f(x, (y_1, x_1), (y_2, x_2)) = \min\{x, x_1\}y_1^+ + \min\{(x - x_1)^+, x_2\}y_2^+$ for $y_1 \geq y_2$.

Proof. The proof is akin to [40] (see Appendix C), so we will only provide an interpretation of the GDoF result here.

First, the DoF of downlink and uplink is limited by the number of transmit and receive antennas, much like the point-to-point MIMO channel. Next we will explain the sum GDoF. Let $\text{DoF}_{u,c}$ and $\text{DoF}_{u,p}$ denote the DoF of the uplink common message and private message, respectively.

Adopting the singular value decomposition (SVD), we can decompose the interference channel as $H_I = U\Lambda V^\dagger$, where U and V are $N_d \times N_d$ and $M_u \times M_u$ unitary matrices, respectively, Λ is $N_d \times M_u$ diagonal matrix containing singular values of H_I . Thus H_I is decomposed into m_I parallel channels, leaving $(M_u - m_I)^+ = (M_u - N_d)^+$ effective inputs at uplink transmitter that do not cause any interference to the downlink receiver. The uplink transmitter divides the private streams into two parts. The first part is sent along the $(M_u - N_d)^+$ -dimensional null space of interference channel H_I and reaches BS at an SNR of ρ with N_u receive antennas. In the remaining m_I dimensions, the second part is transmitted at a power level of $\rho^{-\alpha_I}$ such that it reaches the unintended receiver at the noise floor and reaches BS at an SNR of $\rho^{(1-\alpha_I)^+}$. The process can be viewed as a combination of signal space and signal scale interference

alignment. Thus the DoF of the uplink private message is

$$\text{DoF}_{u,p} = f\left(N_u, ((1 - \alpha_1)^+, m_1), (1, (M_u - N_d)^+)\right). \quad (3.16)$$

Since the common message can be decoded at both receivers, the downlink receiver with N_d receive antennas is a side-channel assisted multiple access channel receiver. The downlink message ω_d reaches the downlink receiver at an SNR of ρ with M_d transmit antennas. The uplink common message $\omega_{u,c}$ reaches the downlink receiver through both main-channel at an SNR of ρ^{α_1} and side-channel as an orthogonal spectral space at an SNR of $\rho^{W\alpha_s}$ with M_u transmit antennas. Thus we have

$$\text{DoF}_d + \text{DoF}_{u,c} = f(N_d, (\alpha_1, M_u), (1, M_d)) + Wf(N_d, (\alpha_s, M_u)). \quad (3.17)$$

Combining (3.16) and (3.17) leads to the sum GDoF. □

Remark 1. *When $W = 0$, i.e., there is no side-channel, the GDoF is the same as that of MIMO Z-interference channel in [40], hence we conclude that the implicit feedback at the full-duplex capable BS does not help improve GDoF regime in the two-user MIMO full-duplex network. This is due to the fact there is only one-sided interference. When $W > 0$, the implicit feedback is still not useful in terms of GDoF because our scheme does not rely on any feedback.*

3.3.4 Special cases

In this section, we give several special cases to illustrate the GDoF results above.

Theorem 2. *(Case A) When $M_d = M_u = M, N_d = N_u = N$, and $\alpha_u = \alpha_d = 1$, the sum GDoF per antenna denoted as $\frac{\text{GDoF}_{\text{sum}}}{\min(M,N)}$ for the symmetric side-channel assisted*

MIMO full-duplex network is given by

$$\frac{\text{GDoF}_{\text{sum}}}{\min(M, N)} = \begin{cases} \min \left\{ 2, 2 - \left(2 - \frac{\max(M, N)}{\min(M, N)} \right)^+ \alpha_I + W\alpha_S \right\} & \alpha_I < 1, \\ \min \left\{ 2, \alpha_I + \frac{\max(M, N)}{\min(M, N)} - 1 + W\alpha_S \right\} & \alpha_I \geq 1. \end{cases}$$

In this case, one can observe that the sum GDoF per antenna increases linearly with the antenna ratio $\frac{\max(M, N)}{\min(M, N)}$ and side-channel quality $W\alpha_S$.

Another case of interest is when the BS has more antennas than mobile clients, i.e., $M_d, N_u \geq M_u, N_d$. This scenario is almost always true in practical systems and the ongoing trend is that the BS can accommodate many antennas such as in massive MIMO systems [5], while the small-form factor mobiles will have a relatively fewer antennas due to its physical size constraint.

Theorem 3. (Case B) When BS has more antennas than mobiles, i.e., $M_d, N_u \geq M_u, N_d$ with $\alpha_u = \alpha_d = 1$, the sum GDoF per antenna denoted as $\frac{\text{GDoF}_{\text{sum}}}{\min(M_u, N_d)}$ is given as

$$\frac{\text{GDoF}_{\text{sum}}}{\min(M_u, N_d)} = \begin{cases} \min \left\{ \frac{m_X}{m_I} + 1, \frac{m_X}{m_I} + 1 - \alpha_I + W\alpha_S \right\} & \alpha_I < 1 \\ \min \left\{ \frac{m_X}{m_I} + 1, \frac{m_X}{m_I} - 1 + \alpha_I + W\alpha_S \right\} & \alpha_I \geq 1. \end{cases}$$

where $m_X = \max(M_u, N_d)$, $m_I = \min(M_u, N_d)$.

Figure 3.5 illustrates how the sum GDoF per antenna varies as the side-channel quality changes when $M_u = N_d$ given an excess of antennas at BS. When $W\alpha_S = 0$, i.e., there is no side-channel, the curve maintains “V” shape as in the Z-interference channel. When $W\alpha_S$ increases, the curve gradually becomes a lifted “V” and finally reach the maximum sum GDoF per antenna of 2 for all regimes that one can achieve without interference.

We also give an example to clarify the DoF of vector bin-and-cancel in Case B

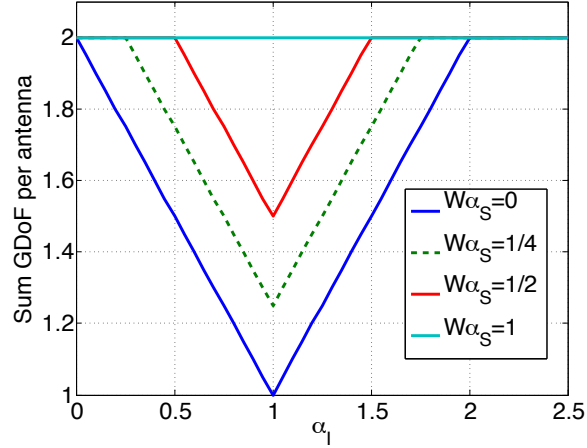


Figure 3.5: The sum GDoF per antenna for $M_u = N_d$ when BS has an excess of antennas.

assuming $\alpha_I = \alpha_S = 1$. Using the standard MIMO SVD of channel matrices, the interference channel and side-channel can be converted to $m_I = \min\{N_d, M_u\}$ parallel paths from uplink node Tx_U to downlink node Rx_D . In Figure 3.6, the diagonalized interference and side-channel paths are depicted in bold.

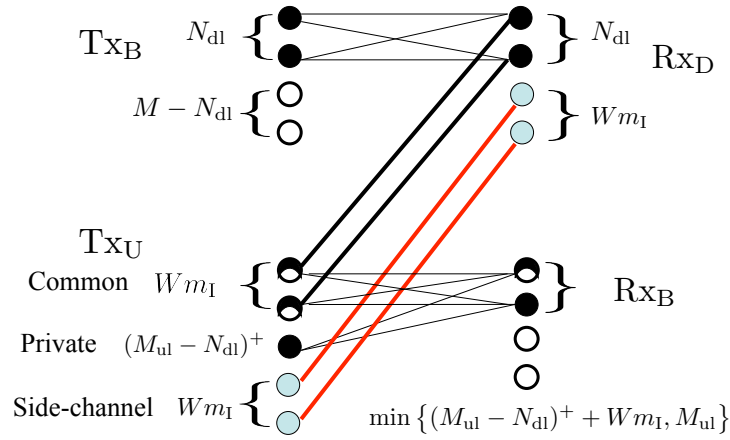


Figure 3.6: The DoF-optimal scheme of two-user side-channel assisted MIMO full-duplex network when $M_u \geq N_d$.

In Figure 3.6, the base station Tx_B sends N_d independent streams to downlink node Rx_D , which is indicated by the black circles. Uplink node Tx_U sets $(1 - W)m_I$

effective inputs ^{*} to zero, which is indicated by the white circles; Tx_U then sends $(M_u - N_d)^+$ independent private streams in the null space of the signal from Tx_B , and Wm_I common message which can be heard at Rx_D . Using vector bin-and-cancel, each transmitter sends Wm_I streams of its common message to the interfering receiver through the side-channel, which is indicated by the blue circles. At the downlink receiver Rx_D , Wm_I streams of the interfering message can be canceled out, thus downlink can achieve N_d DoFs and uplink can achieve $\min\{(M_u - N_d)^+ + Wm_I, M_u\}$ DoFs. Thus, in total, we can obtain $\min\{\max\{N_d, M_u\} + Wm_I, N_d + M_u\}$ DoFs.

3.3.5 GDoF without CSIT

Acquiring the CSIT incurs a large overhead, especially in a MIMO system with many antennas. Hence it is of practical interest to study the GDoF performance of the system without CSIT.

We first describe the encoding and decoding strategy under the no-CSIT assumption. Both transmitters encode their messages using independent Gaussian codebooks for the main-channel. The uplink transmitter sends common message only, and applies vector bin-and-cancel scheme. The side-channel bins all the uplink message and encodes the bin indices using an independent Gaussian codebook. From the downlink user's perspective, the channel is a MAC with side-channel. At the decoding process, the downlink user uses joint maximum likelihood (ML) decoder to decode both downlink message and uplink messages with the help of side-channel. Hence we

^{*}The effective input is a product of the unitary matrices by SVD and the initial input vector.

can obtain the achievable rate region $\mathcal{R}^{\text{No-CSIT}}$ as

$$\begin{aligned} \mathcal{R}^{\text{No-CSIT}} = & \left\{ (R_d, R_u) : R_d \leq W_m \log \left| I_{N_d} + \frac{\rho_d}{M_d} H_d H_d^\dagger \right|, \right. \\ R_u \leq & W_m \min \left\{ \log \left| I_{N_u} + \frac{\bar{\lambda} \rho_u}{M_u} H_u H_u^\dagger \right|, \log \left| I_{N_d} + \frac{\bar{\lambda} \rho_I}{M_u} H_1 H_1^\dagger \right| + W \log \left| I_{N_d} + \frac{\lambda \rho_S}{W M_u} H_S H_S^\dagger \right| \right\}, \\ R_d + R_u \leq & W_m \left(\log \left| I_{N_d} + \frac{\rho_d}{M_d} H_d H_d^\dagger + \frac{\bar{\lambda} \rho_I}{M_u} H_1 H_1^\dagger \right| + W \log \left| I_{N_d} + \frac{\lambda \rho_S}{W M_u} H_S H_S^\dagger \right| \right) \Bigg\}, \end{aligned} \quad (3.18)$$

where $\lambda \in (0, 1)$, for instance, we can fix $\lambda = \bar{\lambda} = 0.5$. The achievable rate region given above can be calculated easily from Equation (3.12) with uplink private message set to null and equal power allocation among transmit antennas which does not require any CSIT.

Now we can obtain the lower bound of the GDoF under the no-CSIT assumption.

Corollary 3. *Assuming $\alpha_d = \alpha_u = 1$ and no-CSIT, the achievable GDoF region of (M_d, N_d, M_u, N_u) side-channel assisted MIMO full-duplex network satisfies the following constraints*

$$\begin{aligned} \text{DoF}_d \leq m_d, \quad \text{DoF}_u \leq \min \{m_u, \alpha_I m_I + W \alpha_S m_I\}, \\ \text{DoF}_d + \text{DoF}_u \leq f(N_d, (\alpha_I, M_u), (1, M_d)) + W f(N_d, (\alpha_S, M_u)). \end{aligned} \quad (3.19)$$

Proof. The achievable GDoF region without CSIT can be derived following the same argument as in the case with CSIT. \square

Remark 2. *Comparing the Corollaries 2 and 3, we conclude that when $\alpha_I \geq 1$ and $N_d \geq M_u$, acquiring CSIT is of no use as the GDoF without CSIT achieves the optimal GDoF with CSIT. In the strong interference regime where $\text{INR} > \text{SNR}$, larger number of receiver antennas is sufficient to null out the interference to achieve the optimal GDoF regime.*

3.3.6 Spatial and spectral tradeoff in GDoF

In this section, we will compare three systems: (i) the side-channel assisted full-duplex network with CSIT, (ii) the side-channel assisted full-duplex network without CSIT, and (iii) an idealized full-duplex network without interference, i.e., a parallel uplink and a downlink channel; the last network provides us the benchmark for the best possible performance. By comparing these three systems, we aim to quantify the relationship between the spatial resources of multiple antennas and spectral resources of the side-channel. We start by presenting several corollaries to Theorems 2 and 3.

Corollary 4. *(Case A with CSIT) The effect of interference can be completely eliminated if the bandwidth ratio of the side-channel to main-channel satisfies the following condition,*

$$W_{CSIT} = \begin{cases} \frac{\alpha_I}{\alpha_S} \left(2 - \frac{\max(M,N)}{\min(M,N)} \right)^+, & \text{for } \alpha_I < 1, \\ \frac{1}{\alpha_S} \left(3 - \frac{\max(M,N)}{\min(M,N)} - \alpha_I \right)^+, & \text{for } \alpha_I \geq 1. \end{cases} \quad (3.20)$$

From Corollary 4, we can see that the required bandwidth ratio is a linearly decreasing function of the antenna number ratio $\frac{\max(M,N)}{\min(M,N)}$ to achieve the interference-free performance. Therefore the spatial resources of the number of antennas at transmitters and receivers is interchangeable with the spectral resources of the side-channel bandwidth to eliminate interference. The intuition behind it is that the additional spatial signaling dimension to perform transmit/receive beamforming is equivalent to leveraging the extra spectral signaling dimension of the side-channel for interference cancellation.

From Corollary 3, we can also find out the required bandwidth ratio under the no-CSIT assumption in order to achieve the no-interference upper bound. The required

bandwidth ratio without CSIT in Case A for $\alpha_I = 1$ is given by

$$W_{\text{No-CSIT}} = \begin{cases} \frac{1}{\alpha_S} \left(2 - \frac{N}{M}\right)^+, & \text{for } N \geq M, \\ \frac{1}{\alpha_S}, & \text{for } M > N. \end{cases} \quad (3.21)$$

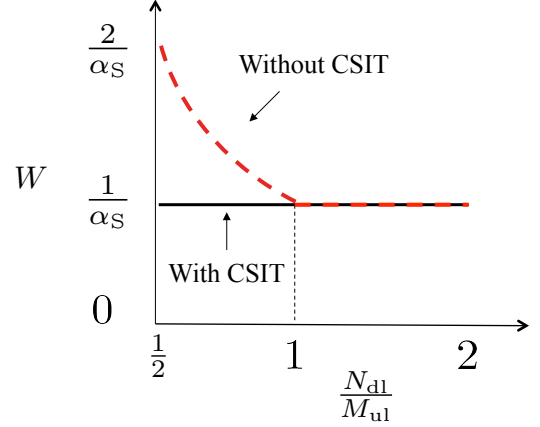
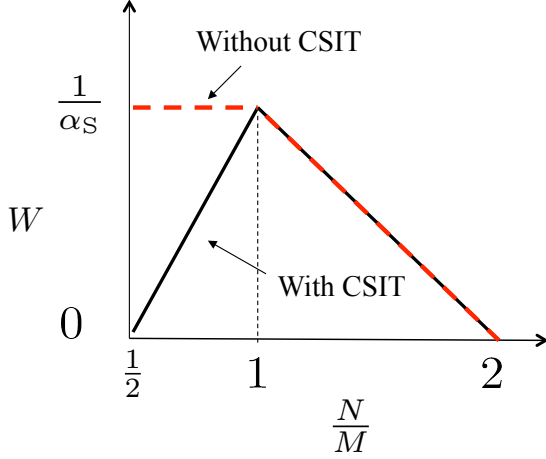


Figure 3.7: Spatial spectral tradeoff in Case A when $\alpha_I = 1$.

Figure 3.8: Spatial spectral tradeoff in Case B when $\alpha_I = 1$.

Corollary 5. (*Case B with CSIT*) *The effect of interference can be completely eliminated if the bandwidth ratio of the side-channel to main-channel satisfies the following condition,*

$$W_{\text{CSIT}} = \begin{cases} \frac{\alpha_I}{\alpha_S}, & \text{for } \alpha_I < 1, \\ \frac{(2-\alpha_I)^+}{\alpha_S}, & \text{for } \alpha_I \geq 1. \end{cases}$$

We observe that in Case B, the required side-channel bandwidth to achieve the no-interference sum GDoF is not affected by the number of antennas in the system but received interference signal strength and side-channel signal strength levels. For $\alpha_I < 1$, lower interference level requires less side-channel bandwidth while for $\alpha_I \geq 1$, higher interference level leads to smaller side-channel bandwidth requirement.

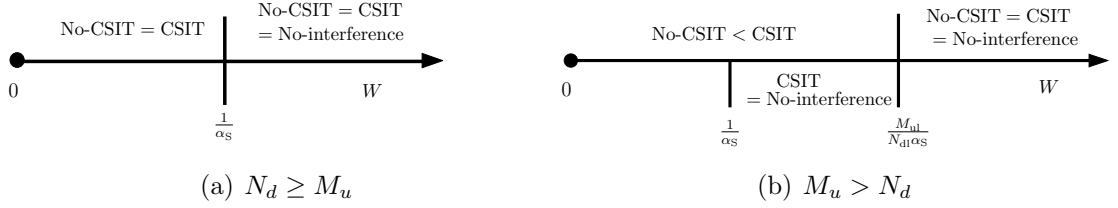


Figure 3.9: Comparison of the three systems in DoF as a function of the side-channel bandwidth when $\alpha_I = 1$.

In Case B, we can also derive the required bandwidth ratio under the no-CSIT assumption from Corollary 3, to achieve the no-interference performance. The required bandwidth ratio without CSIT in Case B for $\alpha_I = 1$ is given by

$$W_{\text{No-CSIT}} = \begin{cases} \frac{1}{\alpha_S}, & \text{for } N_d \geq M_u, \\ \frac{M_u}{N_d \alpha_S}, & \text{for } M_u > N_d. \end{cases} \quad (3.22)$$

In Figs. 3.7 and 3.8, we show the spatial and spectral tradeoff in both Case A and Case B when $\alpha_I = 1$. We observe that when there are more downlink receive antennas than uplink transmit antennas, obtaining CSIT is unavailing since with and without CSIT require the same amount of side-channel bandwidth to completely eliminate interference. However, when we have more uplink transmit antennas, if we do not have CSIT, the extra spatial degrees-of-freedom are wasted and we need more side-channel bandwidth to achieve the no-interference performance.

In Figure 3.9, we give an illustration of the comparisons of the three systems in DoF as a function of the side-channel bandwidth when there is an excess of BS antennas.

3.4 Diversity and Multiplexing Tradeoff

In this section, we consider a slow-fading scenario. When the channel experiences slow fading, an important metric to characterize the MIMO system performance is the

diversity and multiplexing tradeoff (DMT), which delineates the asymptotic tradeoff between data rate and reliability in the high SNR limit. The optimal DMT, first introduced in MIMO point-to-point channels [41], represents the optimal diversity gain $d^*(r)$ for each multiplexing gain r among all possible schemes. Similar to our definition of GDoF, we define the multiplexing gain of both downlink and uplink channel in our system as follows

$$r_i = \lim_{\rho \rightarrow \infty} \frac{R_i(\rho_i)}{W_m \log \rho}, \quad i \in \{\text{d}, \text{ul}\}, \quad (3.23)$$

where R_d and R_u are the achievable rates (bit/s) of downlink and uplink, respectively.

Assuming the overall average error probability is $P_e(r_d, r_u)$, the DMT is

$$d(r_d, r_u) = \lim_{\rho \rightarrow \infty} \frac{-\log P_e(r_d, r_u)}{\log \rho}. \quad (3.24)$$

We define $d^{\text{opt}}(r_d, r_u)$ as the supremum of $d(r_d, r_u)$ computed over all possible schemes. Thus $d^{\text{opt}}(r_d, r_u)$ is the optimal DMT of the system.

In this section, we will study the DMT performance under different assumptions regarding the availability of CSIT. We assume that the channel knowledge is known at the receivers. In the following, we will first obtain the optimal DMT with CSIT which can be achieved by vector bin-and-cancel as described in Section 3.3. Next, we study the case without CSIT and derive the corresponding achievable DMT. Finally, based on the DMT result, we will investigate the spatial and spectral tradeoff as well as the interplay between CSIT and side-channel.

3.4.1 With CSIT case

In a slow fading scenario, the channel matrices remain fixed over a fade period with a short-term power constraint given in (3.4), thus the capacity region in time-invariant

channels can serve as instantaneous capacity region in each fade period. We define the outage event as the target rate pair not contained in the instantaneous capacity region: $\mathfrak{B} \triangleq \{(R_d, R_u) \notin \mathcal{C}(\mathcal{H})\}$, where $\mathcal{C}(\mathcal{H})$ is given in Corollary 1. From [41], it can be easily shown that $P_e^*(r_d, r_u) \doteq \Pr(\mathfrak{B})$, where $P_e^*(r_d, r_u)$ is the infimum of the overall average error probability among all possible schemes. In the high SNR limit, we can obtain that

$$\Pr(\mathfrak{B}) \doteq \max_{i \in \{d, u, \text{sum}\}} \Pr(C_i < R_i), \implies \rho^{-d^*(r_d, r_u)} \doteq \max_{i \in \{d, u, \text{sum}\}} \Pr(C_i < R_i),$$

where C_i is given in (3.13) and $R_{\text{sum}} = R_d + R_u$. Thus the optimal diversity order is

$$d^*(r_d, r_u) = \min_{i \in \{d, u, \text{sum}\}} d_{\mathfrak{B}_i}(r_i), \quad \text{where } d_{\mathfrak{B}_i}(r_i) = \lim_{\rho \rightarrow \infty} -\frac{\log \Pr(C_i < W_m r_i \log \rho)}{\log \rho}, \quad (3.25)$$

In Section 3.3, we showed that vector bin-and-cancel achieves the asymptotic capacity region. Hence in the asymptotic DMT characterization, the optimal DMT with CSIT can be achieved by vector bin-and-cancel which only requires CSIT of the interference channel between the up- and downlink nodes since the uplink message splitting depends on the interference channel. The derivation of the optimal DMT curve of side-channel assisted MIMO full-duplex network follows from two steps. In [41], we know that the optimal DMT for MIMO point-to-point channel is $d_{M,N}(r) = (M - r)(N - r)$, which is a piecewise linear curve joining the integer point $r \in [0, \min(M, N)]$. For a general channel level $\alpha_i, i \in \{d, u\}$ of a point-to-point channel, we will invoke Lemma 6 in [29] (see Appendix C) for our calculation. Hence we first obtain the optimal diversity order of each individual downlink and uplink given as

$$d_{\mathfrak{B}_i}(r_i) = \alpha_i d_{M_i, N_i} \left(\frac{r_i}{\alpha_i} \right), \quad \forall r_i \in [0, \min\{M_i, N_i\} \alpha_i], i \in \{d, u\}. \quad (3.26)$$

Next, we evaluate $d_{\mathfrak{B}_{\text{sum}}}(r_{\text{sum}})$ in the following lemma.

Lemma 3. *The diversity order with CSIT given the sum multiplexing gain of both uplink and downlink is the minimum of the following objective function:*

$$\begin{aligned}
d_{\mathfrak{B}_{\text{sum}}}(r_{\text{sum}}) &= \min_{\bar{\mu}, \bar{\sigma}, \bar{\theta}, \bar{\nu}} \sum_{i=1}^{m_d} (M_d + N_d + 1 - 2i)\mu_i + \sum_{j=1}^{m_u} (M_u + N_u + 1 - 2j)\sigma_j - (M_d + N_u)m_{\text{I}}\alpha_{\text{I}} \\
&\quad + \sum_{k=1}^{m_{\text{I}}} (M_d + N_u + M_u + N_d + 1 - 2k)\theta_k + \sum_{l=1}^{m_{\text{I}}} (M_u + N_d + 1 - 2l)\nu_l \\
&\quad + \sum_{i=1}^{m_d} \sum_{k=1}^{\min\{N_d-i, M_u\}} (\alpha_{\text{I}} - \mu_i - \theta_k)^+ + \sum_{j=1}^{m_u} \sum_{k=1}^{\min\{M_u-j, N_d\}} (\alpha_{\text{I}} - \sigma_j - \theta_k)^+; \\
\text{Subject to } &\sum_{i=1}^{m_d} (\alpha_1 - \mu_i)^+ + \sum_{j=1}^{m_u} (\alpha_2 - \sigma_j)^+ + \sum_{k=1}^{m_{\text{I}}} (\alpha_{\text{I}} - \theta_k)^+ + W \sum_{l=1}^{m_{\text{I}}} (\alpha_{\text{S}} - \nu_l)^+ < r_{\text{sum}}; \\
&0 \leq \mu_1 \leq \dots \leq \mu_{m_d}; \quad 0 \leq \sigma_1 \leq \dots \leq \sigma_{m_u}; \quad 0 \leq \theta_1 \leq \dots \leq \theta_{m_{\text{I}}}; \quad 0 \leq \nu_1 \leq \dots \leq \nu_{m_{\text{I}}}; \\
&\mu_i + \theta_k \geq \alpha_{\text{I}}, \quad \forall (i+k) \geq N_d + 1; \\
&\sigma_j + \theta_k \geq \alpha_{\text{I}}, \quad \forall (j+k) \geq M_u + 1,
\end{aligned} \tag{3.27}$$

where $\bar{\mu} = \{\mu_1, \dots, \mu_{m_d}\}$, $\bar{\sigma} = \{\sigma_1, \dots, \sigma_{m_u}\}$, $\bar{\theta} = \{\theta_1, \dots, \theta_{m_{\text{I}}}\}$, $\bar{\nu} = \{\nu_1, \dots, \nu_{m_{\text{I}}}\}$ and m_d , m_u and m_{I} are defined in (3.8).

Proof. We provide the proof in Appendix D in [29]. \square

With $d_{\mathfrak{B}_i}$ for $i \in \{d, u, \text{sum}\}$ derived above, we have the following theorem which gives the optimal DMT in its most general form, allowing different channel parameters and multiplexing gains for uplink and downlink with arbitrary number of antennas at each node.

Theorem 4. *The optimal DMT of (M_d, N_d, M_u, N_u) side-channel assisted MIMO*

full-duplex network with CSIT denoted as $d^{CSIT,opt}$ is given by

$$d_{(M_d, N_d, M_u, N_u)}^{CSIT,opt}(r_d, r_u) = \min_{i \in \{d, u, \text{sum}\}} d_{\mathfrak{B}_i}(r_i),$$

where $d_{\mathfrak{B}_i}(r_i)$ is given in (3.26) and Lemma 3.

The optimization problem in Lemma 3 is a convex optimization problem [42] with linear constraints, which can be solved using linear programming. The general form of the optimal DMT with CSIT in Theorem 4, though can be calculated using numerical methods, does not result in a closed-form solution. In the following corollary, a closed-form DMT result is derived in the case of single-antenna mobiles communicating with multiple-antenna BS with M transmit and receive antennas, i.e., $M_d = N_u = M$.

Corollary 6. *In the case of $(M, 1, 1, M)$ with symmetric DMT $r_u = r_d = r$ when $\alpha_d = \alpha_u = \alpha_1 = 1$. The closed-form optimal DMT with CSIT is given which completely characterizes the optimal DMT under all side-channel conditions:*

- when $W \leq \frac{1}{2M+1}$ and $W\alpha_S < 1$,

$$d_{(M,1,1,M)}^{CSIT,opt}(r) = \begin{cases} M(1-r), & 0 \leq r \leq \frac{M+1+(2M+1)W\alpha_S}{3M+2} \\ (2M+1)(1+W\alpha_S) - (4M+2)r, & \frac{M+1+(2M+1)W\alpha_S}{3M+2} \leq r \leq \frac{1+W\alpha_S}{2} \end{cases} \quad (3.28)$$

- when $\frac{1}{2M+1} \leq W < \frac{2}{M}$, $\alpha_S \geq \frac{M}{2}$, and $W\alpha_S < 1$,

$$d_{(M,1,1,M)}^{CSIT,opt}(r) = \begin{cases} M(1-r), & 0 \leq r \leq \beta^* \\ \alpha_S + \frac{1}{W}(1-2r), & \beta^* \leq r \leq \frac{1+W\alpha_S}{2} \end{cases} \quad (3.29)$$

- when $W \geq \frac{1}{2M+1}$, $\alpha_S < \frac{M}{2}$, and $W\alpha_S < 1$,

$$d_{(M,1,1,M)}^{CSIT,opt}(r) = \begin{cases} M(1-r), & 0 \leq r \leq \frac{M+1+\alpha_S}{3M+2} \\ 2M+1+\alpha_S - (4M+2)r, & \frac{M+1+\alpha_S}{3M+2} \leq r \leq \frac{1}{2} \\ \alpha_S + \frac{1}{W}(1-2r), & \frac{1}{2} \leq r \leq \frac{1+W\alpha_S}{2} \end{cases} \quad (3.30)$$

- when $W \geq \frac{1}{2M+1}$, $\alpha_S < \frac{M}{2}$, and $W\alpha_S \geq 1$,

$$d_{(M,1,1,M)}^{CSIT,opt}(r) = \begin{cases} M(1-r), & 0 \leq r \leq \frac{M+1+\alpha_S}{3M+2} \\ 2M+1+\alpha_S - (4M+2)r, & \frac{M+1+\alpha_S}{3M+2} \leq r \leq \frac{1}{2} \\ \alpha_S + \frac{1}{W}(1-2r), & \frac{1}{2} \leq r \leq \beta^* \\ M(1-r), & \beta^* \leq r \leq 1 \end{cases} \quad (3.31)$$

- when $\alpha_S \geq \frac{M}{2}$ and $W\alpha_S \geq 1$,

$$d_{(M,1,1,M)}^{CSIT,opt}(r) = M(1-r), 0 \leq r \leq 1 \quad (3.32)$$

$$\text{where } \beta^* = \frac{\alpha_S + \frac{1}{W} - M}{\frac{2}{W} - M}.$$

Proof. The DMT of the point-to-point channel is $M(1-r)$, $\forall r \in [0, 1]$. Thus we only need to solve for the optimization problem given sum multiplexing gain. One way to find the minimum of the optimization problem in Lemma 3 is to apply the Karush-Kuhn-Tucker condition. Here we will provide another approach which is the key to the proof of a general case. The method we adopt is gradient descent which finds the local optimum. Since the optimization problem we have is convex with linear constraints, the local optimum is actually the global optimum in convex optimization [42]. Hence we can obtain the global optimum via gradient descent algorithm.

We first simplify the objective function of the diversity order in Lemma 3 given

sum multiplexing gain. By substituting $\nu'_i = W\nu_i$ in (3.27), we can express the objective function as

$$d_{\text{sum}}^{\text{CSIT}} = \min M\mu_1 + M\sigma_1 + (2M+1)\theta_1 + \frac{\nu'_1}{W} - 2M,$$

$$\text{Subject to } (1 - \mu_1)^+ + (1 - \sigma_1)^+ + (1 - \theta_1)^+ + (W\alpha_S - \nu'_1)^+ < r_{\text{sum}};$$

$$\mu_1, \sigma_1, \theta_1, \nu'_1 \geq 0;$$

$$\mu_1 + \theta_1 \geq 1; \sigma_1 + \theta_1 \geq 1.$$
(3.33)

Next, we differentiate the objective function in (3.33) with respect to different variables

$$\frac{\partial d_{\text{sum}}^{\text{CSIT}}}{\partial \nu'_1} = \frac{1}{W};$$
(3.34)

$$\frac{\partial d_{\text{sum}}^{\text{CSIT}}}{\partial \theta_1} = 2M + 1;$$
(3.35)

$$\frac{\partial d_{\text{sum}}^{\text{CSIT}}}{\partial \mu_1} = \frac{\partial d_{\text{sum}}^{\text{CSIT}}}{\partial \sigma_1} = M < \frac{\partial d_{\text{sum}}^{\text{CSIT}}}{\partial \theta_1}.$$
(3.36)

Comparing the gradient of each variable, when $W \leq \frac{1}{2M+1}$, the steepest descent of the objective function is along the decreasing value of ν'_1 with $\theta_1 = \mu_1 = \sigma_1 = 1$, for $r_{\text{sum}} \leq W\alpha_S$. Thus we have $d_{\text{sum}}^{\text{CSIT}}(r) = 2M + 1 + \alpha_S - \frac{r_{\text{sum}}}{W}, \forall r_{\text{sum}} \in [0, W\alpha_S]$. This also implies that for $r_{\text{sum}} \geq W\alpha_S$, $\nu'_1 = 0$ in the optimal solution. Now the steepest descent of the objective function in (3.33) is along the decreasing value of θ_1 with $\mu_1 = \sigma_1 = 1$, and the corresponding minimum is $d_{\text{sum}}^{\text{CSIT}}(r_{\text{sum}}) = (2M+1)(1+W\alpha_S) - (2M+1)r_{\text{sum}}, \forall r_{\text{sum}} \in [W\alpha_S, 1+W\alpha_S]$.

When $W \geq \frac{1}{2M+1}$, the steepest descent of the objective function is along the decreasing value of θ_1 with $\mu_1 = \sigma_1 = 1, \nu'_1 = W\alpha_S$, for $r_{\text{sum}} \leq 1$. Thus we have $d_{\text{sum}}^{\text{CSIT}}(r_{\text{sum}}) = 2M + 1 + \alpha_S - (2M+1)r_{\text{sum}}, \forall r_{\text{sum}} \in [0, 1]$. Again, for $r_{\text{sum}} \geq 1$, the

optimal solution has $\theta_1 = 0$. We will rewrite the objective function as

$$\begin{aligned}
d_{\text{sum}}^{\text{CSIT}} &= \min M\mu_1 + M\sigma_1 + \frac{\nu'_1}{W} - 2M, \\
\text{Subject to } & (1 - \mu_1)^+ + (1 - \sigma_1)^+ + (W\alpha_S - \nu'_1)^+ \leq r_{\text{sum}} - 1; \\
& \mu_1, \sigma_1, \nu'_1 \geq 0; \\
& \mu_1 \geq 1; \sigma_1 \geq 1.
\end{aligned} \tag{3.37}$$

To minimize the objective function above, we should let $\mu_1 = \sigma_1 = 1$. Hence the minimum of the objective function is $d_{\text{sum}}^{\text{CSIT}}(r_{\text{sum}}) = \alpha_S + \frac{1}{W}(1 - r_{\text{sum}})$, $\forall r_{\text{sum}} \in [1, 1 + W\alpha_S]$. Now combining all the results above, we have

$$d_{(M,1,1,M)}^{\text{CSIT,opt}}(r) = \min\{M(1 - r), d_{\text{sum}(M,1,1,M)}^{\text{CSIT}}(r)\} \text{ for } 0 \leq r \leq 1. \tag{3.38}$$

where $d_{\text{sum}(M,1,1,M)}^{\text{CSIT}}(r)$ is given as

- when $W \leq \frac{1}{2M+1}$

$$d_{\text{sum}(M,1,1,M)}^{\text{CSIT}}(r) = \begin{cases} 2M + 1 + \alpha_S - \frac{2r}{W}, & 0 \leq r \leq \frac{W\alpha_S}{2} \\ (2M + 1)(1 + W\alpha_S) - (4M + 2)r, & \frac{W\alpha_S}{2} \leq r \leq \frac{1+W\alpha_S}{2} \end{cases} \tag{3.39}$$

- when $W \geq \frac{1}{2M+1}$

$$d_{\text{sum}(M,1,1,M)}^{\text{CSIT}}(r) = \begin{cases} 2M + 1 + \alpha_S - (4M + 2)r, & 0 \leq r \leq \frac{1}{2} \\ \alpha_S + \frac{1}{W}(1 - 2r), & \frac{1}{2} \leq r \leq \frac{1+W\alpha_S}{2} \end{cases} \tag{3.40}$$

Further simplification of (3.38) will lead to the analytical expression in Corollary 6.

□

Remark 3. *The optimal DMT with CSIT in the no side-channel case is a special case of Corollary 6 when $W = 0$, and is given as*

$$d_{(M,1,1,M)}^{\text{No-SC,CSIT,opt}}(r) = \begin{cases} M(1-r), & 0 \leq r \leq \frac{M+1}{3M+2} \\ (2M+1)(1-2r), & \frac{M+1}{3M+2} \leq r \leq \frac{1}{2} \end{cases} \quad (3.41)$$

From Corollary 6, we can completely quantify the improvement of DMT with side-channel under all side-channel conditions. Figure 3.10 depicts the comparison of DMT with/without (w/wo) side-channel when $W = \frac{1}{2M+1}$, $\alpha_S = \frac{M}{2}$. We define the light loading threshold as the multiplexing gain threshold within which the system error event is dominated by single-user performance. In the case with CSIT, the light loading threshold of the system without side-channel is B shown in Figure 3.10. When $r > B$, the dominant error event is that all users are in error. With the help of side-channel, the light loading threshold is increased by Δ_1 , where $\Delta_1 = \frac{(2M+1)W\alpha_S}{3M+2}$. Moreover, we can see that the side-channel also improves system maximum multiplexing gain (when the diversity order is zero) by Δ_3 , where $\Delta_3 = \frac{W\alpha_S}{2}$. Both improvement amount Δ_1 and Δ_3 will scale with side-channel quality $W\alpha_S$ (for $W \leq \frac{1}{2M+1}$) till either point C or D reaches the symmetric maximum multiplexing gain of one which corresponds to the no-interference point.

When $W = \frac{1}{2M+1}$, $\alpha_S = \frac{M}{2}$, we have $\Delta_1 = \frac{M}{6M+4}$ and $\Delta_3 = \frac{M}{8M+4}$. We conclude that in this case, both improvement amount Δ_1 and Δ_3 will scale with the number of antennas at the BS. In the limit of M (as in massive MIMO, BS has unlimited number of antennas), we will have improvement of $\lim_{M \rightarrow \infty} \Delta_1 = \frac{1}{6}$ and $\lim_{M \rightarrow \infty} \Delta_3 = \frac{1}{8}$.

3.4.2 Without CSIT case

We define the outage event \mathbf{O} in the case without CSIT as the target rate pair does not lie in the achievable rate region $\mathcal{R}^{\text{No-CSIT}}$: $\mathbf{O} \triangleq \{(R_d, R_u) \notin \mathcal{R}\}$, where \mathcal{R} is given

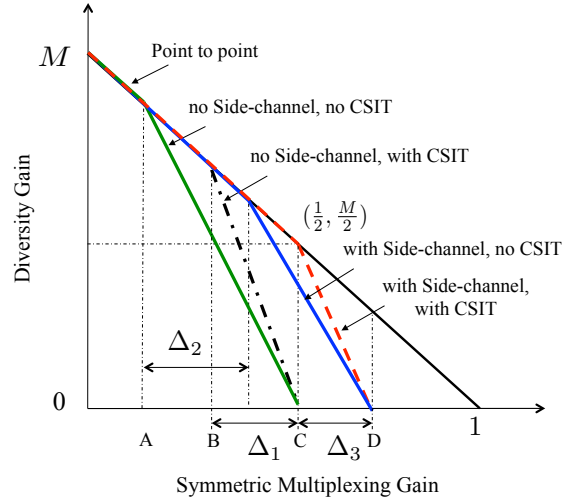


Figure 3.10: DMT comparison w/wo side-channel w/wo CSIT when $W = \frac{1}{2M+1}$, $\alpha_S = \frac{M}{2}$.

(with $\lambda = \bar{\lambda} = 0.5$)

$$\mathcal{R} = \left\{ (R_d, R_u) : R_d \leq W_m \log \left| I_{N_d} + \frac{\rho_d}{M_d} H_d H_d^\dagger \right| ; R_u \leq W_m \log \left| I_{N_u} + \frac{\bar{\lambda} \rho_u}{M_u} H_u H_u^\dagger \right| ; \right. \\ \left. R_d + R_u \leq W_m \left(\log \left| I_{N_d} + \frac{\rho_d}{M_d} H_d H_d^\dagger + \frac{\bar{\lambda} \rho_u}{M_u} H_u H_u^\dagger \right| + W \log \left| I_{N_d} + \frac{\lambda \rho_S}{W M_u} H_S H_S^\dagger \right| \right) \right\}, \quad (3.42)$$

The difference between (3.42) and the achievable rate region in (3.18) is that (3.42) does not have a constraint on R_u for the transmission from up- to downlink mobile. This is because the downlink mobile is not interested in the uplink's message, thereby the failure of decoding uplink's message alone will not be declared as an error event at the downlink receiver.

Under the no-CSIT assumption, the diversity order of each MIMO downlink/uplink channel is still the same as given in (3.26). As for the diversity order for a given sum multiplexing gain, it is characterized by the following lemma.

Lemma 4. *The diversity order at a given sum multiplexing gain in the case without*

CSIT is the minimum of the following objective function:

$$\begin{aligned}
d_{o_{\text{sum}}}(r_{\text{sum}}) &= \min_{\bar{\mu}, \bar{\theta}, \bar{\nu}} \sum_{i=1}^{m_d} (M_d + N_d + 1 - 2i)\mu_i + \sum_{k=1}^{m_I} (M_u + N_d + M_d + 1 - 2k)\theta_k \\
&\quad + \sum_{l=1}^{m_I} (M_u + N_d + 1 - 2l)\nu_l - M_d m_I \alpha_I + \sum_{i=1}^{m_d} \sum_{k=1}^{\min\{N_d-i, M_u\}} (\alpha_I - \mu_i - \theta_k)^+ \\
\text{Subject to} \quad &\sum_{i=1}^{m_d} (\alpha_d - \mu_i)^+ + \sum_{k=1}^{m_I} (\alpha_I - \theta_k)^+ + W \sum_{l=1}^{m_I} (\alpha_S - \nu_l)^+ < r_{\text{sum}}; \\
&0 \leq \mu_1 \leq \dots \leq \mu_{m_d}; \quad 0 \leq \theta_1 \leq \dots \leq \theta_{m_I}; \quad 0 \leq \nu_1 \leq \dots \leq \nu_{m_I}; \\
&\mu_i + \theta_k \geq \alpha_I, \quad \forall (i+k) \geq N_d + 1;
\end{aligned} \tag{3.43}$$

Proof. The proof is proved in the Appendix E in [29]. \square

Theorem 5. *A lower bound of the DMT of (M_d, N_d, M_u, N_u) side-channel assisted MIMO full-duplex network without CSIT is given as*

$$d_{(M_d, N_d, M_u, N_u)}^{\text{No-CSIT}}(r_d, r_u) = \min_{i \in \{d, u, \text{sum}\}} d_{o_i}(r_i).$$

where $d_{o_i}(r_i)$ is given in (3.26) and Lemma 4.

In line with the analysis in Section 3.4.1, we also give the closed-form no-CSIT DMT in the case of single-antenna mobiles communicating with multiple-antenna BS.

Corollary 7. *In the case of $(M, 1, 1, M)$ with symmetric DMT $r_u = r_d = r$ when $\alpha_d = \alpha_u = \alpha_I = 1$. The closed-form lower bound of the DMT without CSIT is given that completely characterizes the achievable DMT under all side-channel conditions:*

- when $W \leq \frac{1}{M+1}$ and $W\alpha_S < 1$,

$$d_{(M,1,1,M)}^{No-CSIT}(r) = \begin{cases} M(1-r), & 0 \leq r \leq \frac{1+(M+1)W\alpha_S}{M+2} \\ (M+1)(1+W\alpha_S) - (2M+2)r, & \frac{1+(M+1)W\alpha_S}{M+2} \leq r \leq \frac{1+W\alpha_S}{2} \end{cases} \quad (3.44)$$

- when $\frac{1}{M+1} \leq W < \frac{2}{M}$, $\alpha_S \geq \frac{M}{2}$, and $W\alpha_S < 1$,

$$d_{\text{sum}(M,1,1,M)}^{No-CSIT}(r) = \begin{cases} M(1-r), & 0 \leq r \leq \beta^* \\ \alpha_S + \frac{1}{W}(1-2r), & \beta^* \leq r \leq \frac{1+W\alpha_S}{2} \end{cases} \quad (3.45)$$

- when $W \geq \frac{1}{M+1}$, $\alpha_S < \frac{M}{2}$, and $W\alpha_S < 1$,

$$d_{\text{sum}(M,1,1,M)}^{No-CSIT}(r) = \begin{cases} M(1-r), & 0 \leq r \leq \frac{1+\alpha_S}{M+2} \\ M+1+\alpha_S - (2M+2)r, & \frac{1+\alpha_S}{M+2} \leq r \leq \frac{1}{2} \\ \alpha_S + \frac{1}{W}(1-2r), & \frac{1}{2} \leq r \leq \frac{1+W\alpha_S}{2} \end{cases} \quad (3.46)$$

- when $W \geq \frac{1}{M+1}$, $\alpha_S < \frac{M}{2}$, and $W\alpha_S \geq 1$,

$$d_{\text{sum}(M,1,1,M)}^{No-CSIT}(r) = \begin{cases} M(1-r), & 0 \leq r \leq \frac{1+\alpha_S}{M+2} \\ M+1+\alpha_S - (2M+2)r, & \frac{1+\alpha_S}{M+2} \leq r \leq \frac{1}{2} \\ \alpha_S + \frac{1}{W}(1-2r), & \frac{1}{2} \leq r \leq \beta^* \\ M(1-r), & \beta^* \leq r \leq 1 \end{cases} \quad (3.47)$$

- when $\alpha_S \geq \frac{M}{2}$ and $W\alpha_S \geq 1$,

$$d_{\text{sum}(M,1,1,M)}^{No-CSIT}(r) = M(1-r), 0 \leq r \leq 1 \quad (3.48)$$

where $\beta^* = \frac{\alpha_S + \frac{1}{W} - M}{\frac{2}{W} - M}$.

Proof. The proof is similar to that in Corollary 6 which uses gradient descent method. \square

Remark 4. *The lower bound of the DMT without CSIT in the no side-channel case is a special case of Corollary 7 when $W = 0$, and is given by*

$$d_{(M,1,1,M)}^{No-SC,No-CSIT}(r) = \begin{cases} M(1-r), & 0 \leq r \leq \frac{1}{M+2} \\ (M+1)(1-2r), & \frac{1}{M+2} \leq r \leq \frac{1}{2} \end{cases} \quad (3.49)$$

Remark 3 and Remark 4 describe the DMT without side-channel under CSIT and no-CSIT assumptions. One can easily verify that the no-side-channel cases in [43] and [44] w/wo CSIT are special cases incorporated in our derivation of DMT.

Now we compare the lower bound of the DMT w/wo side-channel under the no-CSIT assumption. When $W \leq \frac{1}{M+1}$, in the case without CSIT, with the help of side-channel, the light loading threshold over the no-side-channel system is increased by Δ_2 , where $\Delta_2 = \frac{(M+1)W\alpha_S}{M+2}$. In Figure 3.10, the DMT without CSIT w/wo side-channel is given when $W = \frac{1}{2M+1}$ and $\alpha_S = \frac{M}{2}$. Compared with the light loading improvement under the CSIT assumption, we can see that the side-channel is more effective in increasing the DMT performance in the lack of CSIT as $\Delta_2 \geq \Delta_1$.

3.4.3 Spatial and spectral tradeoff in DMT

In this section, we will derive symmetric DMT in closed form for a more general case where the mobiles have multiple antennas communicating with the BS with M transmit and receive antennas. Using the closed-form DMT expressions, again we will compare the three systems: with and without CSIT and the no-interference idealized full-duplex network. We will characterize the relationship between the spatial degrees

of freedom of the antenna resources and the extra spectral degrees of freedom due to the side-channels under slow-fading channels.

We still assume BS has more antennas i.e., $M \geq M_u, N_d$. The closed-form symmetric DMT of the general (M, N_d, M_u, M) system with $\alpha_d = \alpha_u = \alpha_I = 1$ and $r_d = r_u = r$ are given under CSIT and no-CSIT assumptions in Lemma 9 and Lemma 10 in [29] (see Appendix F), respectively.

First we ask the question that how much side-channel bandwidth is required to compensate for the lack of CSIT such that the DMT of the system without CSIT achieves that of the system with CSIT. The sufficient condition is given in the following theorem.

Theorem 6. *In case of (M, N_d, M_u, M) , sufficient conditions such that no CSIT DMT is same as full CSIT DMT are given by*

1. $W = \min \left\{ \frac{N_d + M_u - 1}{M + N_d - M_u + 1}, \frac{1}{\alpha_S} \left(2 - \frac{N_d}{M_u} \right)^+ \right\}$ where $\alpha_S \geq \frac{d_{M, M_u} \left(\frac{M_u}{2} \right) - M(N_d - M_u)}{M_u N_d}$, when $N_d \geq M_u, M_u = 1, 2$;
2. $W = 0$, when $N_d \geq \frac{d_{M_u, M} \left(\frac{M_u}{2} \right)}{M} + M_u, M_u = 1, 2$.

Proof. With the conditions given above, we can verify that the symmetric DMT with CSIT in Lemma 9 in [29] is the same as the DMT without CSIT in Lemma 10 in [29]. □

Corollary 8. *When $M_u > N_d$, if $W < \frac{1}{\alpha_S}$, the DMT without CSIT is strictly smaller than that with CSIT.*

Corollary 8 can be readily obtained by comparing Lemma 9 and Lemma 10 in [29]. If $M_u > N_d$ and $W < \frac{1}{\alpha_S}$, the availability of CSIT is crucial in performing transmit beamforming to yield higher DMT.

The next question we will ask is how much side-channel bandwidth is required to eliminate the effect of interference such that the DMT of the system w/wo CSIT achieves that of a system without interference. The following theorem characterizes the effect of the side-channel bandwidth on the performance of the symmetric DMT to reach no-interference DMT.

Theorem 7. *In case of (M, N_d, M_u, M) , the sufficient conditions are given under CSIT and no-CSIT assumptions, respectively, where the effect of interference can be completely eliminated to achieve the optimal no-interference DMT:*

$$1. W_{CSIT} = \frac{1}{\alpha_S} \left(2 - \frac{m_X}{m_I}\right)^+, \quad \alpha_S \geq \frac{(2m_I - m_X)(M - m_I + 1)}{m_I(2|N_d - M_u| + 2)};$$

$$2. W_{No-CSIT} = \begin{cases} \frac{1}{\alpha_S}, & \alpha_S \geq \frac{M - N_d + 1}{2(M_u - N_d + 1)}, \text{ when } M_u \geq N_d \\ \frac{1}{\alpha_S} \left(2 - \frac{m_X}{m_I}\right)^+, & \alpha_S \geq \frac{(2m_I - m_X)(M - m_I + 1)}{m_I(2|N_d - M_u| + 2)}, \text{ when } N_d \geq M_u \end{cases}$$

where $m_X = \max(M_u, N_d)$, $m_I = \min(M_u, N_d)$.

Proof. We need to show that with the conditions above, the DMT of our system w/wo CSIT is not dominated by the diversity order given sum multiplexing gain $d_{\text{sum}(M, N_d, M_u, M)}^{\text{w/wo CSIT}}(r_{\text{sum}})$, $\forall r \in [0, m_I]$. It is sufficient if we show that the conditions above indicate that the decay slope of $d_{\text{sum}(M, N_d, M_u, M)}^{\text{w/wo CSIT}}(r_{\text{sum}})$ is larger than that of the PTP channel $d_{M, m_I}(r) \forall r$, and the maximum symmetric multiplexing gain of $d_{\text{sum}(M, N_d, M_u, M)}^{\text{w/wo CSIT}}(r_{\text{sum}})$ is larger than m_I .

The decay slope of the piecewise linear function $d_{M, N}^k(r)$ is $(M + N - 2k + 1)$ in each interval $r \in [k - 1, k]$, where $k \in [1, \min(M, N)]$ is an integer. Thus the decay slope of $d_{M, N}^k(r)$ decreases as the interval k increases. Also, the decay slope difference between $d_{M, N}^{k-1}(r)$ and $d_{M, N}^k(r)$ is a constant of 2. We know that the DMT performance will be improved as side-channel bandwidth ratio W increases. Therefore with W large enough, $d_{\text{sum}(M, N_d, M_u, M)}^{\text{w/wo CSIT}}(r_{\text{sum}})$ will lastly be dominated by side-channel condition in

the last admissible interval. With the special structure of the decay slope, in order to find the conditions where DMT w/o achieves PTP performance, it suffices to show: (A) the decay slope of side-channel given sum multiplexing gain is larger than $d_{M,m_I}(r)$ in their last admissible intervals, respectively; (B) $\max(r_{\text{sum}}) \geq 2m_I$.

Under the CSIT assumption, from Corollary 3, we know the maximum sum multiplexing gain is $m_X + m_I W \alpha_S$. We set $m_X + m_I W \alpha_S = 2m_I$ to meet Condition (B) thus $W = \frac{1}{\alpha_S} \left(2 - \frac{m_X}{m_I}\right)^+$. Next to meet condition (A), the decay slope of the side-channel in the last interval $\alpha_S d_{M_u, N_d} \left(\frac{r_{\text{sum}} - m_X}{W \alpha_S}\right)$, $\forall r_{\text{sum}} \in [m_X, m_X + m_I W \alpha_S]$, i.e., $\frac{2}{W} (|M_u - N_d| + 1)$ should be larger than the decay slope of $d_{M,m_I}(r)$, $\forall r \in [0, m_I]$ in its last interval, i.e., $M - m_I + 1$. Hence $\frac{2}{W} (|M_u - N_d| + 1) \geq (M - m_I + 1)$. By substituting $W = \frac{1}{\alpha_S} \left(2 - \frac{m_X}{m_I}\right)^+$ into the inequality above, we have $\alpha_S \geq \frac{(2m_I - m_X)(M - m_I + 1)}{m_I(2|N_d - M_u| + 2)}$. With the side-channel condition derived above, the DMT with CSIT achieves the PTP DMT.

Under the no-CSIT assumption, when $N_d \geq M_u$, the results can be derived similarly. When $M_u > N_d$, the maximum multiplexing gain is $N_d(1 + W \alpha_S)$ according to Corollary 3. To satisfy condition II, we set $N_d(1 + W \alpha_S) = 2N_d$, hence we have $W = \frac{1}{\alpha_S}$. To meet Condition (A), the decay slope of the side-channel in the last interval $\alpha_S d_{M_u, N_d} \left(\frac{r_{\text{sum}} - N_d}{W \alpha_S}\right)$, $\forall r_{\text{sum}} \in [N_d, N_d(1 + W \alpha_S)]$, i.e., $\frac{2}{W} (M_u - N_d + 1)$, should be greater than the decay slope of $d_{M,N_d}(r)$ in its last interval, i.e., $(M - N_d + 1)$. By substituting $W = \frac{1}{\alpha_S}$, we obtain that $\alpha_S \geq \frac{M - N_d + 1}{2(M_u - N_d + 1)}$. \square

3.4.4 Discussion of the results

Figure 3.11 illustrates the comparison of the three systems in DMT as a function of the side-channel bandwidth. When $N_d \geq M_u$, there are three regimes in comparison of DMT. In the first regime, the performance the system without CSIT is worse than that with CSIT. In the second regime, with side-channel bandwidth ratio W greater

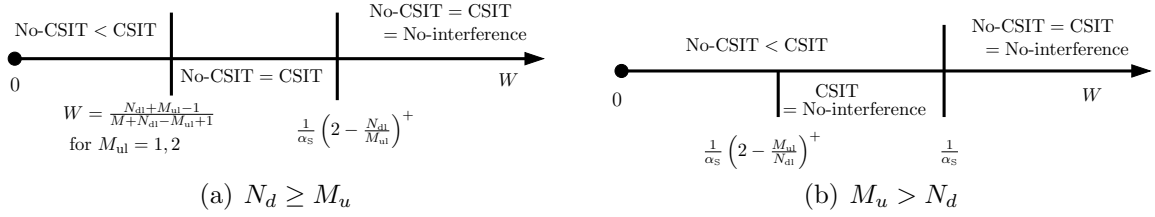


Figure 3.11: Comparison of the three systems in DMT as a function of the side-channel bandwidth.

than a threshold, CSIT is of no use. In the last regime, the use of side-channel helps reduce the probability of outage event where all users are in error such that the dominant error event is single-user error. On the other hand, when $M_u > N_d$, the availability of CSIT always provides an additional gain in performing transmit beamforming. However, larger side-channel bandwidth aids the no-CSIT system to achieve the no-interference upper bound. Note that the strength of the side-channel level α_s is implicitly incorporated in Theorems 6 and 7, thus is omitted in Figure 3.11.

In the following section, we will elaborate the findings in single-antenna mobiles and multiple-antenna mobiles cases, respectively.

3.4.4.1 Single-antenna mobiles

We first show the symmetric DMT w/wo side-channel and w/wo CSIT when $\alpha_d = \alpha_u = \alpha_I = 1$. From Figure 3.12, we can see that in the two-user uplink and downlink system, the full-duplex capable BS is always superior to its half-duplex (HD) counterpart where the BS adopts either time-division multiplexing (TDM) or frequency-division multiplexing (FDM) for uplink and downlink. In the special case of $W = 0$, i.e., no side-channel, having CSIT always yields a better DMT performance. However, with the help of side-channel, as shown in Figure 3.12, when $W = \frac{1}{M+1}$ and $\alpha_s \geq \frac{M}{2}$, there is no benefit to obtain CSIT as the DMT without CSIT already achieves the optimal DMT with CSIT. Such result indicates that as BS accommodates more antennas (tens or hundreds of BS antennas as in massive MIMO), the required side-channel

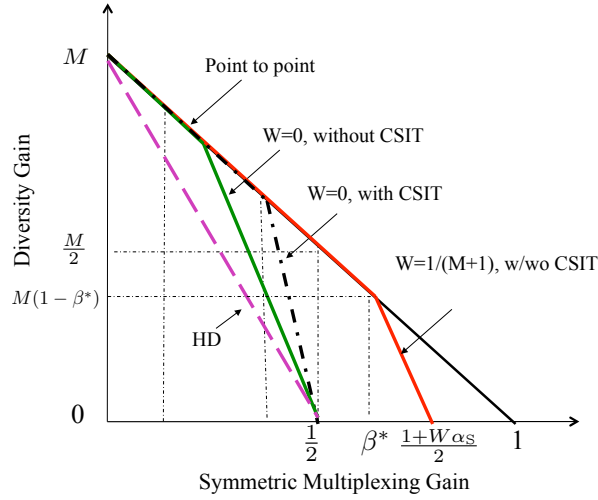


Figure 3.12: DMT of $(M, 1, 1, M)$ w/wo side-channel w/wo CSIT when $\alpha_S \geq \frac{M}{2}$, where $\beta^* = \frac{\alpha_S + \frac{1}{W} - M}{\frac{2}{W} - M}$.

bandwidth can be reduced superlinearly to combat interference.

Figure 3.13 illustrates the side-channel bandwidth ratio required to compensate for CSIT as stated in Theorem 6 with single-antenna mobiles. The required W is inversely proportional to the antenna resources at the BS. The caveat is that the side-channel level α_S , in the meantime, has to grow with increasing number of antennas at the BS.

To understand the result above, let us look at the different decay slopes in DMT in the network. From the downlink's viewpoint, the channel is MAC with side-channel. The decay slope of MAC without CSIT is $M + 1$, while the the decay slope of the side-channel is $\frac{1}{W}$. When the symmetric multiplexing gain $r \leq \frac{1}{2}$, if $W \geq \frac{1}{M+1}$, the users in MAC will first be in error followed by the users' error event in the side-channel. Moreover, if $\alpha_S \geq \frac{M}{2}$, the error event w/wo CSIT is dominated by single-user performance when $r \leq \frac{1}{2}$. And when $r \geq \frac{1}{2}$, the dominant error event is determined by the side-channel, which is the same for both CSIT and no-CSIT cases.*

*The DMT of MAC channel with CSIT is different from that without CSIT as shown in Figure 3.12.

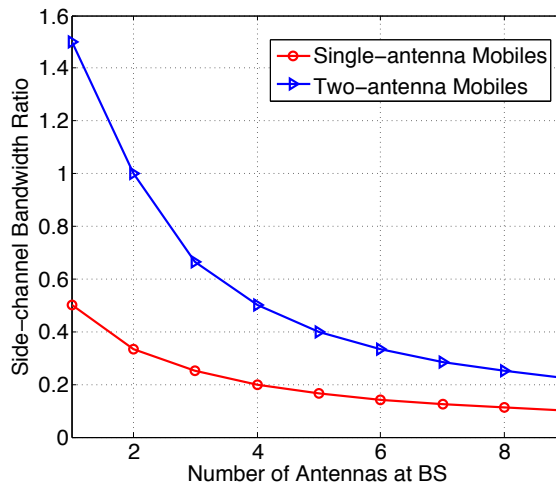


Figure 3.13: The required side-channel bandwidth ratio to compensate for CSIT as a function of the number of antennas at the BS with equal number of antennas at mobiles when $\alpha_S = \frac{M}{2}$.

In order to eliminate the effect of interference such that the DMT w/wo CSIT achieve no-interference upper bound, it is sufficient if the side-channel condition satisfies that $W\alpha_S \geq 1$ according to Theorem 7. Hence the required side-channel bandwidth is inversely proportional to the strength of the side-channel as to eliminate the effect of interference. The implication of such result is that in a highly clustered urban scenario, when the mobile devices are close to each other indicating higher side-channel strength, less side-channel bandwidth is required to achieve the single-user DMT performance.

3.4.4.2 Multiple-antenna mobiles

Figure 3.14 shows the DMT in the absence of the side-channel when both the mobiles have multiple antennas. First, we can find out that the gains due to the full-duplex capable BS over half-duplex BS is particularly larger for MIMO channels. Second, a larger number of downlink receive antennas alone can completely eliminate the effect of CSIT such that the DMT w/wo CSIT have the same performance as stated in Theorem 6. For example, the DMT of $(3, 3, 2, 3)$ without CSIT is the same as that

with CSIT. While in the case of $(3, 2, 3, 3)$, the lack of CSIT will result in significant loss.

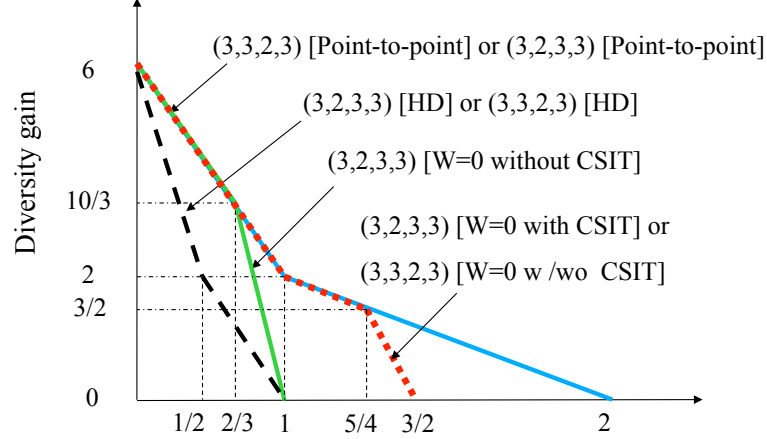


Figure 3.14: The symmetric DMT of MIMO full-duplex network without side-channel for $\alpha_d = \alpha_u = \alpha_I = 1$.

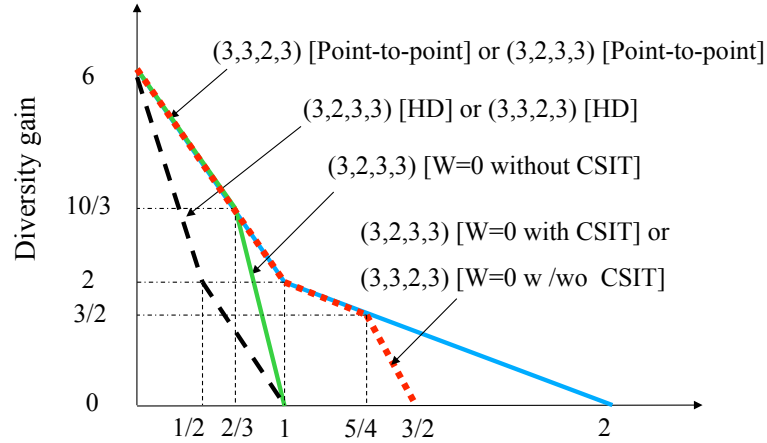


Figure 3.15: The symmetric DMT with side-channel for $\alpha_d = \alpha_u = \alpha_I = \alpha_S = 1$.

Comparing Figure 3.14 and Figure 3.15, we can quantify the gains due to the extra side-channel bandwidth, which is significant especially in MIMO. In the case of $(3, 2, 3, 3)$ when the system is lightly loaded, for instance, $r \leq 2/3$, there is no additional gain due to CSIT or $r \leq 5/4$, there is no gain due to the side-channel since the error event is dominated by single-user error. Beyond those points, the dominant error event is that all users are in error, thus leveraging the CSIT for

transmit beamforming or side-channel to perform vector bin-and-cancel will reduce the probability that such outage event happens.

The required side-channel bandwidth ratio for compensation of CSIT in the case of two-antenna mobiles is also depicted in Figure 3.13, which again demonstrates that the required $W \propto \frac{1}{M}$ similar as in the single-antenna-mobile case.

From Theorem 7, we conclude that with CSIT, as the antenna number ratio $\frac{\max\{M_u, N_d\}}{\min\{M_u, N_d\}}$ increases, the side-channel bandwidth required to completely eliminate the effect of interference reduces. Hence the spatial resources of the multiple antennas at mobiles is interchangeable with the spectral resources of the side-channel bandwidth to reduce the outage probability at a given multiplexing gain such that single-user DMT can be achieved.

We also infer from Theorem 7 that when $M_u > N_d$, the system with CSIT always outperforms that without CSIT by requiring less side-channel bandwidth to reach single-user performance.* However, when $N_d \geq M_u$, there is no advantage due to CSIT to achieve the single-user DMT since, with and without CSIT require the same amount of side-channel bandwidth to achieve interference-free performance. Thus we conclude that having more spatial degree-of-freedom at the interfered downlink receiver or larger side-channel bandwidth can simplify transceiver design by ruling out the necessity of obtaining CSIT to null out the effect of inter-mobile interference.

*The system with CSIT also has a weaker requirement of the side-channel strength level as compared to that without CSIT.

ARQ Design in Multi-User MIMO Full-Duplex System

4.1 Introduction

As we have already pointed out in the previous chapter, in a single-cell MU-MIMO full-duplex system where multiple uplink and downlink users can be supported by the multi-antenna full-duplex BS in the same time-frequency slot, the interference from uplink users to the downlink users can limit the system performance. In this chapter, from a cross-layer design perspective, we will study the side-channel protocol design in a ARQ-based MU-MIMO full-duplex system.

At the data link layer or MAC layer, ARQ is often used to improve the reliability of data transmission in addition to the coding schemes used at the PHY. With ARQ, incorrectly decoded packets sent through the PHY can be detected and a feedback message is sent back to the transmitter for retransmission. The joint PHY-MAC protocols studied in this chapter will enable an enhanced PHY scheme via side-channels to mitigate interference by exploiting the information offered by the MAC layer.

In this chapter, we propose two different side-channel assisted ARQ protocols

which use the side-channels at the PHY to manage interference in a single-cell MU-MIMO full-duplex network. One protocol is a proactive side-channel assisted ARQ protocol and the other one is a reactive side-channel assisted ARQ protocol. In the proactive protocol, the side-channels are used proactively irrespective of the downlink feedback but depending on the conventional uplink ARQ feedback. In contrast, in the reactive protocol, the use of side-channel is triggered by the conventional uplink ARQ feedback and our designed downlink ARQ feedback mechanisms which will be described in the following sections.

4.2 System Model

In a single-cell (M, K_u, K_d, W) side-channel assisted MU-MIMO full-duplex network, the full-duplex capability is available only at the BS, and there are K_u half-duplex uplink users (UE) and K_d half-duplex downlink users (UE). We denote $\mathcal{K}_u = \{1, \dots, K_u\}$, $\mathcal{K}_d = \{1, \dots, K_d\}$ as the sets of uplink and downlink UEs, respectively, with $|\mathcal{K}_u| = K_u$ and $|\mathcal{K}_d| = K_d$. We assume that $M \geq \max(K_u, K_d)$ such that the BS can use M antennas to serve all the single-antenna half-duplex uplink and downlink UEs in the same time-frequency slot. The uplink and downlink communication occur in main-channel (i.e., cellular band), there also exists an orthogonal band among users where users can communicate over such side-channels (i.e., unlicensed band). For simplicity, we assume that the main-channel has unit bandwidth while the side-channels have a total bandwidth of W . The channel model in our system considers both small-scale fading due to mobility and multi path, and large-scale fading due to path loss. We start by presenting the system input-output relationship.

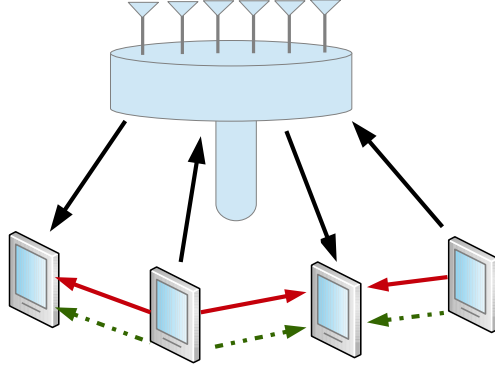


Figure 4.1: (M, K_u, K_d, W) side-channel assisted MU-MIMO full-duplex network, where the side-channels are highlighted in green dash lines.

The received uplink signal at the BS is $\mathbf{y}_u \in \mathbb{C}^{M \times 1}$ and is given as

$$\mathbf{y}_u = \mathbf{H}_u \mathbf{D}_u^{\frac{1}{2}} \mathbf{x}_u + \mathbf{n}_u, \quad (4.1)$$

where $\mathbf{H}_u \in \mathbb{C}^{M \times K_u}$ denotes the fast fading channels between uplink users and the BS, all fast fading channel coefficients are drawn independent and identically distributed (i.i.d.) from circularly-symmetric complex Gaussian distribution $\mathcal{CN}(0, 1)$; $\mathbf{D}_u^{\frac{1}{2}} \in \mathbb{C}^{K_u \times K_u}$ is a diagonal matrix whose diagonal entry denotes the path loss of each uplink channel, i.e., $(\mathbf{D}_u^{\frac{1}{2}})_i = \sqrt{\beta_{u,i}}$, $i \in \mathcal{K}_u$; $\mathbf{x}_u \in \mathbb{C}^{K_u \times 1}$ denotes the K_u uplink transmit signals, $\mathbf{x}_u \triangleq [x_i, \dots, x_{K_u}]$; each uplink transmitter satisfies the power constraint $|x_{u,i}|^2 = P_{u,i} \forall i \in \mathcal{K}_u$; \mathbf{n}_u is the receiver thermal noise which contains i.i.d. $\mathcal{CN}(0, 1)$ entries.

The received downlink signal at each downlink user can be written together as a vector $\mathbf{y}_d \in \mathbb{C}^{K_d \times 1}$ such that

$$\mathbf{y}_d = \mathbf{D}_d^{\frac{1}{2}} \mathbf{H}_d \mathbf{x}_d + \mathbf{G}_I \mathbf{x}_u + \mathbf{n}_d, \quad (4.2)$$

where $\mathbf{H}_d \in \mathbb{C}^{K_d \times M}$ denotes the fast fading channels between the BS and downlink

users which contains i.i.d. $\mathcal{CN}(0,1)$ entries; $\mathbf{D}_d^{\frac{1}{2}} \in \mathbb{C}^{K_d \times K_d}$ is a diagonal matrix whose diagonal entry denotes the path loss of each downlink channel, i.e., $(\mathbf{D}_d^{\frac{1}{2}})_j = \sqrt{\beta_{d,j}}$, $j \in \mathcal{K}_d$; $\mathbf{G}_I \in \mathbb{C}^{K_d \times K_u}$ denotes the interference channel between uplink users and downlink users, and each entry $(\mathbf{G}_I)_{j,i} = g_{I,j}^{(i)}$ incorporates both fast fading and path loss, and $g_{I,j}^{(i)} \sim \mathcal{CN}(0, \beta_{I,j}^{(i)})$; $\mathbf{x}_d \in \mathbb{C}^{M \times 1}$ denotes the downlink transmit vector signal and satisfies the power constraint $\|\mathbf{x}_d\|^2 = P_d$; \mathbf{n}_d denotes the receiver noise which contains i.i.d. $\mathcal{CN}(0,1)$ entries.

For the side-channel communication, we will divide the total side-channel bandwidth into K_u orthogonal bands such that each uplink user will broadcast its side-channel signal over the allocated side-channel band. Hence the j -th downlink user will receive a side-channel signal from the i -th uplink user over the i -th side-channel band as

$$\mathbf{y}_{s,j}^{(i)} = g_{s,j}^{(i)} x_{s,i} + n_{s,j}^{(i)}, \quad (4.3)$$

where $g_{s,j}^{(i)}$ is the side-channel coefficient which models both fast fading and path loss between the i -th uplink user and the j -th downlink user, and $g_{s,j}^{(i)} \sim \mathcal{CN}(0, \beta_{s,j}^{(i)})$, $i \in \mathcal{K}_u, j \in \mathcal{K}_d$; $x_{s,i}$ denotes the side-channel transmit signal and satisfies the power constraint $|x_{s,i}|^2 = P_{s,i}$; $n_{s,j}^{(i)}$ denotes the receiver noise which contains i.i.d. $\mathcal{CN}(0, W)$ entries.

The path loss of each channel is inversely proportional to the channel distance such that $\beta_{u,i} \propto d_{u,i}^{-\alpha}$, $\beta_{d,j} \propto d_{d,j}^{-\alpha}$, $i \in \mathcal{K}_u, j \in \mathcal{K}_d$, where α is the main-channel path-loss parameter, $d_{u,i}$ denotes the distance between the i -th uplink user and BS and $d_{d,j}$ denotes the distance between the j -th downlink user and BS.

4.3 ARQ Protocol Design with Side-Channels

In this section, we present our ARQ design with side-channels in the MU-MIMO full-duplex network. Our protocol design will integrate ARQ at the MAC layer with enhanced interference management scheme via side-channel at the PHY. When an uplink or downlink user fails to decode its packet, a negative-acknowledgment (NACK) will be sent back to the transmitter to request for retransmission. Otherwise, an acknowledgment (ACK) will be sent back so that the transmitter can start new transmission in the next time. We assume that the receivers can perfectly detect the packet errors and ACK/NACK will be fed back to the transmitters for acknowledgement or retransmission. At the PHY, we assume that the optimal channel codes are used to support instantaneous channel capacity. Outage will happen if the transmission rate exceeds the channel capacity due to channel fading and interference.

We assume that all the users use orthogonal resource blocks to feedback up- and downlink ARQ signals such that uplink users can overhear the downlink feedback. We further assume that all the channel state information is available at the downlink users, including the interference channel and side-channel. We will exploit the ARQ feedback information at the MAC layer to design a PHY scheme using side-channels to improve the system goodput. The goodput is defined as the number of successful delivered data bits over transmission time.

4.3.1 Goodput of baseline systems without side-channels

We first derive the goodput of full-duplex system without side-channels. Assuming the transmitter has J packets to transmit, each packet has L bits and the transmission rate is R bits/sec. Each packet require X_i number of ARQ rounds for successful

delivery. As $J \rightarrow \infty$, the long-term goodput G can be calculated according to [45]:

$$G = \lim_{J \rightarrow \infty} \frac{JL}{\frac{L}{R} \sum_{i=1}^J X_i} = \lim_{J \rightarrow \infty} \frac{R}{\frac{1}{J} \sum_{i=1}^J X_i} = \frac{R}{\mathbb{E}(X)}, \quad (4.4)$$

where X is a random variable denoting the number of retransmission of a packet till success. If we define a link error probability as ϵ , X is geometric distributed with parameter $1 - \epsilon$. Thus we have $\mathbb{E}(X) = \frac{1}{1-\epsilon}$ and the goodput is $R(1 - \epsilon)$.

4.3.1.1 Full-duplex baseline system

In order to calculate the goodput of our MU-MIMO full-duplex system, we need to first find out link error probability of each uplink and downlink channel.

To decode the uplink streams, we apply zero-forcing beamforming (ZFBBF) at the BS receiver in equation (4.1) such that $\mathbf{r}_u = \mathbf{A}^H \mathbf{y}_u$, where $\mathbf{A}^H = (\mathbf{H}_u^H \mathbf{H}_u)^{-1} \mathbf{H}_u^H$, and H denotes the Hermitian operator. The received uplink stream sent by the i -th uplink user can be written as $r_{u,j} = \sqrt{\beta_{u,i}} x_{u,i} + (\mathbf{A}^H)_i \mathbf{n}_u$, where $(\mathbf{A}^H)_i$ denotes the i -th row of \mathbf{A}^H . Now we can compute the SINR for the i -th uplink user as follows

$$\begin{aligned} \text{SINR}_{u,i}^{fd} &= \frac{P_{u,i} \beta_{u,i}}{\|(\mathbf{A}^H)_i\|^2} = \frac{P_{u,i} \beta_{u,i}}{[(\mathbf{H}_u^H \mathbf{H}_u)^{-1}]_{i,i}} \\ &\triangleq P_{u,i} \beta_{u,i} X_{u,i}, \end{aligned} \quad (4.5)$$

where $X_{u,i} \triangleq \frac{1}{[(\mathbf{H}_u^H \mathbf{H}_u)^{-1}]_{i,i}}$ follows Erlang distribution [46] with shape parameter $M - K_u + 1$ and scale parameter 1, and the probability density function (PDF) can be represented by

$$f_{X_{u,i}}(x) = \frac{e^{-x}}{(M - K_u)!} x^{M - K_u}. \quad (4.6)$$

For the downlink transmit signal, we apply ZFBBF precoder at BS in equation (5.3)

such that $\mathbf{x}_d = \sqrt{\frac{P_d}{\sigma}} \mathbf{W} \mathbf{s}_d$, where $\mathbf{W} \in \mathbb{C}^{M \times K_d}$ is the precoder, $\mathbf{s}_d \in \mathbb{C}^{K_d \times 1}$ denotes the downlink messages and contains i.i.d. $\mathcal{CN}(0, 1)$ entries, σ is the BS power normalization factor; and we have $\mathbf{W} = \mathbf{H}_d^H (\mathbf{H}_d \mathbf{H}_d^H)^{-1}$, $\sigma = \|\mathbf{W} \mathbf{s}_d\| = \mathbf{s}_d^H (\mathbf{H}_d \mathbf{H}_d^H)^{-1} \mathbf{s}_d$. The received signal at the j -th downlink user can be written as $y_{d,j} = \sqrt{\frac{P_d \beta_{d,j}}{\sigma}} \mathbf{s}_{d,j} + \sum_{i=1}^{K_u} g_{I,j}^{(i)} x_{u,i} + n_{d,j}$. The SINR of the j -th downlink user can be calculated as

$$\text{SINR}_{d,j}^{fd} = \frac{P_d \beta_{d,j}}{\sigma \left(1 + \sum_{i=1}^{K_u} |g_{I,j}^{(i)}|^2 P_{u,i}\right)} \triangleq \frac{P_d \beta_{d,j} X_{d,j}}{1 + Y_{d,j}}, \quad (4.7)$$

where $X_{d,j} \triangleq \frac{1}{\sigma}$ and $Y_{d,j} \triangleq \sum_{i=1}^{K_u} |g_{I,j}^{(i)}|^2 P_{u,i}$. $X_{d,j}$ follows scaled F-distribution [47] with parameter $n_1 = 2(M - K_d + 1)$, $n_2 = 2K_d$, and is given as

$$X_{d,j} \sim \frac{M - K_d + 1}{K_d} \mathcal{F}_{2(M-K_d+1), 2K_d}. \quad (4.8)$$

and the PDF is

$$f_{X_{d,j}}(x) = \frac{M!}{(K_d - 1)!(M - K_d)!} \frac{x^{M-K_d}}{(1+x)^{M+1}}. \quad (4.9)$$

The F-distribution can further be approximated by a Chi-square distribution with degrees-of-freedom $n_1 = 2(M - K_d + 1)$ [48] such that $X_{d,j} \sim \mathcal{G}(n_2 x, n_1)$ and the corresponding PDF can be approximated as

$$f_{X_{d,j}}(x) \approx \frac{K_d^{M-K_d+1}}{(M - K_d)!} e^{K_d x} x^{M-K_d}. \quad (4.10)$$

The received interference power from the i -th uplink user to the j -th downlink user, i.e., $|g_{I,j}^{(i)}|^2 P_{u,i}$ follows exponential distribution such that $|g_{I,j}^{(i)}|^2 P_{u,i} \sim \exp\left(\frac{1}{P_{u,i} \beta_{I,j}^{(i)}}\right)$. We assume that we have pairwise distinct respective parameters $P_{u,i} \beta_{I,j}^{(i)}, \forall i \in \{1, \dots, K_u\}$, $j \in \{1, \dots, K_d\}$, and the heterogeneous interference can be caused by different inter-

ference channel strengths and uplink user transmit power. Hence $Y_{d,j}$ follows Hypo-exponential distribution and the PDF of $Y_{d,j}$ is given below [49]

$$f_{Y_{d,j}}(y) = \left(\prod_{i=1}^{K_u} \frac{1}{P_{u,i}\beta_{I,j}^{(i)}} \right) \sum_{k=1}^{K_u} \frac{\exp\left(-\frac{y}{P_{u,k}\beta_{I,j}^{(k)}}\right)}{\prod_{t \neq k, t=1}^{K_u} \left(\frac{1}{P_{u,t}\beta_{I,j}^{(t)}} - \frac{1}{P_{u,k}\beta_{I,j}^{(k)}}\right)}. \quad (4.11)$$

Based on the up- and downlink SINRs that we have calculated above, next we compute link error probability of each up- and downlink channel as follows. When a strong channel code with a blocklength long enough is used for transmission, outage will occur if the transmission rate exceeds the instantaneous Shannon capacity [45]. For simplicity, we assume that the transmission rate of each packet is R bits/sec.

The link error probability of the i -th uplink user in the MU-MIMO full-duplex network is given below, where $i \in \mathcal{K}_u$

$$\begin{aligned} \epsilon_{u,i}^{fd} &= \Pr(\log(1 + \text{SINR}_{u,i}^{fd}) < R) \\ &= \Pr(\text{SINR}_{u,i}^{fd} < \gamma_{th}) \\ &= 1 - \exp\left(-\frac{\gamma_{th}}{P_{u,i}\beta_{u,i}}\right) \sum_{k=0}^{M-K_u} \frac{1}{k!} \left(\frac{\gamma_{th}}{P_{u,i}\beta_{u,i}}\right)^k, \end{aligned} \quad (4.12)$$

where $\gamma_{th} = 2^R - 1$.

Similarly, the link error probability of the j -th downlink user, where $j \in \mathcal{K}_d$, is given as

$$\begin{aligned} \epsilon_{d,j}^{fd} &= \Pr(\log(1 + \text{SINR}_{d,j}^{fd}) < R) \\ &= \Pr(\text{SINR}_{d,j}^{fd} < \gamma_{th}) \\ &= \Pr\left(\frac{X_{d,j}}{1 + Y_{d,j}} < \frac{\gamma_{th}}{P_d\beta_{d,j}}\right) \end{aligned} \quad (4.13)$$

In the Interference limited regime, where $Y_{d,j} \gg 1$, we can further approximate the

link error probability as

$$\begin{aligned}
\epsilon_{d,j}^{fd} &\approx \Pr\left(\frac{X_{d,j}}{Y_{d,j}} < \frac{\gamma_{th}}{P_d\beta_{d,j}}\right) \text{ (in the interference limited regime)} \\
&= \int_0^\infty \int_0^{\frac{\gamma_{th}y}{P_d\beta_{d,j}}} f_{X_{d,j}}(x)dx f_{Y_{d,j}}(y)dy \\
&= \int_0^\infty \frac{1}{a!} \gamma(a, b_j) f_{Y_{d,j}}(y)dy \\
&= \int_0^\infty \frac{1}{a!} \gamma(a, b_j) \left(\prod_{i=1}^{K_u} c_{j,i}\right) \sum_{i=1}^{K_u} \frac{e^{-c_{j,i}y}}{d_{j,i}} dy \text{ (substitute (4.11))} \\
&= \prod_{i=1}^{K_u} c_{j,i} b_j^a \sum_{i=1}^{K_u} \frac{{}_2F_1\left(1, 1+a; 1+a; \frac{b_j}{b_j+c_{j,i}}\right)}{(b_j+c_{j,i})^{a+1} d_{j,i}} \text{ (eq. 6.455-2 in [50])} \\
&= \prod_{i=1}^{K_u} c_{j,i} b_j^a \sum_{i=1}^{K_u} \frac{1}{c_{j,i} (b_j+c_{j,i})^a d_{j,i}},
\end{aligned} \tag{4.14}$$

where $\gamma(.,.)$ is the lower incomplete Gamma function, $a = M - K_d + 1$, $b_j = \frac{K_d \gamma_{th}}{P_d \beta_{d,j}}$, $c_{j,i} = \frac{1}{P_{u,i} \beta_{1,j}^{(i)}}$, $d_{j,i} = \prod_{t \neq i} (c_{j,t} - c_{j,i})$, ${}_2F_1(.,.,.;.)$ is the Gauss' hypergeometric function [50] and ${}_2F_1(1, x; x; z) = \frac{1}{1-z}$.

Proposition 1. *In a (M, K_u, K_d) MU-MIMO full-duplex network with transmit and receive zero-forcing beamforming, the goodputs of uplink and downlink transmission are given by*

$$\begin{aligned}
G_{u,i}^{fd} &= R(1 - \epsilon_{u,i}^{fd}), \quad i \in \mathcal{K}_u \\
G_{d,j}^{fd} &= R(1 - \epsilon_{d,j}^{fd}), \quad j \in \mathcal{K}_d \\
G_{sum}^{fd} &= \sum_{i \in \mathcal{K}_u} G_{u,i}^{fd} + \sum_{j \in \mathcal{K}_d} G_{d,j}^{fd},
\end{aligned} \tag{4.15}$$

where $\epsilon_{u,i}^{fd}$ and $\epsilon_{d,j}^{fd}$ are given in (4.12) and (4.14), respectively.

Note that if we have a delay constraint imposed on the system which only allows finite number of retransmission. Our goodput expressions will not be affected, the

delay constraint will only affect the sequence of the packet delivery. We give an outline of the proof. We assume that the maximum number of retransmission for each packet is $d - 1$ with a link error probability ϵ , meaning the probability of a packet being discarded is ϵ^d . We also assume that the packet loss probability after delay limit is no more than q such that $\epsilon^d \leq q$. By applying the renewal-reward theorem, we can compute the goodput. The average reward considering the limit d is $R(1 - \epsilon^d)$, and $\mathbb{E}(x)$ is the average renewal interval per packet. Hence the goodput is $\frac{R(1-\epsilon^d)}{\mathbb{E}(x)}$ [45], and the goodput further can be calculated to be $R(1 - \epsilon)$, subject to $\epsilon^d \leq q$.

4.3.1.2 Half-duplex baseline system

In the half-duplex system, the uplink and downlink transmissions are in different time-frequency slots. We first calculate the link error probability in the half-duplex system. The uplink SINR in the half-duplex is the same as that in the full-duplex system, i.e., $\text{SINR}_{u,i}^{hd} = \text{SINR}_{u,i}^{fd}$, where $i \in \mathcal{K}_u$. Hence the corresponding uplink error probability in the half-duplex system is also same as that in the full-duplex system,

$$\epsilon_{u,i}^{hd} = \epsilon_{u,i}^{fd}, \quad i \in \mathcal{K}_u. \quad (4.16)$$

The downlink SINR in the half-duplex system will be different than that in the full-duplex system, since there is no UE-UE interference in the half-duplex system. The SINR of the j -th downlink user, where $j \in \mathcal{K}_d$, is given as

$$\text{SINR}_{d,j}^{hd} = \frac{P_d \beta_{d,j}}{\sigma} \triangleq P_d \beta_{d,j} X_{d,j}, \quad (4.17)$$

where $X_{d,j}$ is a scaled F-distributed random variable whose PDF and approximation are given in (4.9) and (4.10), respectively.

Hence the link error probability of the j -th downlink user is

$$\begin{aligned}
\epsilon_{d,j}^{hd} &= \Pr(\log(1 + \text{SINR}_{d,j}^{hd}) < R) \\
&= \Pr(\text{SINR}_{d,j}^{hd} < \gamma_{th}) \\
&= \Pr\left(X_{d,j} < \frac{\gamma_{th}}{P_d \beta_{d,j}}\right) \\
&\approx \frac{\gamma\left(M - K_d + 1, \frac{K_d \gamma_{th}}{P_d \beta_{d,j}}\right)}{(M - K_d)!},
\end{aligned} \tag{4.18}$$

where $\gamma(\cdot, \cdot)$ is the lower incomplete gamma function.

Proposition 2. *In a (M, K_u, K_d) MU-MIMO half-duplex network with transmit and receive zero-forcing beamforming, the goodputs of uplink and downlink transmission are given by*

$$\begin{aligned}
G_{u,i}^{hd} &= R(1 - \epsilon_{u,i}^{hd}), \quad i \in \mathcal{K}_u \\
G_{d,j}^{hd} &= R(1 - \epsilon_{d,j}^{hd}), \quad j \in \mathcal{K}_d \\
G_{sum}^{hd} &= \alpha \sum_{i \in \mathcal{K}_u} G_{u,i}^{hd} + (1 - \alpha) \sum_{j \in \mathcal{K}_d} G_{d,j}^{hd},
\end{aligned} \tag{4.19}$$

where $\alpha \in [0, 1]$, $\epsilon_{u,i}^{hd}$ and $\epsilon_{d,j}^{hd}$ are given in (4.16) and (4.18), respectively.

4.3.2 Decode-and-cancel over side-channels

In the main-channel, we have the ARQ process where the erroneous data will be detected for retransmission. In contrast, there is no ARQ for the data transmission over the side-channels such that no delay is introduced to the main-channel communication. Hence the side-channel data transmission will only depend on the side-channel link quality. The SINR of each side-channel between the i -th uplink user and the j -th

downlink is

$$\text{SINR}_{s,j}^{(i)} = \frac{|g_{s,j}^{(i)}|^2 P_{s,i}}{W}. \quad (4.20)$$

Now we can calculate the link error probability of the side-channel between the i -th uplink user and the j -th downlink as,

$$\begin{aligned} \epsilon_{s,j}^{(i)} &= \Pr \left(W \log(1 + \text{SINR}_{s,j}^{(i)}) < R \right) \\ &= \Pr(\text{SINR}_{s,j}^{(i)} < \gamma_{s,th}) \\ &= 1 - \exp \left(-\frac{\gamma_{s,th} W}{P_{s,i} \beta_{s,j}^{(i)}} \right), \end{aligned} \quad (4.21)$$

where $\gamma_{s,th} = 2^{\frac{R}{W}} - 1$.

Given different side-channel conditions, the SINR of the j -th downlink user after applying decode-and-cancel is

$$\text{SINR}_{d,j}^{fd-sc} = \frac{P_d \beta_{d,j}}{\sigma \left(1 + \sum_{i \in \mathcal{S}_j} |g_{I,j}^{(i)}|^2 P_{u,i} \right)}, \quad (4.22)$$

where $\mathcal{S}_j = \{i \mid i \in \mathcal{K}_u : \text{SINR}_{s,j}^{(i)} < \gamma_{s,th}\}$, \mathcal{S}_j is the set of uplink users whose interfering signal can't be decoded and cancelled at the j -th downlink user.

Next, we calculate the downlink error probability in the full-duplex system with side-channels. By considering all the conditional probability of j -th downlink failure given the side-channel condition, we have

$$\begin{aligned} \epsilon_{d,j}^{fd-sc} &= \mathbb{E} \left[\Pr(\text{SINR}_{d,j}^{fd-sc} < \gamma_{th}) \mid \text{SINR}_{s,j}^{(i)}, \forall i \in \mathcal{K}_u \right] \\ &= \epsilon_{d,j}^{fd} \prod_{i \in \mathcal{K}_u} \epsilon_{s,j}^{(i)} + \sum_{\substack{\mathcal{S}_j \neq \emptyset \\ \mathcal{S}_j \neq \mathcal{K}_u}} P(\mathcal{S}_j) \prod_{l \in \mathcal{K}_u \setminus \mathcal{S}_j} (1 - \epsilon_{s,j}^{(l)}) \prod_{k \in \mathcal{S}_j} \epsilon_{s,j}^{(k)} + \epsilon_{d,j}^{hd} \prod_{i \in \mathcal{K}_u} (1 - \epsilon_{s,j}^{(i)}), \end{aligned} \quad (4.23)$$

where $P(\mathcal{S}_j) = \prod_{i \in \mathcal{S}_j} c_{j,i} b_j^a \sum_{i \in \mathcal{S}_j} \frac{1}{c_{j,i} (b_j + c_{j,i})^a d_{j,i}}$, $a = M - K_d + 1$, $b_j = \frac{K_d \gamma_{th}}{P_d \beta_{d,j}}$, $c_{j,i} = \frac{1}{P_{u,i} \beta_{f,j}^{(i)}}$, $d_{j,i} = \prod_{t \neq i} (c_{j,t} - c_{j,i})$, ${}_2F_1(\cdot, \cdot; \cdot; \cdot)$ is the Gauss' hypergeometric function, and ${}_2F_1(1, x; x; z) = \frac{1}{z}$. The notation of $\sum_{\substack{\mathcal{S}_j \neq \emptyset \\ \mathcal{S}_j \neq \mathcal{K}_u}}$ denotes the summation over all possible sets of \mathcal{S}_j except the empty set and the full set.

4.3.3 Proactive side-channel assisted ARQ protocol

The proactive protocol will use side-channels proactively irrespective of the downlink feedback. The use of side-channel is triggered only by the conventional uplink ARQ feedback. In the first round of transmission, each uplink user transmits its packet over both main-channel and side-channel. At the end of the data transmission, each uplink user will receive ARQ feedback from the BS. When an uplink user receives an ACK, it will transmit a new packet over both main-channel and side-channel in the next round. However, if an uplink user receives a NACK, there is no need to retransmit the previous packet over the side-channel in the next round because the downlink users already have the old copy of the interfering uplink packet. Hence the side-channel assisted ARQ based full-duplex system is a memory system.

At the downlink receiver, it will first attempt to decode downlink data sent from the BS over the main-channel, if the data fails to be decoded, then the downlink user will perform decode-and-cancel scheme [38] to decode the packet sent from the side-channel, re-generate interfering main-channel signal locally, then cancel the interference from the main-channel. Next, the downlink user will decode its intended packet from the main-channel. If the side-channel packet fails to be decoded, the downlink user will continue to perform its main-channel decoding, and thus our side-channel assisted ARQ protocol will not impose any delay for main-channel communication. The proactive protocol communication process is given in Figure 4.2 where $K_u = K_d = 2$.

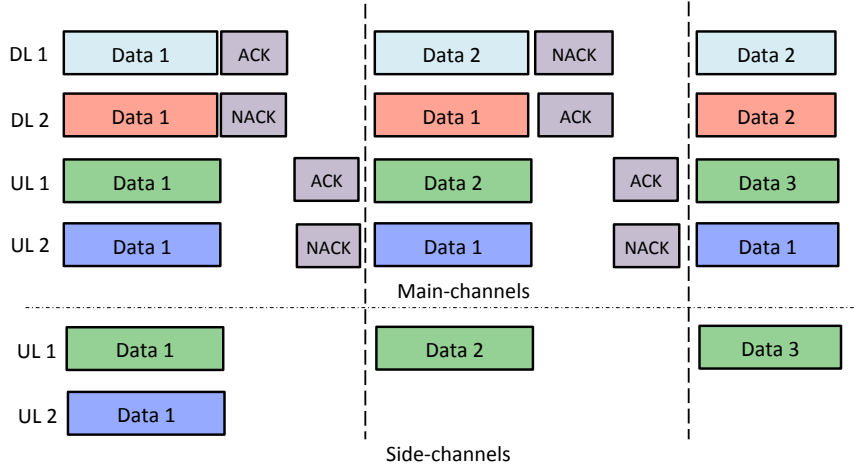


Figure 4.2: Proactive protocol process where $K_u = K_d = 2$.

Based on the proactive protocol, we can use the side-channel to help improve downlink goodput by mitigating UE-UE interference, which is presented in the following proposition.

Proposition 3. *In a (M, K_u, K_d, W) side-channel assisted MU-MIMO full-duplex network, the goodputs of uplink and downlink transmission using proactive protocol, are given by*

$$\begin{aligned} G_{u,i}^{pro} &= G_{u,i}^{fd}, \quad i \in \mathcal{K}_u \\ G_{d,j}^{pro} &= R \left(1 - \epsilon_{d,j}^{fd-sc} \right), \quad j \in \mathcal{K}_d \end{aligned} \quad (4.24)$$

where $G_{u,i}^{fd}$ is given (4.15) and $\epsilon_{d,j}^{fd-sc}$ is given in (4.23).

Proof. Since the use of side-channels will only help alleviate the interference for the downlink users, the uplink goodput will not be affected by the proactive protocol. The effective link error probability of the j -th downlink user after applying proactive protocol can be computed by considering all the conditional probability of j -th downlink failure given the side-channel condition. Hence the downlink goodput can

be derived accordingly. □

4.3.4 Reactive side-channels assisted ARQ protocol

The reactive protocol will use the side-channels on demand. The use of side-channels is triggered based on both uplink ARQ and our designed downlink ARQ feedback. We design two different downlink ARQ feedback mechanisms when a packet is in error: one is NACK-N which indicates that the erroneous packet is due to noise; the other one is NACK-I which indicates the erroneous packet is due to interference. When an uplink user overhears NACK-I from downlink users and its previous uplink ARQ feedback is ACK, the uplink user will send a new packet over both main-channel and side-channel in the next time slot. Each downlink user will first decode the intended packets on the main-channel. If the downlink user encounters decoding failure, it will perform decode-and-cancel to cancel interference from uplink users using the side-channel information.

Each uplink user will not use side-channels if it overhears downlink ACK or NACK-N, neither will the uplink user use side-channels if its uplink feedback is NACK (except for the first time to use side-channels) since the the downlink users already have the previous uplink packet. The reactive protocol communication process is given in Figure 4.3 where $K_u = K_d = 2$.

We first compute downlink error probability due to noise which will be used later in our goodput analysis. We denote $p_{N,j}$ as the link error probability of the j -th downlink user due to noise. The link error is caused by noise if the interference level is below a certain noise threshold. The aggregated interference at the j -th downlink user is $Y_{d,j} \triangleq \sum_{i=1}^{K_u} |g_{I,j}^{(i)}|^2 P_{u,i}$, and $Y_{d,j}$ follows Hypoexponential distribution whose

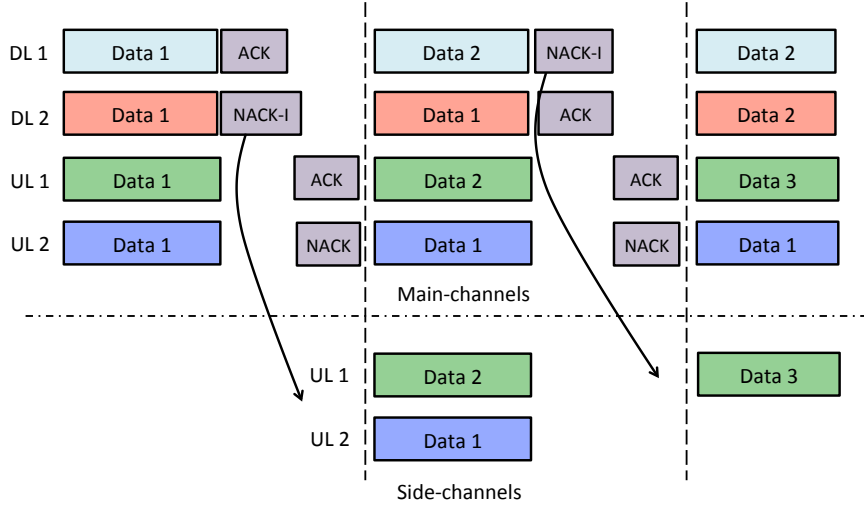


Figure 4.3: Reactive protocol process where $K_u = K_d = 2$.

PDF is given in (4.11). Hence we have

$$\begin{aligned}
 p_{N,j} &= \Pr(Y_{d,j} < N_{th}) \\
 &= \left(\prod_{i=1}^{K_u} \frac{1}{P_{u,i} \beta_{I,j}^{(i)}} \right) \sum_{k=1}^{K_u} \frac{P_{u,k} \beta_{I,j}^{(k)} \left(1 - \exp \left(- \frac{N_{th}}{P_{u,k} \beta_{I,j}^{(k)}} \right) \right)}{\prod_{t \neq k, t=1}^{K_u} \left(\frac{1}{P_{u,t} \beta_{I,j}^{(t)}} - \frac{1}{P_{u,k} \beta_{I,j}^{(k)}} \right)}, \quad (4.25)
 \end{aligned}$$

where N_{th} is the noise threshold.

In the following proposition, we state the goodput of the side-channel assisted full-duplex system using reactive protocol.

Proposition 4. *In a (M, K_u, K_d, W) side-channel assisted MU-MIMO full-duplex network, the goodputs of uplink and downlink transmission using reactive protocol, are given by*

$$\begin{aligned}
 G_{u,i}^{rea} &= G_{u,i}^{fd}, \quad i \in \mathcal{K}_u \\
 G_{d,j}^{rea} &= R \left(1 - \frac{\epsilon_{d,j}^{fd}}{1 + \epsilon_{d,j}^{fd} - P_{N,j} \epsilon_{d,j}^{hd} - (1 - P_{N,j}) \epsilon_{d,j}^{fd-sc}} \right), \quad j \in \mathcal{K}_d, \quad (4.26)
 \end{aligned}$$

where $\epsilon_{d,j}^{fd-sc}$ is given in (4.23), and $p_{N,j}$ is given in (4.25).

Proof. In the reactive protocol, since the use of side-channels will be triggered starting from the second transmission time based on the downlink ARQ feedback, we can compute the downlink link error probability in the reactive protocol $\epsilon_{d,j}^{rea}$ as

$$\begin{aligned}
\epsilon_{d,j}^{rea} &= \mathbb{E}_T[\Pr(\text{SINR}_{d,j}^{fd-sc} < \gamma_{th})|T] \\
&= \Pr(T = 1)\Pr(\text{SINR}_{d,j}^{fd-sc} < \gamma_{th})|T = 1 \\
&+ \Pr(T \neq 1)\Pr(\text{SINR}_{d,j}^{fd-sc} < \gamma_{th})|T \neq 1 \\
&= (1 - \epsilon_{d,j}^{rea})\epsilon_{d,j}^{fd} + \epsilon_{d,j}^{rea}(\Pr(\text{SINR}_{d,j}^{fd-sc} < \gamma_{th})|\text{NACK-N}) \\
&+ \Pr(\text{SINR}_{d,j}^{fd-sc} < \gamma_{th})|\text{NACK-I}) \\
&= (1 - \epsilon_{d,j}^{rea})\epsilon_{d,j}^{fd} + \epsilon_{d,j}^{rea} \left(P_{N,j}\epsilon_{d,j}^{hd} + (1 - P_{N,j})\epsilon_{d,j}^{fd-sc} \right) \\
&\Rightarrow \epsilon_{d,j}^{rea} = \frac{\epsilon_{d,j}^{fd}}{1 + \epsilon_{d,j}^{fd} - P_{N,j}\epsilon_{d,j}^{hd} - (1 - P_{N,j})\epsilon_{d,j}^{fd-sc}}.
\end{aligned} \tag{4.27}$$

With the derived $\epsilon_{d,j}^{rea}$, the downlink goodput in the reactive protocol is $G_{d,j}^{rea} = R(1 - \epsilon_{d,j}^{rea})$. And the uplink goodput is the same as the baseline full-duplex system. \square

4.3.5 Energy efficiency for side-channel protocols

In this section, we will evaluate the energy-efficiency (bits/Joule) of both proactive and reactive side-channel assisted ARQ protocols. Since we exploit the use of side-channel to manage UE-UE interference, only downlink performance will be enhanced. Therefore we define the energy-efficiency as the ratio between downlink goodput (bits/s) and average side-channel transmit power (Joule/s). We only need to calculate how much downlink goodput can be achieved for every Joule spent on the side-channels. As we would expect, the proactive protocol will achieve higher

downlink goodput while reactive protocol will spend less energy on the side-channel transmission. Hence there exists regimes where one protocol will outperform the other in terms of energy-efficiency.

For the ease of analysis, we assume the side-channel transmit power is fixed as P_s for all uplink users. Now we will compute the average side-channel transmit power per packet for all uplink users in the proactive protocol as

$$P_{pro} = \sum_{i \in \mathcal{K}_u} (1 - \epsilon_{u,i}^{fd}) P_s. \quad (4.28)$$

And the average side-channel transmit power per packet for all uplink user in the reactive protocol is

$$P_{rea} = \begin{cases} 0, & \text{if } \min_{j \in \mathcal{K}_d} p_{N,j} = 1 \text{ or } \max_{j \in \mathcal{K}_d} \epsilon_{d,j}^{fd} = 0 \\ \left(\sum_{i \in \mathcal{U}} (1 - \min_{j \in \mathcal{K}_d} p_{N,j}) \frac{\max_{j \in \mathcal{K}_d} \mathbb{E}(J_j) - 1}{\max_{j \in \mathcal{K}_d} \mathbb{E}(J_j)} \right) P_s \\ + \sum_{i' \in \mathcal{K}_u \setminus \mathcal{U}} (1 - \min_{j \in \mathcal{K}_d} p_{N,j}) (1 - \epsilon_{u,i'}^{fd}) P_s, & \text{otherwise} \end{cases} \quad (4.29)$$

where $\mathcal{U} = \{i \mid i \in \mathcal{K}_u : \epsilon_{u,i}^{fd} = 0\}$; $\mathbb{E}(J_j)$ is the average retransmission time of each packet for the j -th downlink user in the reactive protocol, $\mathbb{E}(J_j) = 1/(1 - \epsilon_{d,j}^{rea})$, and $\epsilon_{d,j}^{rea} = \frac{\epsilon_{d,j}^{fd}}{1 + \epsilon_{d,j}^{fd} - p_{N,j} \epsilon_{d,j}^{hd} - (1 - p_{N,j}) \epsilon_{d,j}^{fd-sc}}$.

Now we can compute the energy efficiency as bit per Joule for proactive and reactive protocols as follows:

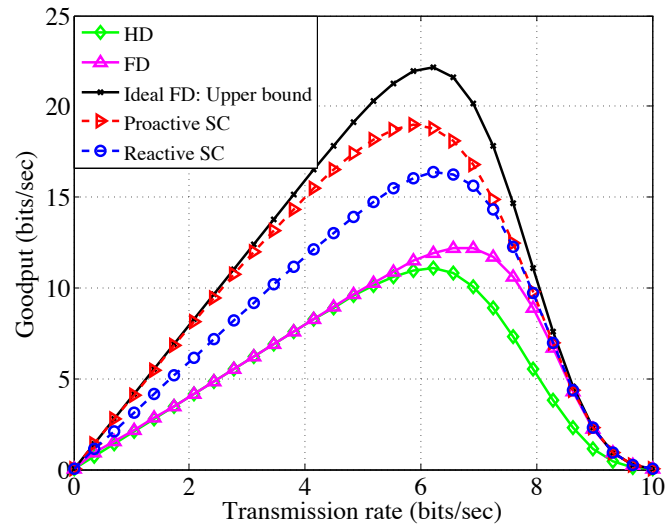
$$\begin{aligned} \eta_{pro} &= \frac{\sum_{j \in \mathcal{K}_d} G_{d,j}^{pro}}{P_{pro}}, \\ \eta_{rea} &= \frac{\sum_{j \in \mathcal{K}_d} G_{d,j}^{rea}}{P_{rea}}. \end{aligned} \quad (4.30)$$

4.4 Numerical Results

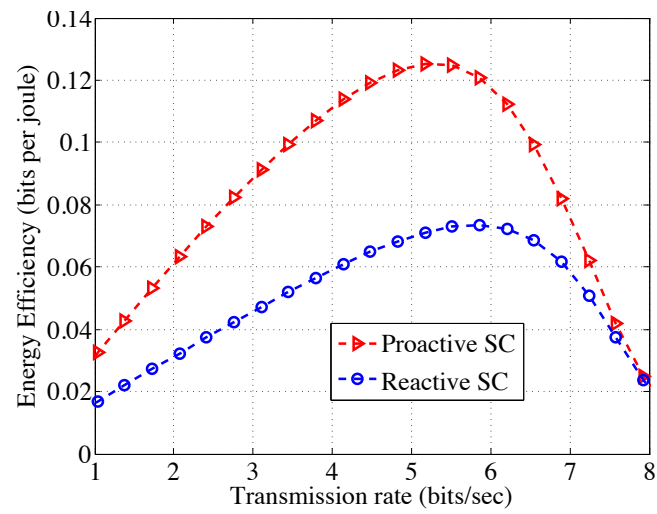
In this section, we present the numerical results to verify our protocol analysis. In the numerical simulation, we assume that the number of BS antennas $M = 4$, and up- and downlink users $K_u = K_d = 2$. The main-channel transmit power is 20 dB and the side-channel transmit power is 15 dB. For the large-scale fading parameters, we let $\beta_{u,i} = \beta_{d,j} = 1$, and $\beta_{I,j}^{(i)} = \beta_{s,j}^{(i)} \sim \text{uniform}(3, 5)$, $\forall i \in \mathcal{K}_u, j \in \mathcal{K}_d$. We further assume the side-channel bandwidth $W = 3$ while the main-channel bandwidth is normalized as 1. We run hundreds of simulation to compare sum goodput for the following five systems: 1) half-duplex system with an equal time/frequency sharing between up- and downlink transmission; 2) full-duplex system without side-channels; 3) full-duplex system with reactive protocol; 4) full-duplex with proactive protocol; 5) ideal full-duplex upper bound (no interference in the system).

Figure 4.4 illustrates the system performance with different transmission rates. The goodputs of five different systems are given in Figure 4.4(a), and energy efficiency of proactive and reactive side-channel protocols is given in Figure 4.4(b). The goodput of each system is a convex function of the transmission rate. This is because when the transmission rate is low, the corresponding goodput also becomes low. When the transmission rate is high, the link error probability will increase and result in more retransmission, thus reducing the system goodput. With our side-channel protocols, the system goodput can be significantly improved over the half-duplex and full-duplex baseline systems, and proactive protocol achieves higher energy efficiency.

The system performance with various number of BS antennas M is shown in Figure 4.5 when $R = 3$ bits/s. We observe that the performance of full-duplex system without side-channels will scale with M much faster than other systems. Proactive side-channel protocol achieves higher energy efficiency when M is small while reactive protocol achieves higher energy efficiency when M is large. The reason behind this



(a) Goodput



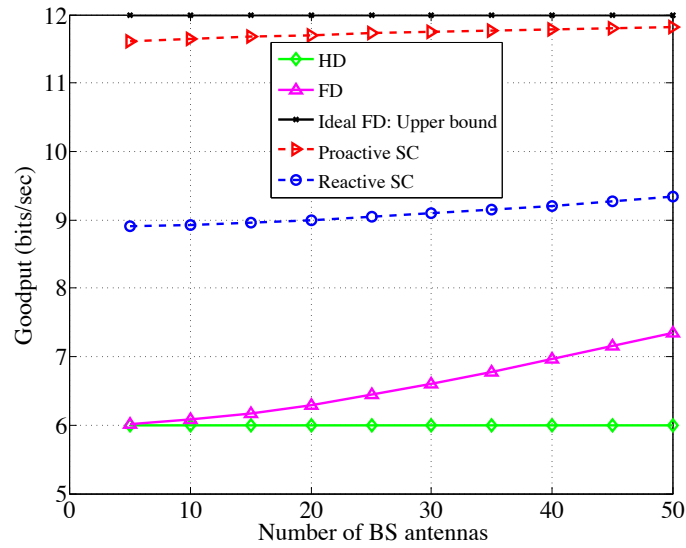
(b) Energy efficiency

Figure 4.4: Performance versus transmission rate.

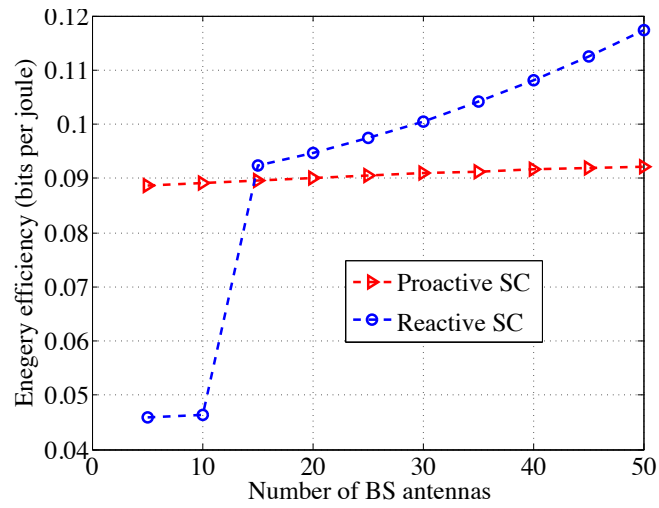
result is that as M increases, the signal link strength will increase and the number of data retransmission will reduce. As a result, we use side-channel less often to mitigate interference for large M and reactive protocol is better choice. In contrast, when M is small, we need to use the side-channels more often to evoke enhanced interference management, and proactive protocol is more effective. We conclude that large number BS antennas can help reduce side-channel bandwidth/power to maintain the same goodput performance.

Figure 4.6 shows the system performance with different side-channel bandwidths when $R = 6$ bits/s. As we increase the side-channel bandwidth, the performance of both proactive and reactive side-channel protocols will improve, and proactive will achieve close to the upper bound goodput performance.

Figure 4.7 demonstrates the system performance with varying interference level when $R = 4$ bits/s. The goodput of both side-channel protocols will scale with increasing interference level, while the performance of full-duplex system without side-channel decays as interference level increases. This is because as the average interference link strength become stronger, i.e., uplink user to downlink user distance become closer, the side-channel strength will also increase. Hence the use of side-channels for decoding and canceling the interference is more effective as interference level increases. Moreover, the proactive protocol outperforms the reactive protocol in the high interference regime in energy efficiency as we need to use the side-channels more frequently to combat interference.

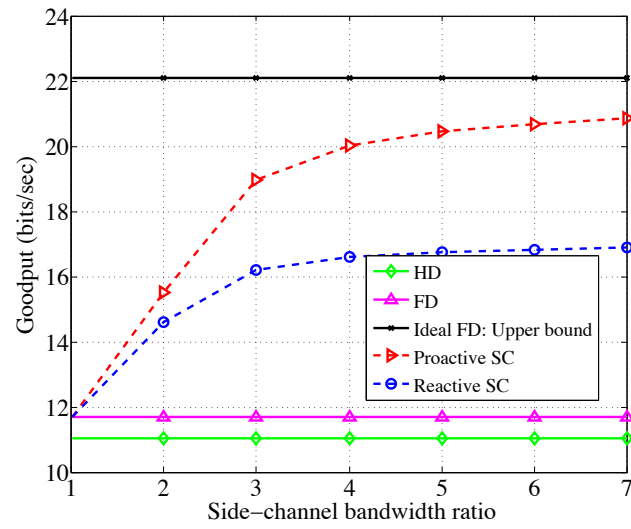


(a) Goodput

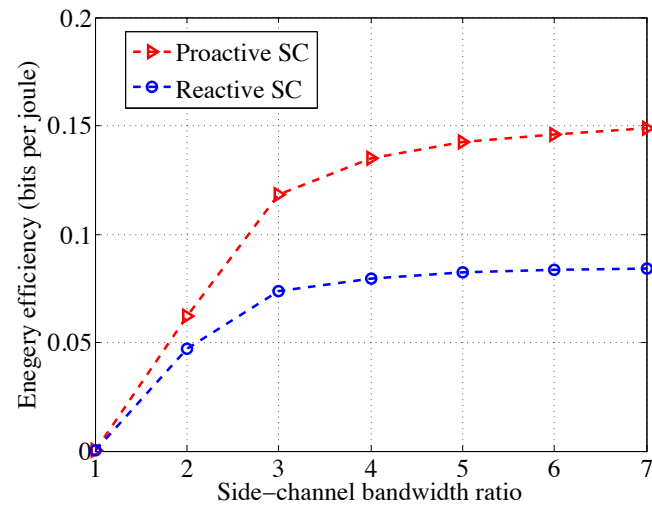


(b) Energy efficiency

Figure 4.5: Performance versus number of BS antennas when $R = 3$ bits/s.

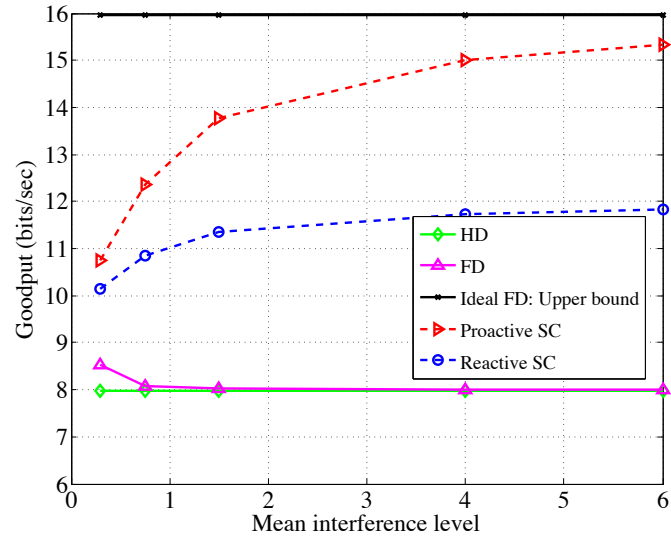


(a) Goodput

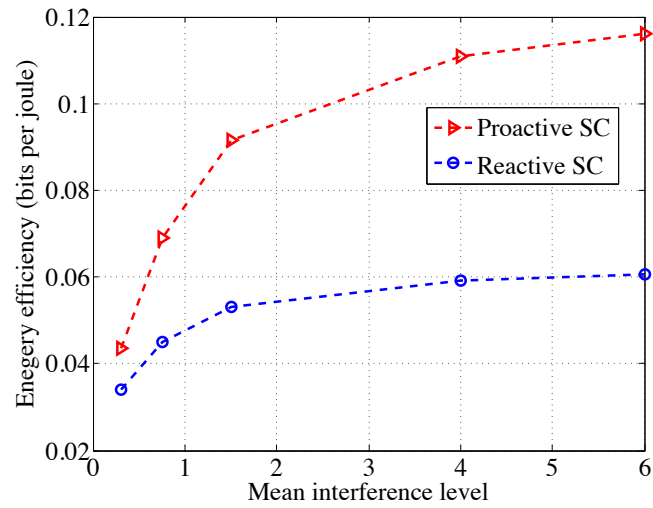


(b) Energy efficiency

Figure 4.6: Performance versus side-channel bandwidth when $R = 6$ bits/s.



(a) Goodput



(b) Energy efficiency

Figure 4.7: Performance versus interference level when $R = 4$ bits/s.

Large Antenna Analysis of Multi-Cell Full-Duplex System

5.1 Introduction

In this chapter, we will extend our study of MU-MIMO full-duplex networks to a multi-cell scenario. In a multi-cell MU-MIMO full-duplex system, there are more simultaneous active links compared to the half-duplex counterpart, which result in additional interference. In the example of multi-cell MU-MIMO full-duplex network shown in Figure 5.1, the uplink rate will be affected by the new interference from neighboring full-duplex BSs, and downlink rate will be affected by the new interference from uplink users (UE). There is a possibility that in the multi-cell MU-MIMO full-duplex networks, full-duplex gains can be offset by the loss due to additional interference. Managing interference is therefore critical to retain the full-duplex gain in such multi-cell networks.

In this paper, we study if and how large antenna arrays at BSs can be used to manage the increased intra- and inter-cell interference in full-duplex enabled networks. Recently, the use of a very large antenna array at the BS has become very attractive [4,

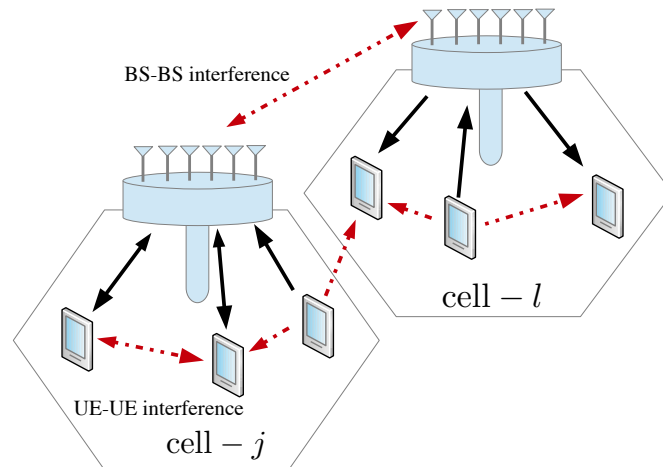


Figure 5.1: The full-duplex BS in each cell has M antennas, and the UE has single antenna with either full-duplex or half-duplex radio. Besides the conventional uplink and downlink interference that exist in the half-duplex system, there will be new BS-BS and UE-UE interference highlighted by the red dash lines.

5, 6], where a BS has orders of magnitude more antennas compared with the current use. The large antenna array at the BS not only can increase the network capacity many-fold, but also enable a new network architecture to simplify baseband signal processing [4], eliminate inter-cell interference [1], and reduce node transmit power for energy saving [3]. The experimental evidence on the benefits of massive MIMO has already sparked strong industry interest and 64-antenna configuration is now being considered for 5G systems.

In the rest of the chapter, we characterize the ergodic achievable rates for the case of simple linear receivers and precoders. Our rate analysis takes into account practical constraints such as imperfect full-duplex radio chains, channel estimation error, training overhead and pilot contamination. We also analyze the system performance in the asymptotic regime where the number of BS antennas grows infinitely large. Numerical evaluation is provided in the end.

5.2 Multi-Cell Full-Duplex System Model

We consider a multi-cell MU-MIMO full-duplex system with $L (\geq 1)$ cells, where each cell has one in-band full-duplex BS with M antennas. In each cell, single-antenna UEs with either full-duplex or half-duplex radios are supported. Each BS can serve K_f full-duplex (FD) users, K_h^u half-duplex (HD) uplink users and K_h^d half-duplex downlink users. We denote $\mathcal{K}_u = \underbrace{\{1, \dots, K_f\}}_{\text{FD UE}}, \underbrace{\{K_f + 1, \dots, K_f + K_h^u\}}_{\text{HD UE}}$ as the set of all uplink users, where the first K_f elements represent K_f full-duplex users; and the last K_h^u elements represent half-duplex uplink users. The set of all downlink users are denoted as $\mathcal{K}_d = \underbrace{\{1, \dots, K_f\}}_{\text{FD UE}}, \underbrace{\{K_f + 1, \dots, K_f + K_h^d\}}_{\text{HD UE}}$, where the first K_f elements represent full-duplex users, and the last K_h^d elements represent half-duplex downlink users. We further denote the set of full-duplex users as $\mathcal{K}_f \triangleq \{1, \dots, K_f\}$ and set of half-duplex downlink users as $\mathcal{K}_h^d \triangleq \{K_f + 1, \dots, K_f + K_h^d\}$. The total number of uplink users is $|\mathcal{K}_u| \triangleq K_u = K_f + K_h^u$ and the total number of downlink users is $|\mathcal{K}_d| \triangleq K_d = K_f + K_h^d$.

The uplink and downlink data are transmitted over the same time-frequency slot with block fading. The analysis in this chapter can be applied to wide-band channels such as OFDM system.

In this work, we will consider practical constraints on the full-duplex radio chains such as non-ideal power amplifier, oscillator phase noise, non-ideal digital-to-analog converter and analog-to-digital converter, which can be captured by the dynamic range model [51, 52, 53]. The dynamic range model approximates the imperfect full-duplex transmit radio chain as an additive white Gaussian “transmitter noise” added to each transmit antenna. The variance of the transmitter noise is κ ($\kappa \ll 1$) times the power of the transmit signals, where κ is the dynamic range parameter. The full-duplex transmitter noise will propagate over the self-interference (SI) channel and

is nontrivial compared to receiver thermal noise. However, the effect of transmitter noise that propagates over the uplink/downlink channels is negligible when compared to receiver thermal noise [53].

5.2.1 Uplink

The j -th full-duplex BS will receive an $M \times 1$ uplink signal vector $\mathbf{y}'_{u,j}$:

$$\mathbf{y}'_{u,j} = \sum_{l=1}^L \mathbf{G}_{u,jl} \mathbf{x}_{u,l} + \sum_{l=1}^L \mathbf{V}_{jl} \mathbf{x}_{d,l} + \mathbf{V}_{jj} \mathbf{e}_{bs,j} + \mathbf{n}_{u,j}, \quad (5.1)$$

where $\mathbf{x}_{u,l} = \sqrt{P_u} \mathbf{u}_l$ denotes the uplink transmit signal vector, $\mathbf{u}_l \triangleq [u_{l,1}, \dots, u_{l,K_u}]^T$ is a $K_u \times 1$ vector consisting of uplink messages of the K_u uplink users in the l -th cell. Each user has an average power constraint P_u , and $\mathbb{E}(|u_{l,k}|^2) = 1$, for $k \in \mathcal{K}_u$. $\mathbf{x}_{d,l}$ is an $M \times 1$ vector denoting downlink transmit signal in the l -th cell. Each BS has an average power constraint P_d .

We assume $\mathbf{G}_{u,jl}$ is an $M \times K_u$ matrix denoting the channel between the uplink users in the l -th cell and the j -th BS. The propagation channel model in our system considers both small-scale fading due to mobility and multipath, and large-scale fading due to geometric attenuation and shadowing effect, thus allowing arbitrary cell layout.

The uplink channel $\mathbf{G}_{u,jl}$ encompasses independent small-scale fading and large-scale fading

$$(\mathbf{G}_{u,jl})_{m,n} \triangleq g_{u,jmln} = h_{u,jmln} \sqrt{\beta_{u,jln}},$$

where $j, l \in \{1, \dots, L\}$, $m \in \{1, \dots, M\}$, $n \in \mathcal{K}_u$. $h_{u,jmln}$ is the small-scale fading value between the n -th uplink user in the l -th cell and the m -th antenna at the j -th BS, following independent and identically distributed (i.i.d.) circularly-symmetric complex Gaussian distribution $\mathcal{CN}(0, 1)$. We use $\beta_{u,jln}$ to model the path loss and shadow fading between the n -th uplink user in the l -th cell and the j -th BS, which is

independent of m . Such long-term parameters can be measured at the BS.

The BS-BS channel $\mathbf{V}_{j,l}$ is an $M \times M$ matrix denoting the channel between the l -th BS and the j -th BS, and $\mathbf{V}_{j,j}$ denotes the SI channel for the j -th full-duplex BS. We assume $\mathbf{V}_{j,l}$ contains i.i.d $\mathcal{CN}(0, \beta_{b,jl})$ elements. The imperfect transmit front-end chain is modeled as transmit noise $\mathbf{e}_{bs,j} \in \mathbb{C}^{M \times 1}$ added to each transmit antenna at the j -th full-duplex BS. And $\mathbf{e}_{bs,j}$ will propagate through the SI channel and follow $\mathcal{CN}(0, \frac{\kappa P_d}{M} \mathbf{I}_M)$ assuming equal power allocation among downlink users, where \mathbf{I}_M denotes an $M \times M$ identity matrix. The receiver thermal noise is denoted as $\mathbf{n}_{u,j}$ which contains i.i.d $\mathcal{CN}(0, \sigma^2)$ entries.

The j -th BS then performs SI cancellation by knowing its SI channel and its downlink signal. Hence from (5.1), we have

$$\mathbf{y}_{u,j} = \sum_{l=1}^L \mathbf{G}_{u,jl} \mathbf{x}_{u,l} + \sum_{l \neq j}^L \mathbf{V}_{j,l} \mathbf{x}_{d,l} + \mathbf{z}_{u,j}, \quad (5.2)$$

where $\mathbf{z}_{u,j} \sim \mathcal{CN}(0, (\sigma^2 + \kappa P_d \beta_{b,jj}) \mathbf{I}_M)$.

5.2.2 Downlink

The received signals for the K_d downlink users in the l -th cell can be expressed as a $K_d \times 1$ vector $\mathbf{y}_{d,l}$, given by

$$\mathbf{y}_{d,l} = \sum_{j=1}^L \mathbf{G}_{d,jl}^T \mathbf{x}_{d,j} + \sum_{j=1}^L \mathbf{F}_{lj} \mathbf{x}_{u,j} + \mathbf{J}_l + \mathbf{n}_{d,l}, \quad (5.3)$$

where $\mathbf{G}_{d,jl}$ is an $M \times K_d$ matrix denoting the channel between the downlink users in the l -th cell and the j -th BS, the downlink channel can be represented as $\mathbf{G}_{d,jl}^T$ and we have

$$(\mathbf{G}_{d,jl})_{m,k}^T \triangleq g_{d,jmlk}^T = h_{d,jmlk}^T \sqrt{\beta_{d,jlk}},$$

where $k \in \mathcal{K}_d$, the superscript “ T ” denotes transpose. $h_{d,jmlk}$ is the small-scale fading value between the k -th downlink user in the l -th cell and the m -th antenna at the j -th BS, with zero mean and unit variance. $\beta_{d,jlk}$ incorporates path loss and shadow fading between the k -th downlink user in the l -th cell and the j -th BS .

The UE-UE interference channel \mathbf{F}_{lj} is a $K_d \times K_u$ matrix denoting the interference channel from K_u uplink users in the j -th to K_d downlink users in the l -th cell; $\mathbf{J}_l = \begin{pmatrix} \text{diag}(\mathbf{S}_{ll})\mathbf{e}_{ue,l} \\ \mathbf{0} \end{pmatrix}$ is a $K_d \times 1$ vector, where \mathbf{S}_{ll} is a $K_f \times K_f$ matrix denoting the interference channels between full-duplex users in the l -th cell. The diagonal elements of \mathbf{S}_{ll} constitute SI channels for each full-duplex user in the l -th cell. And \mathbf{S}_{ll} is a sub-matrix of \mathbf{F}_{ll} , where $(\text{diag}(\mathbf{S}_{ll}))_k = (\mathbf{F}_{ll})_{k,k} \triangleq f_{lkk}$, $k \in \mathcal{K}_f$. We assume each entry in $(\mathbf{F}_{lj})_{k,n} \triangleq f_{lkjn}$ models both the large-scale and small-scale fading channel coefficient between the n -th uplink user in the j -th cell and the k -th downlink user in the l -th cell, and follows i.i.d. $\sim \mathcal{CN}(0, \beta_{l,lkjn})$, where $j, l \in \{1, \dots, L\}$ and $n \in \mathcal{K}_u, k \in \mathcal{K}_d$. The transmit noise at each full-duplex user in the l -th cell $\mathbf{e}_{ue,l} \in \mathbb{C}^{K_f \times 1}$ will propagate through the SI channel and follow $\mathcal{CN}(0, \kappa P_u \mathbf{I}_{K_f})$. The receiver thermal noise $\mathbf{n}_{d,l}$ follows $\sim \mathcal{CN}(0, \sigma^2 \mathbf{I}_{K_d})$.

Next, the k -th full-duplex user in the l -th cell where $k \in \mathcal{K}_f$, will perform SI cancellation by subtracting out its own interference from the received signal in (5.3). Thus we have

$$r_{d,lk} = \sum_{j=1}^L \mathbf{g}_{d,jlk}^T \mathbf{x}_{d,j} + \sum_{j=1}^L \sum_{n=1}^{K_u} \sqrt{P_u} f_{lkjn} u_{j,n} - \sqrt{P_u} f_{lkk} u_{l,k} + z_{d,lk}, \quad (5.4)$$

where $\mathbf{g}_{d,jlk}$ is the k -th column of matrix $\mathbf{G}_{d,jl}$ and $z_{d,lk} \sim \mathcal{CN}(0, (\sigma^2 + \kappa P_u \beta_{l,lk}))$.

The expressions of the received downlink signals for full-duplex users and half-duplex users will differ, because for a full-duplex user, after SI cancellation there is no self UE-UE interference but an additional transmit noise is added to the received

signal, while for a half-duplex downlink user, it will suffer the interference from all uplink users. Hence we can rewrite the received downlink signal for the k' -th half-duplex user in the l -th cell where $k' \in \mathcal{K}_h^d$ as

$$r_{d,lk'} = \sum_{j=1}^L \mathbf{g}_{d,jlk'}^T \mathbf{x}_{d,j} + \sum_{j=1}^L \sum_{n=1}^{K_u} \sqrt{P_u} f_{lk'jn} u_{j,n} + n_{d,lk'}, \quad (5.5)$$

where $n_{d,lk'}$ is the k' -th element in $\mathbf{n}_{d,l}$.

5.3 Achievable Rates in Full-Duplex Networks

In this section, we will derive the up- and downlink ergodic achievable rates in multi-cell MU-MIMO full-duplex networks. We first study the case of perfect channel state information (CSI) where the channel information is obtained perfectly at no cost. Next, we consider the channel estimation error, where CSI is estimated from uplink pilot sequences. We assume synchronized reception from all cells, which will reflect the worst possible scenario of pilot contamination [1].

5.3.1 Perfect channel state information

5.3.1.1 Uplink with maximum ratio combining

The j -th BS will receive data transmitted by its associated K_u uplink users, together with the interference from other cells. We apply a low-complexity linear receiver, i.e., maximum ratio combining for uplink signal detection. The j -th BS will multiply the received signal after SI cancellation by the conjugate-transpose of its uplink channel

$\mathbf{G}_{u,jj}^H$ to obtain a $K_u \times 1$ signal vector

$$\begin{aligned} \mathbf{r}_{u,j} &= \mathbf{G}_{u,jj}^H \mathbf{y}_{u,j} \\ &= \mathbf{G}_{u,jj}^H \mathbf{G}_{u,jj} \mathbf{x}_{u,j} + \sum_{l \neq j} \mathbf{G}_{u,jj}^H \mathbf{G}_{u,jl} \mathbf{x}_{u,l} + \sum_{l \neq j} \mathbf{G}_{u,jj}^H \mathbf{V}_{j,l} \mathbf{x}_{d,l} + \mathbf{G}_{u,jj}^H \mathbf{z}_{u,j}, \end{aligned} \quad (5.6)$$

where superscript “ H ” denotes conjugate-transpose, $\mathbf{y}_{u,j}$ is given in (5.2).

5.3.1.2 Downlink with conjugate beamforming

The l -th BS will transmit an $M \times 1$ downlink signal vector $\mathbf{x}_{d,l}$ by precoding the downlink messages using a conjugate beamforming linear precoder

$$\mathbf{x}_{d,l} = \frac{\mathbf{G}_{d,ll}^*}{\sqrt{\gamma_l}} \mathbf{s}_{d,l}, \quad (5.7)$$

where superscript “ $*$ ” denotes conjugate. $\mathbf{s}_{d,l} = \sqrt{\frac{P_d}{K_d}} \mathbf{d}_l$, $\mathbf{d}_l \triangleq [d_{l,1}, \dots, d_{l,K_d}]^T$ is a $K_d \times 1$ vector consisting of downlink messages of the K_d downlink users in the l -th cell with $\mathbb{E}(|d_{l,k}|^2) = 1, k \in \mathcal{K}_d$; γ_l is the l -th cell power normalization factor to meet the average power constraint such that $\mathbb{E}(\mathbf{x}_{d,l}^H \mathbf{x}_{d,l}) = P_d$, hence $\gamma_l = \frac{\mathbb{E}(\mathbf{d}_l^H \mathbf{G}_{d,ll}^T \mathbf{G}_{d,ll}^* \mathbf{d}_l)}{K_d} = \frac{M \sum_{k=1}^{K_d} \beta_{d,llk}}{K_d}$.

Substituting (5.7) into (5.4), we can first obtain the downlink signal at the k -th full-duplex user in the l -th cell where $k \in \mathcal{K}_f$ as

$$r_{d,lk} = \sum_{j=1}^L \sum_{i=1}^{K_d} \sqrt{\frac{P_d}{K_d \gamma_j}} \mathbf{g}_{d,jlk}^T \mathbf{g}_{d,jji}^* d_{j,i} + \sum_{j=1}^L \sum_{n=1}^{K_u} \sqrt{P_u} f_{lkjn} u_{j,n} - \sqrt{P_u} f_{lklk} u_{l,k} + z_{d,lk}. \quad (5.8)$$

Next, we substitute (5.7) into (5.5) to obtain the received downlink signal at the

k' -th half-duplex user in the l -th cell where $k' \in \mathcal{K}_h^d$ as

$$r_{d,lk'} = \sum_{j=1}^L \sum_{i=1}^{K_d} \sqrt{\frac{P_d}{K_d \gamma_j}} \mathbf{g}_{d,jlk'}^T \mathbf{g}_{d,jji}^* d_{j,i} + \sum_{j=1}^L \sum_{n=1}^{K_u} \sqrt{P_u f_{lk'jn}} u_{j,n} + n_{d,lk'}. \quad (5.9)$$

5.3.1.3 Ergodic achievable rates

The interference and noise terms in (5.6), (5.8) and (5.9) can be modeled as an additive independently Gaussian noise. By coding over infinitely large number of the realizations of the small-scale fading channels, we can obtain the ergodic achievable rate of the n -th uplink user in the j -th cell (bits/s/Hz) as

$$\tilde{R}_{u,jn}^{fd,p} = \mathbb{E} \left\{ \log_2 \left(1 + \frac{P_u \|\mathbf{g}_{u,jjn}\|^4}{P_u \sum_{(l,m) \neq (j,n)} |\mathbf{g}_{u,jjn}^H \mathbf{g}_{u,jlm}|^2 + I_{bs-bs} + \|\mathbf{g}_{u,jjn}\|^2 (\sigma^2 + \kappa P_d \beta_{b,jj})} \right) \right\}, \quad (5.10)$$

where $n \in \mathcal{K}_u$, $I_{bs-bs} = \sum_{l \neq j} \sum_{k \in \mathcal{K}_d} \frac{P_d}{K_d \gamma_l} |\mathbf{g}_{u,jjn}^H \mathbf{V}_j \mathbf{g}_{d,llk}^*|^2$. The notation of $\sum_{(l,m) \neq (j,n)}$ denotes the summation over all tuples $(l, m) \in \{1, \dots, L\} \times \mathcal{K}_u \setminus \{(l = j, m = n)\}$.

Similarly, the downlink ergodic achievable rates of the k -th full-duplex user and the k' -th half-duplex user in the l -th cell are respectively given as follows

$$\begin{aligned} \tilde{R}_{d,lk}^{fd,p} &= \mathbb{E} \left\{ \log_2 \left(1 + \frac{\frac{P_d}{K_d \gamma_l} \|\mathbf{g}_{d,llk}\|^4}{\sum_{(j,i) \neq (l,k)} \frac{P_d}{K_d \gamma_j} |\mathbf{g}_{d,jlk}^T \mathbf{g}_{d,jji}^*|^2 + I_{ue-ue}(k) - P_u |f_{lklk}|^2 + \sigma^2 + \kappa P_u \beta_{I,lklk}} \right) \right\}, \\ \tilde{R}_{d,lk'}^{fd,p} &= \mathbb{E} \left\{ \log_2 \left(1 + \frac{\frac{P_d}{K_d \gamma_l} \|\mathbf{g}_{d,llk'}\|^4}{\sum_{(j,i) \neq (l,k')} \frac{P_d}{K_d \gamma_j} |\mathbf{g}_{d,jlk'}^T \mathbf{g}_{d,jji}^*|^2 + I_{ue-ue}(k') + \sigma^2} \right) \right\}, \end{aligned} \quad (5.11)$$

where $k \in \mathcal{K}_f$, $k' \in \mathcal{K}_h^d$. $I_{ue-ue}(k) = \sum_{j=1}^L \sum_{n \in \mathcal{K}_u} P_u f_{lkjn}$. The notation of $\sum_{(j,i) \neq (l,k)}$ denotes the summation over all tuples $(j, i) \in \{1, \dots, L\} \times \mathcal{K}_d \setminus \{(j = l, i = k)\}$.

Proposition 5. *For perfect CSI, lower bounds on the ergodic achievable rates of*

multi-cell MU-MIMO full-duplex networks when $M \geq 3$ are given as

$$\begin{aligned}
\text{Uplink user: } R_{u,jn}^{fd,p} &= \log_2 \left(1 + \frac{P_u(M-1)\beta_{u,jjn}}{I_{up} + \sigma^2 + \kappa P_d \beta_{b,jj}} \right), \\
\text{Downlink, FD user: } R_{d,lk}^{fd,p} &= \log_2 \left(1 + \frac{\eta_l P_d (M-1)(M-2)\beta_{d,llk}^2}{I_{down}(k) - P_u \beta_{I,llkk} + \sigma^2 + \kappa P_u \beta_{I,llkk}} \right), \\
\text{Downlink, HD user: } R_{d,lk'}^{fd,p} &= \log_2 \left(1 + \frac{\eta_l P_d (M-1)(M-2)\beta_{d,llk'}^2}{I_{down}(k') + \sigma^2} \right),
\end{aligned} \tag{5.12}$$

where $n \in \mathcal{K}_u$, $k \in \mathcal{K}_f$, $k' \in \mathcal{K}_h^d$, $I_{up} = P_u \sum_{(l,m) \neq (j,n)} \beta_{u,jlm} + P_d \sum_{l \neq j} \beta_{b,jl}$, $I_{down}(k) = \sum_{i \neq k, i \in \mathcal{K}_d} \eta_l P_d \beta_{d,ulk} \beta_{d,lli} (M-2) + P_d \sum_{j \neq l} \beta_{d,jlk} + \sum_{j=1}^L \sum_{n \in \mathcal{K}_u} P_u \beta_{I,lnkn}$, and $\eta_l = \frac{1}{M \sum_{i \in \mathcal{K}_d} \beta_{d,lli}}$.

Proof. Based on Jensen's inequality and the convexity of $\log_2(1+x^{-1})$, we have $\mathbb{E}[\log_2(1+x^{-1})] \geq \log_2(1+\mathbb{E}^{-1}(x))$. Hence we can lower bound the ergodic achievable rate of the n -th uplink UE in the j -th cell in (5.10) as

$$\begin{aligned}
\tilde{R}_{u,jn}^{fd,p} &\geq R_{u,jn}^{fd,p} \triangleq \log_2 \left(1 + \right. \\
&\mathbb{E}^{-1} \left[\frac{P_u \sum_{(l,m) \neq (j,n)} |\mathbf{g}_{u,jjn}^H \mathbf{g}_{u,jlm}|^2 + I_{bs-bs} + \|\mathbf{g}_{u,jjn}\|^2 (\sigma^2 + \kappa P_d \beta_{b,jj})}{P_u \|\mathbf{g}_{u,jjn}\|^4} \right] \Bigg) \\
&= \log_2 \left(1 + \mathbb{E}^{-1} \left[\frac{P_u \sum_{(l,m) \neq (j,n)} |\tilde{g}_{u,jlm}|^2 + \sum_{l \neq j} \sum_{k \in \mathcal{K}_d} \frac{P_d}{K_d \gamma_l} |\tilde{v}_{jlk}|^2 + \sigma^2 + \kappa P_d \beta_{b,jj}}{P_u \|\mathbf{g}_{u,jjn}\|^2} \right] \right),
\end{aligned} \tag{5.13}$$

where $\tilde{g}_{u,jlm} \triangleq \frac{\mathbf{g}_{u,jjn}^H \mathbf{g}_{u,jlm}}{\|\mathbf{g}_{u,jjn}\|}$, $\tilde{v}_{jlk} \triangleq \frac{\mathbf{g}_{u,jjn}^H \mathbf{V}_{jl} \mathbf{g}_{d,llk}^*}{\|\mathbf{g}_{u,jjn}\|}$. Conditioned on $\mathbf{g}_{u,jjn}$, $\tilde{g}_{u,jlm} \sim$

$\mathcal{CN}(0, \beta_{u,jlm})$ and $\tilde{v}_{jlk} \sim \mathcal{CN}(0, M\beta_{b,jl}\beta_{d,ulk})$ are independent of $\mathbf{g}_{u,jjn}$. Thus we have

$$\begin{aligned} & \mathbb{E} \left[\frac{P_u \sum_{(l,m) \neq (j,n)} |\tilde{g}_{u,jlm}|^2 + \sum_{l \neq j} \sum_{k \in \mathcal{K}_d} \frac{P_d}{K_d \gamma_l} |\tilde{v}_{jlk}|^2 + \sigma^2 + \kappa P_d \beta_{b,jj}}{P_u \|\mathbf{g}_{u,jjn}\|^2} \right] \\ &= \left(\sum_{(l,m) \neq (j,n)} P_u \mathbb{E}[|\tilde{g}_{u,jlm}|^2] + \sum_{l \neq j} \sum_{k \in \mathcal{K}_d} \frac{P_d}{K_d \gamma_l} \mathbb{E}[|\tilde{v}_{jlk}|^2] + \sigma^2 + \kappa P_d \beta_{b,jj} \right) \mathbb{E} \left[\frac{1}{P_u \|\mathbf{g}_{u,jjn}\|^2} \right]. \end{aligned} \quad (5.14)$$

From Lemma 2.10 in [54], for a central Wishart matrix $\mathbf{W} \sim \mathcal{W}_m(n, \mathbf{I})$ with $n \geq m$, we have $\mathbb{E}[\text{tr}\{\mathbf{W}^{-1}\}] = \frac{m}{n-m}$ for $n > m$. Hence

$$\mathbb{E} \left[\frac{1}{P_u \|\mathbf{g}_{u,jjn}\|^2} \right] = \frac{1}{(M-1)P_u \beta_{u,jjn}} \text{ for } M \geq 2. \quad (5.15)$$

Combing (5.13), (5.14) and (5.15), we can obtain the uplink achievable rate in (5.12).

To derive the lower bound on the downlink achievable rate, we need to evoke the Lemma 2.10 in [54] again where $\mathbb{E}[\text{tr}\{\mathbf{W}^{-2}\}] = \frac{mn}{(n-m)^3 - (n-m)}$ for $n > m + 1$. Thus we have

$$\mathbb{E} \left[\frac{1}{\|\mathbf{g}_{d,ulk}\|^4} \right] = \frac{1}{(M-1)(M-2)\beta_{d,ulk}^2} \text{ for } M \geq 3. \quad (5.16)$$

Following the same approach used in the derivation of uplink rate, we can obtain the achievable rate of each downlink user given in proposition 5. The details are omitted to avoid redundancy. \square

5.3.2 Imperfect channel state information

In order to perform up- and downlink beamforming in MU-MIMO networks, the BS needs to know the up- and downlink channels for uplink coherent detection and downlink precoding. In this section, we will derive the ergodic achievable rates in

the presence of channel estimation error. In the full-duplex system, the up- and downlink channels are estimated through uplink training sequences, and thus the pilot overhead is only proportional to the number of users. Simultaneous up-and downlink data transmission starts after uplink training, as shown in Figure 5.2.

5.3.2.1 Pilot-aided channel estimation

During the uplink training period, within a coherence interval of T , $K_{tot} \triangleq K_u + K_d - K_f$ mutually orthogonal pilot sequences of length τ ($\tau \geq K_{tot}$) symbols are used to estimate the channels between each BS and its associated UEs. The same set of pilot sequences will be reused by L cells. The channel estimate will be corrupted by pilot contamination [1] due to the non-orthogonality of the reused pilots. We assume that each user has an average channel training power of P_{tr} , which is a parameter that depends on the length of the pilot sequences.

The j -th BS will correlate the received signal from uplink training with the pilot sequences assigned for the k -th user to obtain an M -dimensional vector $\mathbf{y}_{tr,jk}$

$$\mathbf{y}_{tr,jk} = \mathbf{g}_{\Phi,jjk} + \sum_{l \neq j}^L \mathbf{g}_{\Phi,jlk} + \frac{\mathbf{n}_{jk}}{\sqrt{P_{tr}}}, \quad (5.17)$$

where $\Phi \in \{u, d\}$, $k \in \mathcal{K}_u \cup \mathcal{K}_h^d$, $\mathbf{g}_{\Phi,jjk}$ is the k -th column of the channel matrix $\mathbf{G}_{\Phi,jj}$, and $\mathbf{n}_{jk} \sim \mathcal{CN}(\mathbf{0}, \sigma^2 \mathbf{I}_M)$. For the full-duplex users, due to the channel reciprocity, we have $\mathbf{g}_{u,jji} = \mathbf{g}_{d,jji}$ for $i \in \mathcal{K}_f$. Hence the estimated uplink channels for full-duplex users can be used for downlink precoding.

The MMSE channel estimate of the k -th user in the j -th cell $\mathbf{g}_{\Phi,jjk}$ can be obtained as [55]

$$\hat{\mathbf{g}}_{\Phi,jjk} = \frac{P_{tr} \beta_{\Phi,jjk}}{\lambda_{\Phi,jk}} \left(\sum_{l=1}^L \mathbf{g}_{\Phi,jlk} + \frac{\mathbf{n}_{jk}}{\sqrt{P_{tr}}} \right), \quad (5.18)$$

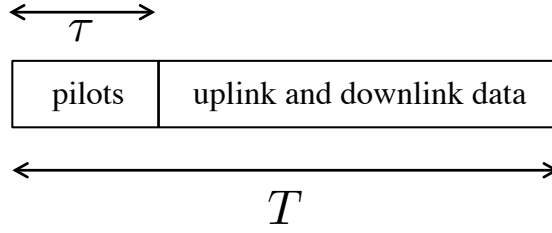


Figure 5.2: Uplink channel training in full-duplex networks.

where $\lambda_{\Phi,jk} = \sigma^2 + P_{tr} \sum_{l=1}^L \beta_{\Phi,jlk}$, and $\hat{\mathbf{g}}_{\Phi,jjk} \sim \mathcal{CN}\left(\mathbf{0}, \frac{P_{tr} \beta_{\Phi,jjk}^2}{\lambda_{\Phi,jk}} \mathbf{I}_M\right)$

Due to the orthogonality principle of the MMSE estimator, the true channel can be decomposed as the estimated channel and channel estimation error. Hence we have

$$\mathbf{g}_{\Phi,jjk} = \hat{\mathbf{g}}_{\Phi,jjk} + \boldsymbol{\epsilon}_{\Phi,jjk}, \quad (5.19)$$

where $\boldsymbol{\epsilon}_{\Phi,jjk} \sim \mathcal{CN}\left(\mathbf{0}, \frac{\beta_{\Phi,jjk}(\sigma^2 + P_{tr} \sum_{l \neq j} \beta_{\Phi,jlk})}{\lambda_{\Phi,jk}} \mathbf{I}_M\right)$, and the error $\boldsymbol{\epsilon}_{\Phi,jjk}$ is independent of the estimate $\hat{\mathbf{g}}_{\Phi,jjk}$.

5.3.2.2 Uplink and downlink data transmission

In the uplink, the j -th BS will apply maximum ratio combining detector by multiplying the conjugate-transpose of channel estimate $\hat{\mathbf{G}}_{u,jj}^H$ with the received signal

$$\mathbf{r}_{u,j} = \hat{\mathbf{G}}_{u,jj}^H \mathbf{y}_{u,j} \quad (5.20)$$

$$= \hat{\mathbf{G}}_{u,jj}^H \mathbf{G}_{u,jj} \mathbf{x}_{u,j} + \sum_{l \neq j} \hat{\mathbf{G}}_{u,jj}^H \mathbf{G}_{u,jl} \mathbf{x}_{u,l} + \sum_{l \neq j} \hat{\mathbf{G}}_{u,jj}^H \mathbf{V}_{j,l} \mathbf{x}_{d,l} + \hat{\mathbf{G}}_{u,jj}^H \mathbf{z}_{u,j} \quad (5.21)$$

$$= \hat{\mathbf{G}}_{u,jj}^H \hat{\mathbf{G}}_{u,jj} \mathbf{x}_{u,j} + \hat{\mathbf{G}}_{u,jj}^H \mathbf{E}_{u,jj} \mathbf{x}_{u,j} + \sum_{l \neq j} \hat{\mathbf{G}}_{u,jj}^H \mathbf{G}_{u,jl} \mathbf{x}_{u,l} + \sum_{l \neq j} \hat{\mathbf{G}}_{u,jj}^H \mathbf{V}_{j,l} \mathbf{x}_{d,l} + \hat{\mathbf{G}}_{u,jj}^H \mathbf{z}_{u,j} \quad (5.22)$$

where the k -th column of $\mathbf{E}_{u,jj}$ is $\boldsymbol{\epsilon}_{u,jjk}$, and (5.22) follows from $\mathbf{G}_{u,jj} = \hat{\mathbf{G}}_{u,jj} + \mathbf{E}_{u,jj}$.

In the downlink, the l -th BS will employ conjugate beamforming to precode the downlink messages using the channel estimate $\hat{\mathbf{G}}_{d,ll}$, and transmit an $M \times 1$ signal vector $\mathbf{x}_{d,l}$,

$$\mathbf{x}_{d,l} = \frac{\hat{\mathbf{G}}_{d,ll}^*}{\sqrt{\tilde{\gamma}_l}} \mathbf{s}_{d,l}, \quad (5.23)$$

$$\text{where } \tilde{\gamma}_l = \frac{\mathbb{E}(\mathbf{d}_l^H \hat{\mathbf{G}}_{d,ll}^T \hat{\mathbf{G}}_{d,ll}^* \mathbf{d}_l)}{K_d} = \frac{M}{K_d} \sum_{i=1}^{K_d} \frac{P_{tr} \beta_{d,lli}^2}{\sigma^2 + P_{tr} \sum_{j=1}^L \beta_{d,lji}}.$$

We assume that the downlink users do not have the channel estimate for reception (otherwise, additional pilot overhead needs to be considered), but are aware of the channel statistics. And each downlink user can perfectly track the average effective channel gain. Thus the received downlink signal can be decomposed as an average effective channel gain times the desired signal symbol, plus a composite term to denote effective noise as in [55].

Substituting (5.23) into (5.4), the received downlink signal at the k -th full-duplex user in the l -th cell where $k \in \mathcal{K}_f$ can be written as

$$\begin{aligned} r_{d,lk} = & \sqrt{\frac{P_d}{K_d \tilde{\gamma}_l}} \mathbb{E}[\mathbf{g}_{d,llk}^T \mathbf{v}_{lk}] d_{l,k} + \sqrt{\frac{P_d}{K_d \tilde{\gamma}_l}} (\mathbf{g}_{d,llk}^T \mathbf{v}_{lk} - \mathbb{E}[\mathbf{g}_{d,llk}^T \mathbf{v}_{lk}]) d_{l,k} \\ & + \sum_{(j,i) \neq (l,k)} \sqrt{\frac{P_d}{K_d \tilde{\gamma}_j}} \mathbf{g}_{d,jlk}^T \mathbf{v}_{ji} d_{j,i} + \sum_{j=1}^L \sum_{n=1}^{K_u} \sqrt{P_u} f_{lkjn} u_{j,n} - \sqrt{P_u} f_{lklk} u_{l,k} + z_{d,lk}. \end{aligned} \quad (5.24)$$

where $\mathbf{v}_{lk} = \hat{\mathbf{g}}_{d,llk}^*$ for conjugate beamforming precoder.

Similarly, we substitute (5.23) into (5.5) to obtain the downlink signal at the k' -th

half-duplex user in the l -th cell where $k' \in \mathcal{K}_h^d$

$$\begin{aligned}
r_{d,lk'} &= \sqrt{\frac{P_d}{K_d \tilde{\gamma}_l}} \mathbb{E}[\mathbf{g}_{d,ulk'}^T \mathbf{v}_{lk'}] d_{l,k'} + \sqrt{\frac{P_d}{K_d \tilde{\gamma}_l}} (\mathbf{g}_{d,ulk'}^T \mathbf{v}_{lk'} - \mathbb{E}[\mathbf{g}_{d,ulk'}^T \mathbf{v}_{lk'}]) d_{l,k'} \\
&+ \sum_{(j,i) \neq (l,k')} \sqrt{\frac{P_d}{K_d \tilde{\gamma}_j}} \mathbf{g}_{d,jlk'}^T \mathbf{v}_{ji} d_{j,i} + \sum_{j=1}^L \sum_{n=1}^{K_u} \sqrt{P_u} f_{lk'jn} u_{j,n} + n_{d,lk'}.
\end{aligned} \tag{5.25}$$

5.3.2.3 Ergodic achievable rates

For the uplink, the channel estimate will be treated as the true channel. Hence we can obtain the ergodic achievable rate for the n -th uplink user in the j -th cell as follows:

$$\tilde{R}_{u,jn}^{fd,ip} = \mathbb{E} \left\{ \log_2 \left(1 + \frac{P_u \|\hat{\mathbf{g}}_{u,jjn}\|^4}{P_u |\hat{\mathbf{g}}_{u,jjn}^H \boldsymbol{\epsilon}_{u,jjn}|^2 + P_u \sum_{(l,m) \neq (j,n)} |\hat{\mathbf{g}}_{u,jjn}^H \mathbf{g}_{u,jlm}|^2 + I_{bs-bs}^{ip} + N} \right) \right\}, \tag{5.26}$$

where $n \in \mathcal{K}_u$, $I_{bs-bs}^{ip} = \sum_{l \neq j} \sum_{k \in \mathcal{K}_d} \frac{P_d}{K_d \tilde{\gamma}_l} |\hat{\mathbf{g}}_{u,jjn}^H \mathbf{V}_{jl} \hat{\mathbf{g}}_{d,ulk}^*|^2$, $N = \|\hat{\mathbf{g}}_{u,jjn}\|^2 (\sigma^2 + \kappa P_d \beta_{b,jj})$.

For the downlink, the effective noise is uncorrelated with the signal, using worst-case independent Gaussian noise results in [56], the downlink ergodic achievable rates of the k -th full-duplex user and the k' -th half-duplex user in the l -th cell are respectively given as

$$\begin{aligned}
R_{d,lk}^{fd,ip} &= \log_2 \left(1 + \frac{\frac{P_d}{K_d \tilde{\gamma}_l} |\mathbb{E}[\mathbf{g}_{d,ulk}^T \hat{\mathbf{g}}_{d,ulk}^*]|^2}{\frac{P_d}{K_d \tilde{\gamma}_l} \text{var}[\mathbf{g}_{d,ulk}^T \hat{\mathbf{g}}_{d,ulk}^*] + I_{other}(k) - P_u \mathbb{E}[|f_{lk}|^2] + \sigma^2 + \kappa P_u \beta_{I,klk}} \right), \\
R_{d,lk'}^{fd,ip} &= \log_2 \left(1 + \frac{\frac{P_d}{K_d \tilde{\gamma}_l} |\mathbb{E}[\mathbf{g}_{d,ulk'}^T \hat{\mathbf{g}}_{d,ulk'}^*]|^2}{\frac{P_d}{K_d \tilde{\gamma}_l} \text{var}[\mathbf{g}_{d,ulk'}^T \hat{\mathbf{g}}_{d,ulk'}^*] + I_{other}(k') + \sigma^2} \right),
\end{aligned} \tag{5.27}$$

where $k \in \mathcal{K}_f$, $k' \in \mathcal{K}_h^d$. $I_{other}(k) = \sum_{(j,i) \neq (l,k)} \frac{P_d}{K_d \tilde{\gamma}_j} \mathbb{E}[|\mathbf{g}_{d,jlk}^T \hat{\mathbf{g}}_{d,jji}^*|^2] + \sum_{j=1}^L \sum_{n \in \mathcal{K}_u} P_u \mathbb{E}[|f_{lkjn}|^2]$.

The notation $\text{var}[x] \triangleq \mathbb{E}[(x - \mu)(x - \mu)^H]$, $\mathbb{E}[x] = \mu$.

Proposition 6. *For imperfect CSI with MMSE estimation, the following sets of rates are achievable in multi-cell MU-MIMO full-duplex networks when $M \geq 3$*

$$\begin{aligned}
\text{Uplink user: } R_{u,jn}^{fd,ip} &= \log_2 \left(1 + \frac{P_{tr} P_u (M-1) \beta_{u,jjn}^2}{P_u \beta_{u,jjn} (\sigma^2 + P_{tr} \sum_{l \neq j} \beta_{u,jln}) + \tilde{I}_{up} + \tilde{N}} \right), \\
\text{Downlink, FD user: } R_{d,lk}^{fd,ip} &= \log_2 \left(1 + \frac{\tilde{\eta}_l P_{tr} P_d M \beta_{d,llk}^4}{\lambda_{d,lk}^2 (\tilde{I}_{down}(k) - P_u \beta_{I,klk} + \sigma^2 + \kappa P_u \beta_{I,klk})} \right), \\
\text{Downlink, HD user: } R_{d,lk'}^{fd,ip} &= \log_2 \left(1 + \frac{\tilde{\eta}_l P_{tr} P_d M \beta_{d,llk'}^4}{\lambda_{d,lk'}^2 (\tilde{I}_{down}(k') + \sigma^2)} \right),
\end{aligned} \tag{5.28}$$

where $\tilde{I}_{up} = P_{tr} P_u \sum_{l \neq j} \left[(M+1) \beta_{u,jln}^2 + \sum_{l_1 \neq l} \beta_{u,jl_1 n} \beta_{u,jln} + \frac{\beta_{u,jln} \sigma^2}{P_{tr}} \right]$, $\tilde{N} = \lambda_{u,jn} (P_d \sum_{l \neq j} \beta_{b,jl} + P_u \sum_{l=1}^L \sum_{m \in \mathcal{K}_u, m \neq n} \beta_{u,jlm} + \sigma^2 + \kappa P_d \beta_{b,jj})$, $\tilde{I}_{down}(k) = \frac{\tilde{\eta}_l P_d \beta_{d,llk}^3}{\lambda_{d,lk}} + \sum_{j \neq l} \frac{\tilde{\eta}_j P_{tr} P_d (M+1) \beta_{d,jlk}^2 \beta_{d,jjk}^2}{\lambda_{d,jk}^2} + \sum_{j \neq l} \frac{\tilde{\eta}_j P_d \beta_{d,jjk}^2 (\sigma^2 + P_{tr} \sum_{l_1 \neq l} \beta_{d,jl_1 k}) \beta_{d,jlk}}{\lambda_{d,jk}^2} + \sum_{j=1}^L \sum_{i \neq k, i \in \mathcal{K}_d} \frac{\tilde{\eta}_j P_d \beta_{d,jji}^2 \beta_{d,jlk}}{\lambda_{d,ji}} + \sum_{j=1}^L \sum_{n \in \mathcal{K}_u} P_u \beta_{I,lnk}$.
 $\tilde{\eta}_l = \left(\sum_{i \in \mathcal{K}_d} \frac{\beta_{d,lli}^2}{\lambda_{d,li}} \right)^{-1}$, $n \in \mathcal{K}_u$, $k \in \mathcal{K}_f$, $k' \in \mathcal{K}_h^d$.

Proof. Similar to the proof of Proposition 5, applying Jensen's inequality, we can lower bound the ergodic achievable rate of the n -th uplink user in the j -th cell in (5.26) as

$$\begin{aligned}
\tilde{R}_{u,jn}^{fd,ip} &\geq R_{u,jn}^{fd,ip} \triangleq \log_2 \left(1 + \right. \\
&\mathbb{E}^{-1} \left[\frac{P_u |\tilde{\epsilon}_{jjn}|^2 + P_u \sum_{(l,m) \neq (j,n)} |\tilde{g}_{u,jlm}|^2 + \sum_{l \neq j} \sum_{k \in \mathcal{K}_d} \frac{P_d}{K_d \gamma_l} |\tilde{v}_{jlk}|^2 + \sigma^2 + \kappa P_d \beta_{b,jj}}{P_u \|\hat{\mathbf{g}}_{u,jjn}\|^2} \right] \Big)
\end{aligned} \tag{5.29}$$

where $\tilde{\epsilon}_{jjn} \triangleq \frac{\hat{\mathbf{g}}_{u,jjn}^H \boldsymbol{\epsilon}_{u,jjn}}{\|\hat{\mathbf{g}}_{u,jjn}\|}$, $\tilde{g}_{u,jlm} \triangleq \frac{\hat{\mathbf{g}}_{u,jjn}^H \mathbf{g}_{u,jlm}}{\|\hat{\mathbf{g}}_{u,jjn}\|}$, $\tilde{v}_{jlk} \triangleq \frac{\hat{\mathbf{g}}_{u,jjn}^H \mathbf{V}_{jl} \hat{\mathbf{g}}_{d,llk}^*}{\|\hat{\mathbf{g}}_{u,jjn}\|}$. Conditioned on $\hat{\mathbf{g}}_{u,jjn}$, $\tilde{\epsilon}_{jjn} \sim \mathcal{CN} \left(0, \frac{\beta_{u,jjk} (\sigma^2 + P_{tr} \sum_{l \neq j} \beta_{u,jlk})}{\lambda_{u,jk}} \right)$, $\tilde{v}_{jlk} \sim \mathcal{CN} \left(0, M \beta_{b,jl} \frac{P_{tr} \beta_{d,llk}^2}{\lambda_{d,lk}} \right)$ and $\tilde{g}_{u,jlm} \sim (0, \text{var}(\tilde{g}_{u,jlm}))$ are independent of $\hat{\mathbf{g}}_{u,jjn}$. Using (5.18), we have

$$\tilde{g}_{u,jlm} = \frac{P_{tr} \beta_{u,jjn}}{\lambda_{u,jn}} \left(\sum_{l_1=1}^L \mathbf{g}_{u,jl_1 n}^H + \frac{\mathbf{n}_{jn}^H}{\sqrt{P_{tr}}} \right) \frac{\mathbf{g}_{u,jlm}}{\|\hat{\mathbf{g}}_{u,jjn}\|}. \tag{5.30}$$

Evoking Lemma 2.9 in [54], where for a central Wishart matrix $\mathbf{W} \sim \mathcal{W}_m(n, \mathbf{I})$ with $n \geq m$, $\mathbb{E}[\text{tr}\{\mathbf{W}^2\}] = mn(m+n)$, we can calculate the variance of $\tilde{g}_{u,jlm}$ as

$$\mathbb{E}[|\tilde{g}_{u,jlm}|^2] = \begin{cases} \frac{P_{tr}}{\lambda_{u,jn}} \left[(M+1)\beta_{u,jln}^2 + \sum_{l_1 \neq l} \beta_{u,jl_1n} \beta_{u,jln} + \frac{\beta_{u,jln} \sigma^2}{P_{tr}} \right] & m = n, l \neq j \\ \beta_{u,jlm} & m \neq n. \end{cases} \quad (5.31)$$

Now we can rewrite the expectation in (5.29) as

$$\begin{aligned} & \mathbb{E} \left[\frac{P_u |\tilde{c}_{jjn}|^2 + P_u \sum_{(l,m) \neq (j,n)} |\tilde{g}_{u,jlm}|^2 + \sum_{l \neq j} \sum_{k \in \mathcal{K}_d} \frac{P_d}{K_d \gamma_l} |\tilde{v}_{jlk}|^2 + \sigma^2 + \kappa P_d \beta_{b,jj}}{P_u \|\hat{\mathbf{g}}_{u,jjn}\|^2} \right] \\ &= \left(P_u \mathbb{E}[|\tilde{c}_{jjn}|^2] + P_u \sum_{(l,m) \neq (j,n)} \mathbb{E}[|\tilde{g}_{u,jlm}|^2] + \sum_{l \neq j} \sum_{k \in \mathcal{K}_d} \frac{P_d}{K_d \gamma_l} \mathbb{E}[|\tilde{v}_{jlk}|^2] + \sigma^2 + \kappa P_d \beta_{b,jj} \right) \mathbb{E} \left[\frac{1}{P_u \|\hat{\mathbf{g}}_{u,jjn}\|^2} \right]. \end{aligned} \quad (5.32)$$

Combing (5.29), (5.31) and (5.32), we can obtain the uplink achievable rate in (5.28).

For the downlink achievable rate in (5.27), we first compute $\mathbb{E}[\mathbf{g}_{d,uk}^T \hat{\mathbf{g}}_{d,uk}^*]$. Let $\mu = \mathbf{g}_{d,uk}^T \hat{\mathbf{g}}_{d,uk}^*$, since $\mathbf{g}_{d,uk} = \hat{\mathbf{g}}_{d,uk} + \boldsymbol{\epsilon}_{d,uk}$ and $\hat{\mathbf{g}}_{d,uk}$ is independently of $\boldsymbol{\epsilon}_{d,uk}$, we have

$$\begin{aligned} \mathbb{E}[\mu] &= \mathbb{E}[(\hat{\mathbf{g}}_{d,uk}^T + \boldsymbol{\epsilon}_{d,uk}^T) \hat{\mathbf{g}}_{d,uk}^*] \\ &= \mathbb{E}[\|\hat{\mathbf{g}}_{d,uk}\|^2] = \frac{M P_{tr} \beta_{d,uk}^2}{\lambda_{d,uk}}. \end{aligned} \quad (5.33)$$

Again invoking Lemma 2.9 in [54], we have

$$\begin{aligned} \mathbb{E}[\mu^2] &= \mathbb{E}[\|\hat{\mathbf{g}}_{d,uk}\|^4] + \mathbb{E}[\boldsymbol{\epsilon}_{d,uk}^T \hat{\mathbf{g}}_{d,uk}^* \hat{\mathbf{g}}_{d,uk}^T \boldsymbol{\epsilon}_{d,uk}^*] \\ &= \frac{M(M+1)P_{tr}^2 \beta_{d,uk}^4 + M P_{tr} \beta_{d,uk}^3 (\sigma^2 + P_{tr} \sum_{j \neq l} \beta_{d,ljk})}{\lambda_{d,uk}^2}. \end{aligned} \quad (5.34)$$

Since $\text{var} [\mathbf{g}_{d,ulk}^T \hat{\mathbf{g}}_{d,ulk}^*] \triangleq \text{var}(\mu) = \mathbb{E}(\mu^2) - \mathbb{E}^2(\mu)$, we can obtain that

$$\text{var}(\mu) = \frac{MP_{tr}\beta_{d,ulk}^3}{\lambda_{d,lk}}. \quad (5.35)$$

Next, we compute $\mathbb{E} [|\mathbf{g}_{d,jlk}^T \hat{\mathbf{g}}_{d,jji}^*|^2]$ as

$$\mathbb{E} [|\mathbf{g}_{d,jlk}^T \hat{\mathbf{g}}_{d,jji}^*|^2] = \begin{cases} \frac{MP_{tr}^2\beta_{d,jjk}^2}{\lambda_{d,jk}^2} \left[(M+1)\beta_{d,jlk}^2 + \sum_{l_1 \neq l} \beta_{d,jl_1k} \beta_{d,jlk} + \frac{\beta_{d,jlk}\sigma^2}{P_{tr}} \right] & i = k, j \neq l \\ \frac{MP_{tr}\beta_{d,jji}^2\beta_{d,jlk}}{\lambda_{d,ji}} & i \neq k. \end{cases} \quad (5.36)$$

The rest terms in (5.27) can be calculated easily, and thus the details are omitted. Combing all the results above, we can obtain downlink achievable rate given in proposition 6. \square

5.3.3 TDD baseline system

We use TDD system as a baseline half-duplex system for comparison since both full-duplex and TDD systems use uplink training for channel estimation.* Compared with a full-duplex system, in a TDD system, the uplink does not have BS-BS interference and transmit noise which accounts for imperfect FD radios, and the downlink does not have UE-UE interference and transmit noise. We assume the corresponding TDD system has an uplink and downlink user sets of \mathcal{K}_u and \mathcal{K}_d , respectively, with the same total number of uplink and downlink users as in the full-duplex system, i.e., $|\mathcal{K}_u| = K_u$ and $|\mathcal{K}_d| = K_d$. For the TDD baseline system, the up- and downlink transmissions are in two different time slots, and we assume an equal time sharing between up- and downlink transmission.

*FDD system requires downlink training with channel feedback which incurs a much higher pilot overhead as the overhead is not only proportional to the number of users but also the number of BS antennas.

The up- and downlink ergodic achievable rates in a TDD system under perfect CSI assumption are given as

$$\begin{aligned} \text{Uplink user: } R_{u,jn}^{tdd,p} &= \frac{1}{2} \mathbb{E} \left\{ \log_2 \left(1 + \frac{P_u \|\mathbf{g}_{u,jjn}\|^4}{P_u \sum_{(l,m) \neq (j,n)} |\mathbf{g}_{u,jjn}^H \mathbf{g}_{u,jlm}|^2 + \|\mathbf{g}_{u,jjn}\|^2 \sigma^2} \right) \right\}, \\ \text{Downlink user: } R_{d,lk}^{tdd,p} &= \frac{1}{2} \mathbb{E} \left\{ \log_2 \left(1 + \frac{\frac{P_d}{K_d \tilde{\gamma}_l} \|\mathbf{g}_{d,llk}\|^4}{\sum_{(j,i) \neq (l,k)} \frac{P_d}{K_d \tilde{\gamma}_j} |\mathbf{g}_{d,jlk}^T \mathbf{g}_{d,jji}^*|^2 + \sigma^2} \right) \right\}, \end{aligned} \quad (5.37)$$

where $\gamma_l = \frac{M \sum_{k=1}^{K_d} \beta_{d,llk}}{K_d}$, $n \in \mathcal{K}_u$, $k \in \mathcal{K}_d$.

When training sequences are used for channel estimation, within a coherence interval T , K_u mutually orthogonal pilot sequences of length τ_u ($\tau_u \geq K_u$) are used for the uplink users and K_d mutually orthogonal pilot sequences of length τ_d ($\tau_d \geq K_d$) are used for the downlink users. The same sets of training sequences are also reused by all cells. The corresponding up- and downlink ergodic achievable rates in TDD system are given

$$\begin{aligned} \text{Uplink user: } R_{u,jn}^{tdd,ip} &= \frac{1}{2} \mathbb{E} \left\{ \log_2 \left(1 + \frac{P_u \|\hat{\mathbf{g}}_{u,jjn}\|^4}{P_u |\hat{\mathbf{g}}_{u,jjn}^H \boldsymbol{\epsilon}_{u,jjn}|^2 + P_u \sum_{(l,m) \neq (j,n)} |\hat{\mathbf{g}}_{u,jjn}^H \mathbf{g}_{u,jlm}|^2 + N'} \right) \right\}, \\ \text{Downlink user: } R_{d,lk}^{tdd,ip} &= \frac{1}{2} \mathbb{E} \left\{ \log_2 \left(1 + \frac{\frac{P_d}{K_d \tilde{\gamma}_l} |\mathbb{E} [\mathbf{g}_{d,llk}^T \hat{\mathbf{g}}_{d,llk}^*]|^2}{Z' + \sigma^2} \right) \right\}, \end{aligned} \quad (5.38)$$

where $N' = \|\hat{\mathbf{g}}_{u,jjn}\|^2 \sigma^2$, $n \in \mathcal{K}_u$, $k \in \mathcal{K}_d$, and $Z' = \frac{P_d}{K_d \tilde{\gamma}_l} |\mathbf{g}_{d,llk}^T \hat{\mathbf{g}}_{d,llk}^* - \mathbb{E}[\mathbf{g}_{d,llk}^T \hat{\mathbf{g}}_{d,llk}^*]|^2 + \sum_{(j,i) \neq (l,k)} \frac{P_d}{K_d \tilde{\gamma}_j} |\mathbf{g}_{d,jlk}^T \mathbf{v}_{ji} d_{j,i}|^2$.

Note that the uplink and downlink ergodic achievable rates in the baseline TDD system follow [3] and [56] but without lower bounding the achievable rates, as we will use them to compute the full-duplex versus half-duplex rate ratios in the next section.

5.4 Large-Scale full-duplex System Performance

While the general ergodic achievable rates in the full-duplex system are given in the previous section, it is of interest to study the impact of large antenna arrays at BSs as the next generation of wireless systems will employ significantly more antennas at the infrastructure nodes [57]. In this section, we will investigate large-scale system performance as the number of full-duplex BS antennas, M , becomes arbitrarily large.

5.4.1 Leveraging large antenna arrays for multi-cell interference mitigation

In this section, we will show that using large BS antenna arrays can mitigate multi-cell interference in the full-duplex system. With increasing number of BS antennas, the signal strength will become stronger due to beamforming, and the transmit power can be scaled down proportionally to maintain the same quality-of-service. In what follows, we will present two theorems which characterize the asymptotic full-duplex spectral efficiency gain over TDD system under both perfect and imperfect CSI assumptions.

Theorem 8 (Asymptotic FD spectral efficiency gain with perfect CSI). *For perfect CSI, we scale the transmit power of each node proportional to $1/M$ as $P_u = E_u/M$ and $P_d = E_d/M$, where E_u and E_d are fixed. As $M \rightarrow \infty$, the full-duplex spectral efficiency gains over the TDD system in the uplink and downlink, denoted by Gain_u^p and Gain_d^p , respectively, are given below, where fixed asymptotic up- and downlink rates*

are maintained.

$$\begin{aligned} \text{Gain}_u^p &\triangleq \lim_{M \rightarrow \infty} \frac{\sum_{j=1}^L \sum_{n \in \mathcal{K}_u} R_{u,jn}^{fd,p}}{\sum_{j=1}^L \sum_{n \in \mathcal{K}_u} R_{u,jn}^{tdd,p}} = 2, \\ \text{Gain}_d^p &\triangleq \lim_{M \rightarrow \infty} \frac{\sum_{l=1}^L \sum_{k \in \mathcal{K}_d} R_{d,lk}^{fd,p}}{\sum_{l=1}^L \sum_{k \in \mathcal{K}_d} R_{d,lk}^{tdd,p}} = 2. \end{aligned} \quad (5.39)$$

The asymptotic ergodic achievable rate of the n -th uplink user in the j -th cell and the achievable rate of the k -th downlink user in the l -th cell are given below,

$$\begin{aligned} R_{u,jn}^{fd,p} &\rightarrow \log_2 \left(1 + \frac{\beta_{u,jjn} E_u}{\sigma^2} \right), \quad n \in \mathcal{K}_u \\ R_{d,lk}^{fd,p} &\rightarrow \log_2 \left(1 + \frac{\beta_{d,llk}^2 E_d}{\sum_{i \in \mathcal{K}_d} \beta_{d,lli} \sigma^2} \right), \quad k \in \mathcal{K}_d. \end{aligned} \quad (5.40)$$

Proof. For two mutually independent $M \times 1$ vectors $\mathbf{a} \triangleq [a_1, \dots, a_M]^T$ and $\mathbf{b} \triangleq [b_1, \dots, b_M]^T$ whose entries are i.i.d. zero-mean random variables with $\mathbb{E}(|a_i|^2) = \sigma_a^2$ and $\mathbb{E}(|b_i|^2) = \sigma_b^2$, $\forall i \in \{1, \dots, M\}$. By law of large numbers, we have the following almost sure convergence according to [58],

$$\frac{1}{M} \mathbf{a}^H \mathbf{a} \xrightarrow{a.s.} \sigma_a^2, \quad \frac{1}{M} \mathbf{a}^H \mathbf{b} \xrightarrow{a.s.} 0, \quad \text{as } M \rightarrow \infty. \quad (5.41)$$

Under the favorable propagation condition in [1] where the fast fading channels are i.i.d. with zero mean and unit variance, from (5.44), in the limit of M , we have $\lim_{M \rightarrow \infty} \frac{\mathbf{G}_{u,jl}^H \mathbf{G}_{u,jl}}{M} = \mathbf{D}_{u,jl} \delta_{jl}$, $\lim_{M \rightarrow \infty} \frac{\mathbf{G}_{d,jl}^H \mathbf{G}_{d,jl}}{M} = \mathbf{D}_{d,jl} \delta_{jl}$, where $\mathbf{D}_{u,jl}$ is a $K_u \times K_u$ diagonal matrix, and each diagonal element is $(\mathbf{D}_{u,jl})_n = \beta_{u,jln}$; $\mathbf{D}_{d,jl}$ is a $K_d \times K_d$ diagonal matrix, and each diagonal element is $(\mathbf{D}_{d,jl})_k = \beta_{d,jlk}$; $\delta_{jl} = 1$ for $j = l$, $\delta_{jl} = 0$ for $j \neq l$. By substituting $P_u = E_u/M$ and $P_d = E_d/M$ into (5.12) and (5.37), we can obtain the desired results as $M \rightarrow \infty$. \square

Remark 5. When a full-duplex BS employs a large antenna array, the transmit power

of each node can possibly be scaled down proportionally to $1/M^C$ to achieve the same rate. As $M \rightarrow \infty$, $1/M$ is the fastest rate at which we can scale down the transmit power to maintain fixed asymptotic up- and downlink rates. Otherwise, if $C > 1$, the rates will go to zero and if $C < 1$, the rates will go to infinity. The same power scaling law in the half-duplex system [3] is also preserved in the full-duplex system despite increased interference in the full-duplex system. And full-duplex system asymptotically doubles the spectral efficiency over TDD system since all K_u uplink streams and K_d downlink streams can be supported in the same time-frequency slot.

Theorem 9 (Asymptotic FD spectral efficiency gain with imperfect CSI). *For imperfect CSI with an MMSE estimator, we scale the power of each node for channel training and data transmission proportional to $1/\sqrt{M}$ as $P_{tr} = E_{tr}/\sqrt{M}$, $P_u = E_u/\sqrt{M}$ and $P_d = E_d/\sqrt{M}$, where E_{tr} , E_u and E_d are fixed. Within a coherence interval T , let $\tau_u = K_u$, $\tau_d = K_d$ and $\tau = K_u + K_d - K_f$. As $M \rightarrow \infty$, the full-duplex spectral efficiency gains over the TDD system in the uplink and downlink, denoted by Gain_u^{ip} and Gain_d^{ip} , respectively, are given below, where fixed asymptotic up- and downlink rates are maintained.*

$$\begin{aligned} \text{Gain}_u^{ip} &\triangleq \lim_{M \rightarrow \infty} \frac{\frac{T-\tau}{T} \sum_{j=1}^L \sum_{n \in \mathcal{K}_u} R_{u,jn}^{fd,ip}}{\frac{T-\tau_u}{T} \sum_{j=1}^L \sum_{n \in \mathcal{K}_u} R_{u,jn}^{tdd,ip}} = 2 \left(1 - \frac{K_h^d}{T - K_u} \right), \\ \text{Gain}_d^{ip} &\triangleq \lim_{M \rightarrow \infty} \frac{\frac{T-\tau}{T} \sum_{l=1}^L \sum_{k \in \mathcal{K}_d} R_{d,lk}^{fd,ip}}{\frac{T-\tau_d}{T} \sum_{l=1}^L \sum_{k \in \mathcal{K}_d} R_{d,lk}^{tdd,ip}} = 2 \left(1 - \frac{K_h^u}{T - K_d} \right). \end{aligned} \quad (5.42)$$

The asymptotic ergodic achievable rate of the n -th uplink user in the j -th cell and the

achievable rate of the k -th downlink user in the l -th cell are given below,

$$\begin{aligned} R_{u,jn}^{fd,ip} &\rightarrow \log_2 \left(1 + \frac{E_{tr} E_u \beta_{u,jjn}^2}{E_{tr} E_u \sum_{l \neq j} \beta_{u,jln}^2 + \sigma^4} \right), \\ R_{d,lk}^{fd,ip} &\rightarrow \log_2 \left(1 + \frac{E_{tr} E_d \beta_{d,llk}^4}{Z_l \left(\sum_{j \neq l} \frac{E_{tr} E_d \beta_{d,jjk}^2 \beta_{d,jlk}^2}{Z_j} + \sigma^6 \right)} \right), \end{aligned} \quad (5.43)$$

where $Z_l = \sum_{i \in \mathcal{K}_d} \frac{\beta_{d,lli}^2}{\sigma^2}$, $n \in \mathcal{K}_u$, $k \in \mathcal{K}_d$.

Proof. When channel estimation overhead is taken into account, the uplink spectral efficiency in the full-duplex system is $\frac{T-\tau}{T} \sum_{j=1}^L \sum_{n \in \mathcal{K}_u} R_{u,jn}^{ip}$ and the downlink spectral efficiency is $\frac{T-\tau}{T} \sum_{l=1}^L \sum_{k \in \mathcal{K}_d} R_{d,lk}^{ip}$. While for the TDD system, since uplink and downlink transmission are in two different time slots, the corresponding up- and downlink spectral efficiency are $\frac{T-\tau_u}{T} \sum_{j=1}^L \sum_{n \in \mathcal{K}_u} R_{u,jn}^{tdd,ip}$ and $\frac{T-\tau_d}{T} \sum_{l=1}^L \sum_{k \in \mathcal{K}_d} R_{d,lk}^{tdd,ip}$, respectively. For two mutually independent $M \times 1$ vectors $\mathbf{a} \triangleq [a_1, \dots, a_M]^T$ and $\mathbf{b} \triangleq [b_1, \dots, b_M]^T$ whose entries are i.i.d. zero-mean random variables with $\mathbb{E}(|a_i|^2) = \sigma_a^2$ and $\mathbb{E}(|b_i|^2) = \sigma_b^2$, $\forall i \in \{1, \dots, M\}$. By law of large numbers, we have the following convergence in distribution according to [58],

$$\frac{1}{\sqrt{M}} \mathbf{a}^H \mathbf{b} \xrightarrow{d} \mathcal{CN}(0, \sigma_a^2 \sigma_b^2), \text{ as } M \rightarrow \infty. \quad (5.44)$$

Similar to the proof of Theorem 8, by substituting $P_{tr} = E_{tr}/\sqrt{M}$, $P_u = E_u/\sqrt{M}$, $P_d = E_d/\sqrt{M}$, $\tau_u = K_u$, $\tau_d = K_d$ and $\tau = K_u + K_d - K_f$ into (5.28) and (5.38), and using the fact that $K_u = K_h^u + K_f$ and $K_d = K_h^d + K_f$, the desired results can be obtained as $M \rightarrow \infty$. \square

Corollary 9. *When $K_u = K_d = K_f$, i.e., when only full-duplex users are served, full-duplex system asymptotically doubles the spectral efficiency over the TDD system under the imperfect CSI assumption, where $\text{Gain}_u^{ip} = \text{Gain}_d^{ip} = 2$. However, if there*

exists half-duplex users (i.e., $K_h^d > 0$ or $K_h^u > 0$), then $\text{Gain}_{u/d}^{ip} < 2$, and the spectral efficiency gains decrease as the number of half-duplex users increases due to channel training overhead.

Remark 6. In case of imperfect CSI, the fastest rate at which we can cut down the transmit power to maintain fixed asymptotic up- and downlink rates is $1/\sqrt{M}$. With power scaling down with increasing M , the impact of imperfect SI cancellation, intra-cell and inter-cell interference in the multi-cell MU-MIMO full-duplex networks will vanish as $M \rightarrow \infty$.

5.4.2 System with only full-duplex users

For tractability, we consider a homogeneous network by assuming all links in the same cell have the same channel statistic and all the cross-cells links have the same channel statistics, i.e., let $\beta_{u,ln} = \beta_{d,lk} = \beta_{I,lkn} = \beta_{b,ul} = 1$, $\beta_{u,jln} = \beta_{d,jlk} = \beta_{I,lkjn} = \beta_{b,jl} = \beta$, where $\beta \in [0, 1]$ for $j \neq l \in [1, \dots, L]$, $n \in \mathcal{K}_u$, $k \in \mathcal{K}_d$, and the noise variance is set as $\sigma^2 = 1$. We consider a simple scenario where all users are full-duplex and the number of full-duplex users in each cell is $K_f \triangleq K$. Similar results can be derived in case of mixed half-duplex UEs or only half-duplex UEs. With the simplification, we can compute the up- and downlink spectral efficiency per cell (bits/s/Hz/cell) when CSI is perfect as

$$\begin{aligned} R_u^{f,d,p} &= K \log_2 \left(1 + \frac{P_u(M-1)}{P_u(K-1) + (L-1)\beta(P_uK + P_d) + \kappa P_d + 1} \right), \\ R_d^{f,d,p} &= K \log_2 \left(1 + \frac{P_d(M-1)(M-2)}{P_d(K-1)(M-2) + MK(L-1)\beta P_d + V + MK(\kappa P_u + 1)} \right), \end{aligned} \quad (5.45)$$

where $V = MK(K-1 + (L-1)K\beta)P_u$.

When CSI is imperfect, the up- and downlink spectral efficiency per cell (bits/s/Hz/cell)

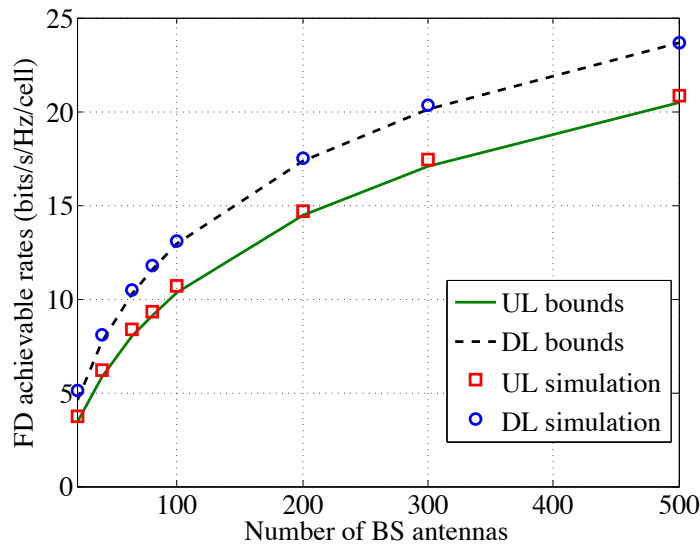
are

$$\begin{aligned} R_u^{fd,ip} &= \frac{K(T - \tau)}{T} \log_2 \left(1 + \frac{P_{tr} P_u (M - 1)}{P_{tr} P_u (K \bar{L}^2 - 1 + \beta (\bar{L} - 1) M) + J} \right), \\ R_d^{fd,ip} &= \frac{K(T - \tau)}{T} \log_2 \left(1 + \frac{P_{tr} P_d M}{(1 + P_{tr} \bar{L}) U_1 + (\bar{L} - 1) U_2} \right), \end{aligned} \quad (5.46)$$

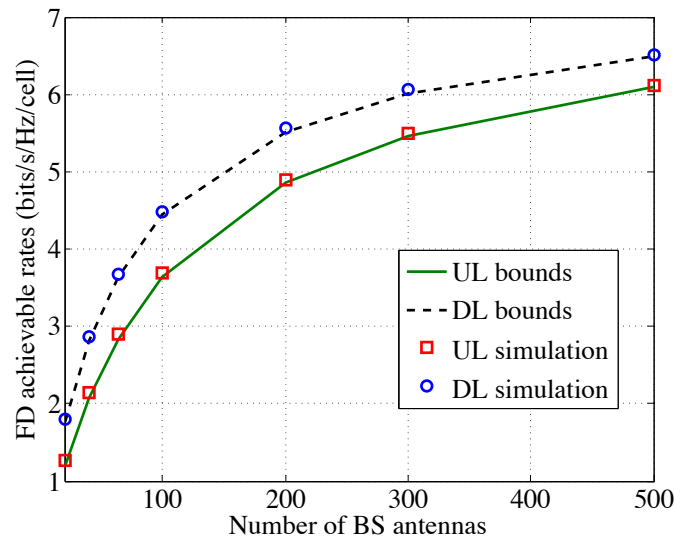
where $J = P_d(1 + P_{tr} \bar{L})(\bar{L} - 1) + P_u K \bar{L} + P_{tr}(1 + \kappa P_d) \bar{L} + \kappa P_d + 1$,
 $U_1 = P_d(1 + (K - 1) \bar{L}) + K(P_u(K - 1) + P_u(\bar{L} - 1)K + 1 + \kappa P_u)$,
 $U_2 = P_{tr} P_d(M\beta + \bar{L}) + P_d$, $\bar{L} = 1 + (L - 1)\beta$.

We first evaluate the tightness of our derived bounds on achievable rates in the homogenous networks. We consider a scenario with $L = 7$ cells and the inter-cell interference level $\beta = 0.3$, each cell has $K = 5$ full-duplex UEs. The up- and downlink transmit power are assumed as $P_{tr} = P_u = 10$ dB and $P_d = 20$ dB, respectively. The dynamic range parameter is $\kappa = -50$ dB. In case of imperfect CSI, considering an OFDM system, we assume the coherence time is 1 ms (one subframe in LTE standard where there are 14 OFDM symbols in each subframe), and the ‘‘frequency smoothness interval’’ is 14 as given in [1]. Hence the coherence interval which is a time-frequency product is equal to $T = 196$. The pilot length is assumed to be the same as the number of users, i.e., $\tau = K$. From Figure 5.3, we can see that all bounds are very tight in both perfect and imperfect CSI cases, particularly with increasing M . Next, we use these bounds for the full-duplex system to compute the uplink and downlink spectral efficiency ratios between full-duplex system and half-duplex system. Note that for the half-duplex system, we still numerically evaluate the ergodic achievable rates with no simplification.

We compute the spectral efficiency ratios between full-duplex and half-duplex by comparing the full-duplex rates given in (5.45) and (5.46) with the half-duplex achievable rates in (5.37) and (5.38) which can be evaluated numerically. We consider



(a) With perfect CSI



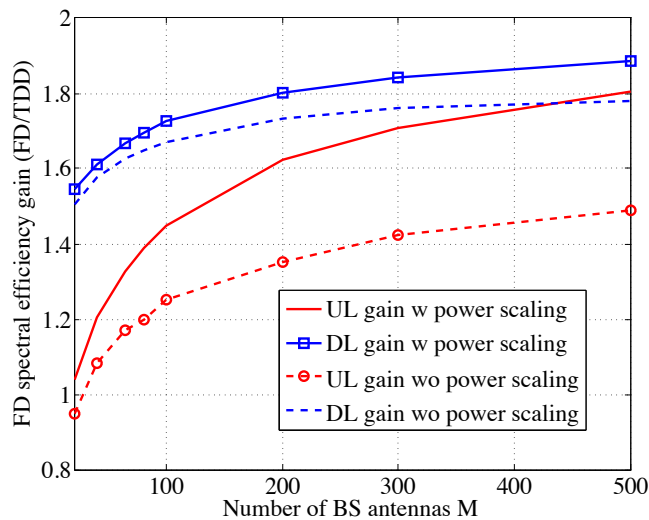
(b) With imperfect CSI

Figure 5.3: Comparisons between lower bounds in Proposition 5 and 6 and numerically evaluated values of the ergodic achievable rates (bits/s/Hz/cell) under both perfect and imperfect CSI assumptions, where $P_{tr} = P_u = 10$ dB and $P_d = 20$ dB.

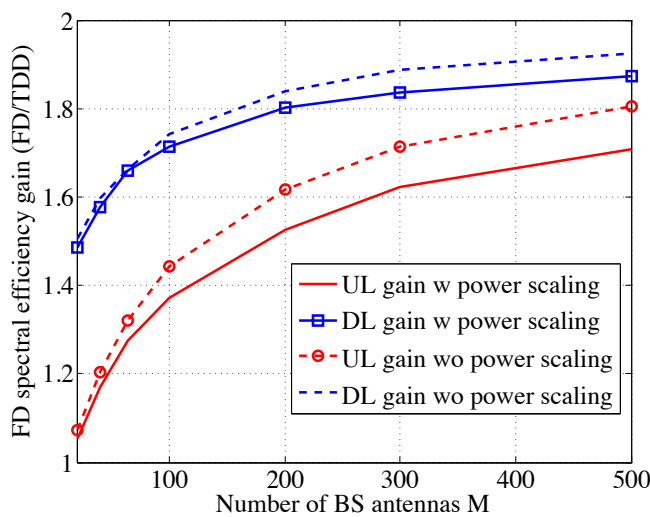
the same setting as in Fig. 5.3 under both perfect and imperfect CSI assumptions. In Figure 5.4(a), in the case of perfect CSI, we can see that as M increases, the up- and downlink spectral efficiency gain between full-duplex system versus TDD system

will converge to 2 as we scale down the transmit power according to Theorem 8. The convergence rate is fast at the beginning, and becomes slower for large M . To reach the asymptotic $2\times$ gain, it will require remarkably large number of BS antennas. However, full-duplex system achieves finite M gains in both uplink and downlink. For example, when $M = 64$, full-duplex achieves about $1.7\times$ downlink gain and $1.3\times$ uplink gain. We numerically show that even without scaling down the transmit power, similar full-duplex gains still can be achieved. Figure 5.4(b) shows the full-duplex over half-duplex spectral efficiency gains in the case of imperfect CSI. We observe that even with channel estimation error and pilot contamination, full-duplex uplink and downlink gains exist for finite M with and without scaling down the transmit power.

We also investigate the spectral efficiency gain and antenna reduction tradeoff between full-duplex system and TDD system. The antenna reduction is the reduction of BS antennas due to full-duplex operation which can be characterized by the ratio between the number of BS antennas in TDD system (M_{TDD}) and the number of BS antennas in FD system. In Fig. 5.5, we consider the same setting as in Fig. 5.3 under imperfect CSI assumption. We illustrate the spectral efficiency gain and antenna reduction tradeoff for both uplink and downlink with different M_{TDD} in the TDD system. Larger full-duplex antenna reduction can be achieved at the cost of reducing the spectral efficiency gain. In the regimes above the dashed arrows as shown in Fig. 5.5, full-duplex system achieves both spectral efficiency gain and antenna reduction over TDD system. We can see that full-duplex system can require an order of magnitude fewer BS antennas compared with TDD to obtain the same performance in some cases. In addition, as M_{TDD} increases, full-duplex system can achieve higher spectral efficiency gain and antenna reduction. The spectral efficiency gain and antenna reduction tradeoff is essentially the tradeoff between full-duplex multiplexing gain due



(a) With perfect CSI



(b) With imperfect CSI

Figure 5.4: Full-duplex over half-duplex spectral efficiency ratio in the imperfect CSI system with and without power scaling.

to simultaneous transmission and reception and beamforming gain due to M .

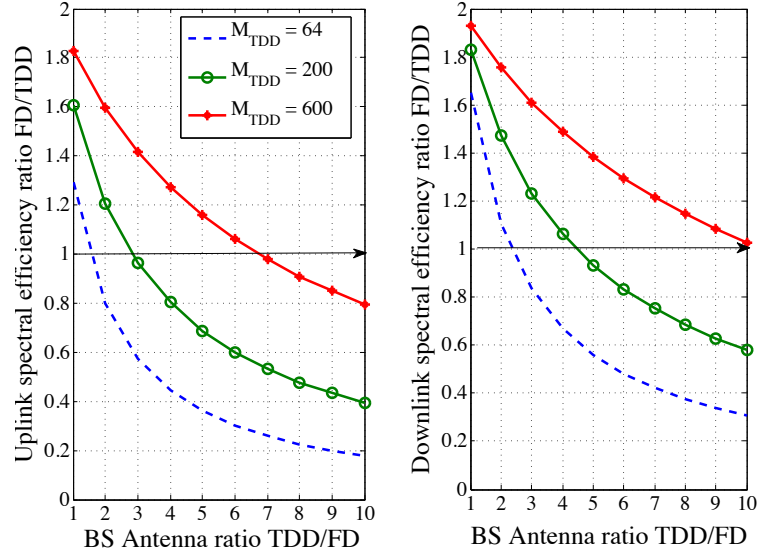


Figure 5.5: Spectral efficiency gain and antenna reduction tradeoff for various numbers of BS antennas employed in the TDD system under imperfect CSI assumption.

5.5 Interference Management via Side-Channels

In addition to the large-antenna array at the BS for interference mitigation, we can explore the wide-spectrum on the mobiles to alleviate UE-UE interference. In this section, we will briefly present the use of side-channels in multi-cell full-duplex networks to manage UE-UE interference in the downlink.

Since we only focus a cellular system without BS cooperation, we will only allow in-cell user cooperation for the use of side-channels. And the side-channels are being controlled by the BSs who will decide when the side-channels should be used. We first define the cooperative user set for each downlink user. The cooperative users set for the k -th downlink user in the l -th cell is \mathcal{S}_{lk} , which contains the $|\mathcal{S}_{lk}|$ most dominant uplink users in the same cell who will interfere with the k -th downlink user in the l -th cell. The uplink users in the cooperative set will be assigned orthogonal side-channel bands to perform interference cancellation. We assume that the cooperative user set for each downlink user is a known parameter which has been determined by the BSs.

Next, we describe the procedure to use the side-channels. The users in the coop-

erative set can apply a decode-and-cancel scheme [25] to send a coded copy of the interfering packet over the side-channel for interference cancellation. For the n -th uplink user in the l -th cell where $n \in \mathcal{S}_{lk}$, it will broadcast the signal $x_{s,ln}$ over the n -th allocated side-channel band. The received signal at the k -th downlink user in the l -th cell over the n -th side-channel band is

$$y_{s,lk}^{(n)} = f_{s,lk}^{(n)} x_{s,ln} + n_{s,lk}^{(n)}. \quad (5.47)$$

The k -th downlink user will then decode the interfering signal, and cancel out the interference from the received signal over the main-channel, and finally decode its intended downlink packet.

5.6 Numerical Results

5.6.1 A small cell scenario

Based on the state-of-art self-interference cancellation capability [2], the coverage of a full-duplex system is more likely to be within a small-cell communication ranges. Hence in this section, we present the numerical simulation in realistic small-cell network settings used in 3GPP [27] to evaluate the system performance. Twelve small cell BSs are uniformly and randomly distributed within a hexagonal region with a radius of 300 meters. All the small-cell BSs have full-duplex capability with multiple antennas. Each small-cell BS is associated with five single-antenna half-duplex uplink UEs and downlink UEs, respectively, which are uniformly and randomly dropped within a radius of 40 meters of the BS. The numerical results are shown for the case of imperfect CSI with channel estimation error. We consider an OFDM system and the coherence interval is $T = 196$. The channel bandwidth is assumed as 20 MHz for both

Parameter	Value
Full-duplex BS power	24 dBm
UE power	23 dBm
BS antenna gain	5 dBi
Number of BS antennas M	{20, 50, 100, 300, 500}
Thermal noise density	-174 dBm/Hz
Noise Figure	BS: 9 dB; UE: 5 dB
Dynamic range κ^{-1}	{50, 60, 70, 80} dB
Minimum distance constraints	BS-BS: 40 m; BS-UE: 10 m; UE-UE: 3 m
Shadowing standard deviation	BS-UE: 10 dB; BS-BS: 12 dB; UE-UE: 6 dB
Pathloss models for BS-UE, UE-UE, and BS-BS channels	Refer to [27]
Fast fading channels	i.i.d. $\mathcal{CN}(0, 1)$
Propagation loss of self-interference channels	40 dB [2]

Table 5.1: Simulation parameters

TDD and full-duplex systems. The large-scale fading models for BS-UE, BS-BS and UE-UE channels which include path loss and shadowing effect follow 3GPP model in [27]. The SI channel model is based on the existing experiment data [2], where the propagation loss of SI channel in a separate-antenna system includes path loss, isolation, cross-polarization and antenna directionality [8], and in a shared-antenna system includes isolation using a circulator. We assume the SI channel has a propagation loss of 40 dB. We run hundreds of random drops of BSs and UEs in the simulation, and parameter details are given in Tabel 5.1.

5.6.2 Performance without side-channels

The average full-duplex spectral efficiency gain is illustrated in Fig. 5.7 with varying numbers of BS antennas, where the dynamic range parameter κ is -60 dB. We verify that the full-duplex gains in realistic network scenarios exist for a range of finite number of BS antennas and the gains will scale with BS antennas. Fig 5.8 depicts the average spectral efficiency gain of the full-duplex system for different dynamic

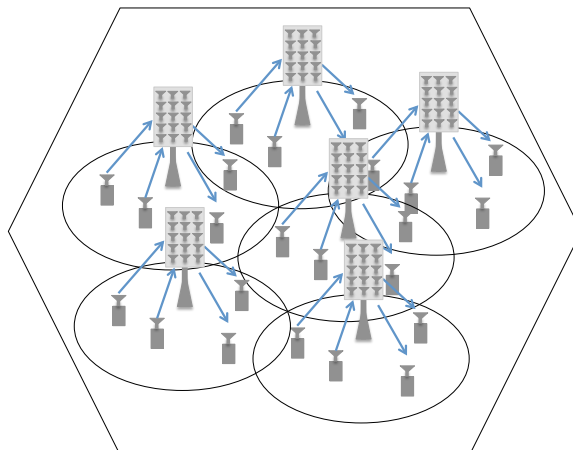
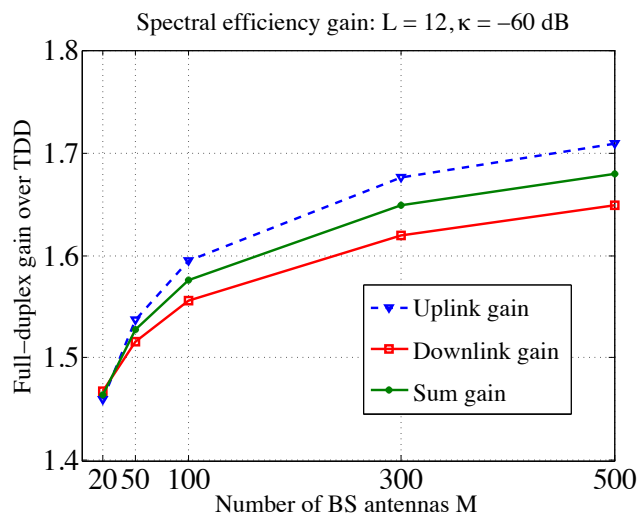


Figure 5.6: Small cell deployment.

Figure 5.7: Average full-duplex spectral efficiency gain with BS antenna arrays when $L = 12$ and $\kappa = -60$.

range parameters κ when $M = 100$, which demonstrates the impact of imperfect SI cancellation. Since all users are half-duplex, the downlink gains are not affected by κ . However, since all the BSs are full-duplex, the uplink gains are severely affected by the dynamic range values especially when the dynamic range value is low. We can see that larger dynamic range κ^{-1} , (i.e., smaller κ) will result in less residual SI, thus increasing the uplink gain. Once the dynamic range κ^{-1} exceeds certain threshold, there is not much impact of residual SI on the uplink performance.

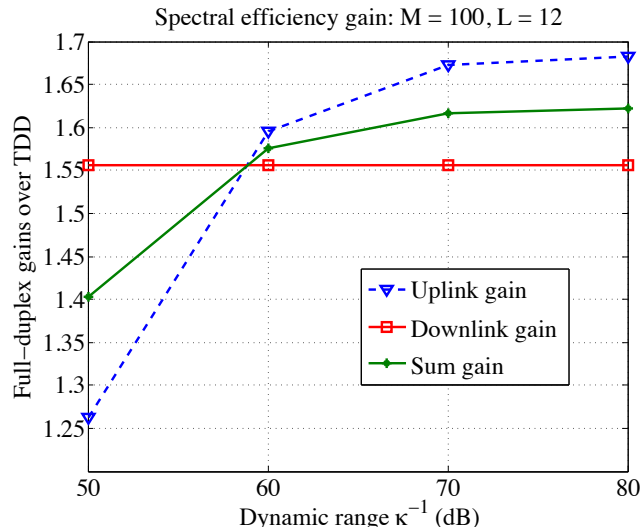


Figure 5.8: Average full-duplex spectral efficiency gain with different dynamic ranges when $M = 100$ and $L = 12$.

Figure 5.9 demonstrates the system performance with varying small cell density from 3 BSs to 30 BSs within the same area. We assume $M = 100$ and dynamic range parameter $\kappa = -60$ dB. We notice that the downlink gain will first decay and then increase with growing number of BSs. As the cell density increases, conventional interference becomes stronger, and the new interference in the full-duplex system will become less dominant. Hence higher average downlink full-duplex gain can be achieved exceeding a certain cell density threshold.

5.6.3 Performance with side-channels

We will demonstrate the effectiveness of using side-channels in the finite regimes by simulation. Under the same realistic network settings as given in Section 5.6.1, we assume that for each downlink user, the UE-UE interference from its cooperative user set can be completely cancelled out. In Figure 5.10, the user spectral efficiency cumulative distribution function (CDF) of uplink and downlink are given for varying size of the cooperative user set. Since we only use side-channels to manage UE-UE interference in the full-duplex networks, only downlink performance will be improved

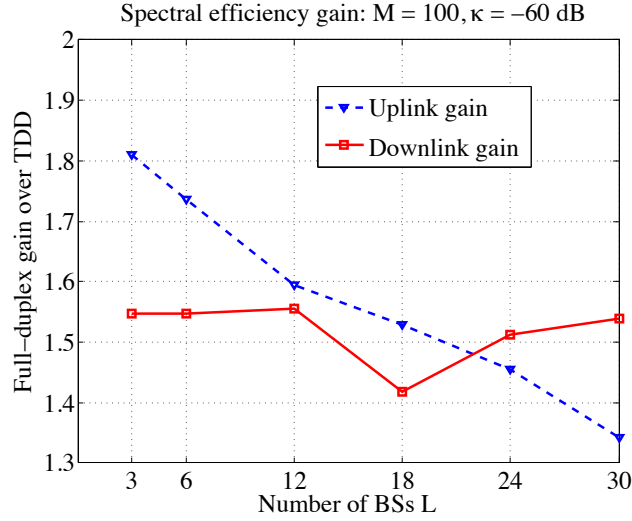


Figure 5.9: Average full-duplex spectral efficiency gain with cell density when $M = 100$ and $\kappa = -60$.

with increasing number of cooperative users while the uplink performance will remain the same. We can see that the use of side-channels will improve the spectral efficiency of all the downlink users.

The 5-percentile and average full-duplex spectral efficiency gains with and without (w/wo) side-channels are shown in Figure 5.11 under the same settings as in Figure 5.10. We vary the number of uplink users in each cooperative user set from 1 to 5 for in-cell cooperation. We first observe that the downlink full-duplex spectral efficiency gains with side-channels of both cell-edge users and average users will scale up with increasing number of cooperative users. Without side-channels, even when $M = 300$, the downlink performance of the cell-edge users in full-duplex system is worse than TDD system as the cell-edge users suffer more from new UE-UE interference due to the full-duplex transmission. However, with the help of side-channels, full-duplex gain of cell-edge users in the downlink can be improved from 48% to 128%. In contrast, side-channels improve the full-duplex gain of average users in the downlink from 5% to 17%. We conclude that the use of side-channels is most effective in

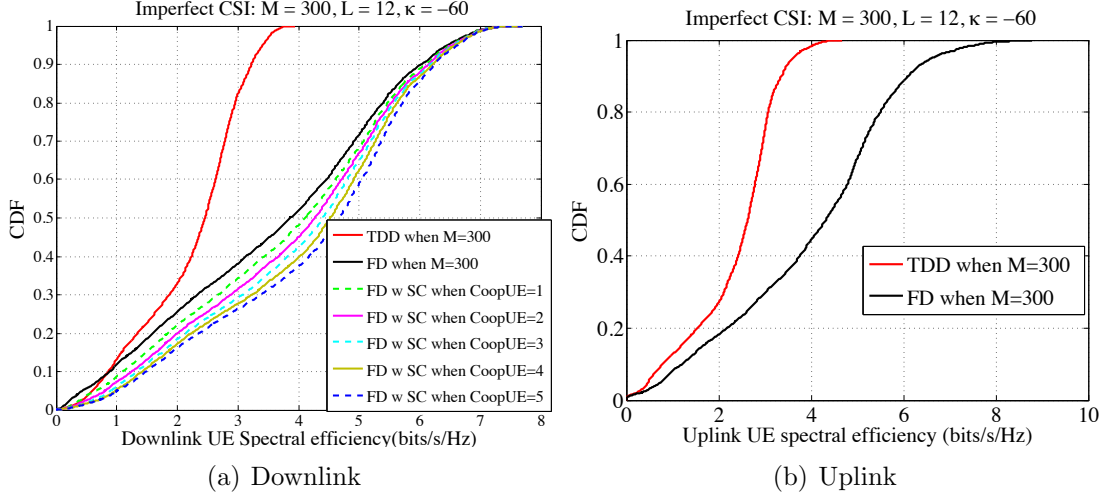
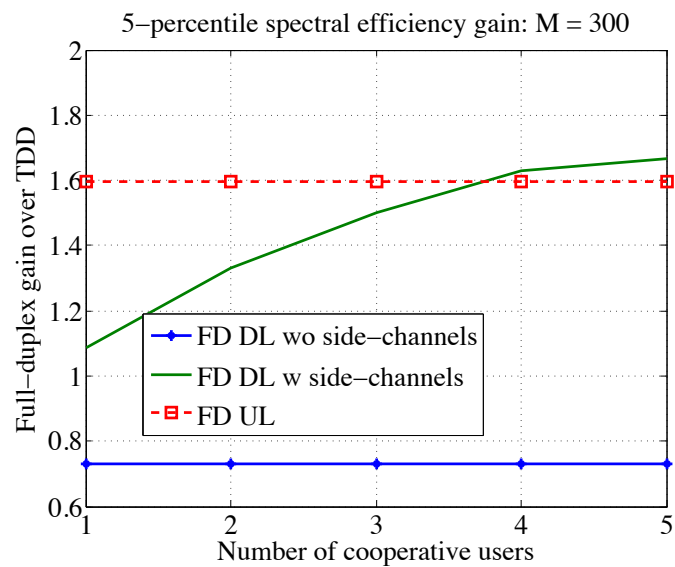


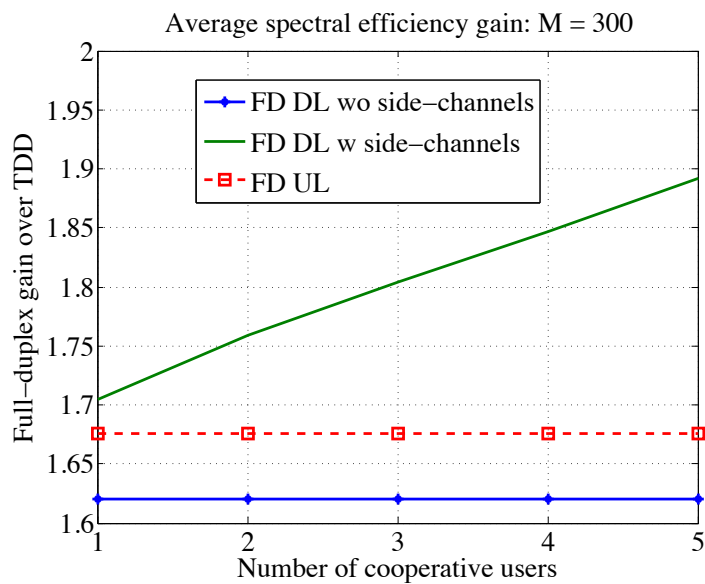
Figure 5.10: User spectral efficiency CDF with the size of cooperative user set when $M = 300$, $L = 12$ and $\kappa = -60$ dB.

improving the cell-edge downlink users in the finite regimes.

In Figure 5.12, the 5-percentile and average full-duplex spectral efficiency gains w/wo side-channels are shown with different number of BS antennas for a fixed size of cooperative user set where $|\mathcal{S}_{lk}| = 5 \forall l, k$. When $M = 20$, the use of side-channels improves the full-duplex gain of cell-edge downlink users without side-channels by 492%, and improves the average users by 25%. However, the improvement of using side-channels on the full-duplex gain will reduce as the number of BS antenna increases. When $M = 500$, side-channel improvement of cell-edge downlink user is 81%, and the improvement of average downlink users is 15%. The reason behind the result is that when the number of BS antennas is small, the use of side-channels is very effective in reducing the downlink interference in the full-duplex networks. As M increases, the large antenna array at BS will help mitigate the effect of interference in the full-duplex system. Consequently, the gain of using side-channel for interference management will gradually vanish as $M \rightarrow \infty$. Hence the use of ISM side-channels



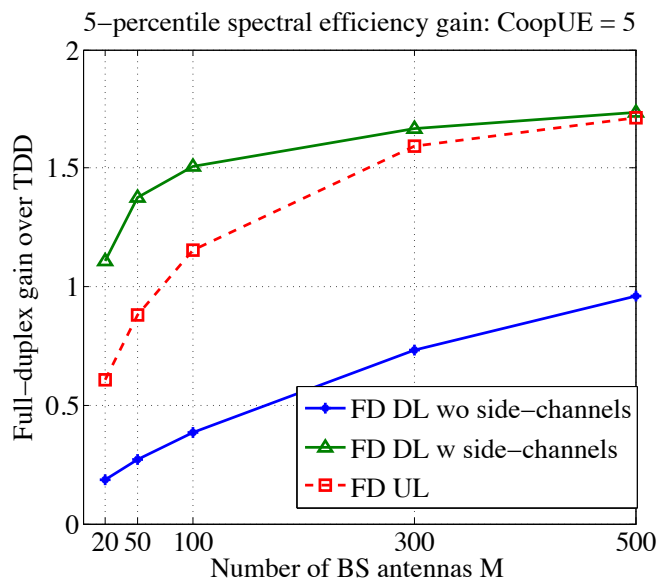
(a) Cell-edge users



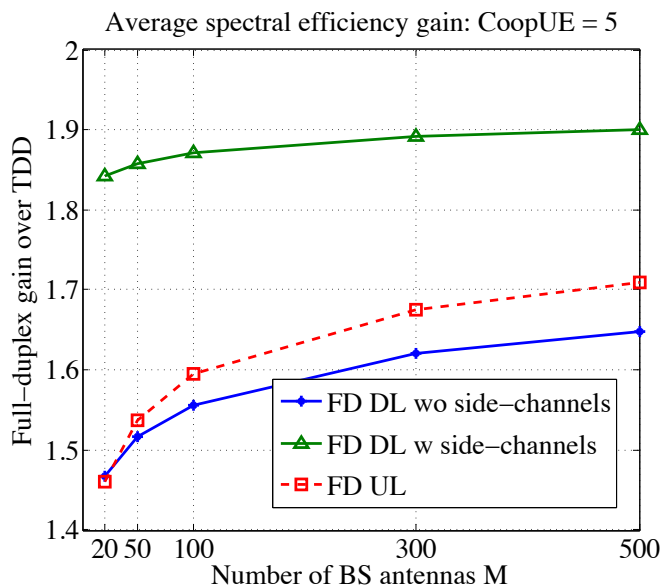
(b) Average users

Figure 5.11: Full-duplex spectral efficiency gain with the size of cooperative user set when $M = 300$, $L = 12$ and $\kappa = -60$ dB.

is not essential for large M .



(a) Cell-edge users



(b) Average users

Figure 5.12: Full-duplex spectral efficiency gain with BS antennas arrays when $|\mathcal{S}_{lk}| = 5$, $\forall l, k$, $L = 12$ and $\kappa = -60$ dB.

Conclusions

6.1 Summary

MIMO full-duplex wireless systems promise to bring many-fold spectral efficiency gains compared with the existing half-duplex paradigms. However, one of biggest challenges in realizing the full-duplex gain is to deal with the increased interference in the full-duplex networks due to increased simultaneous active links.

In this thesis, we propose a new approach for enhanced interference management via wireless side-channels in MIMO full-duplex systems. The prevalence of multiple radio interfaces in smartphones opens up opportunities to use ISM bands in new and unique ways. We explore the use of ISM bands to manage interference in cellular bands, by creating wireless “side-channels” between mobile users. We propose the use of wireless side-channel to manage interference from uplink users to downlink users in a multi-user MIMO full-duplex system, where an in-band full-duplex BS with multiple antennas communicates with multiple uplink and downlink users in the same time-frequency slot.

We first study the availability of wireless side-channels by experimentally quantifying the likelihood of finding ISM side-channels among smartphones in WiFi-free

areas such as highways. Then, we study a side-channel assisted two-user MIMO full-duplex system. For time-invariant channels, we derive a constant-gap capacity region and the GDoF region which can be achieved by our proposed vector bin-and-cancel scheme. For slow-fading channels, we obtain DMTs with and without CSIT of the system. Both the GDoF and DMT results reveal various insights about the effect of the side-channels and the spatial and spectral tradeoff between antenna resources and bandwidth of the side-channels.

Next, we study a side-channel assisted multi-user MIMO full-duplex system from a cross-layer protocol design perspective. We propose two joint PHY-MAC protocols to integrate ARQ at the MAC layer with enhanced interference management via side-channels at the PHY. Our proposed protocols which exploit the ARQ information offered by the MAC layer can effectively help reduce the data retransmission times and improve system goodput.

Finally, we study the multi-cell multi-user MIMO full-duplex networks where single-antenna full-duplex and half-duplex users are served by the full-duplex BSs with multiple antennas. Using low complexity linear receivers and precoders, the ergodic achievable rates of uplink and downlink are characterized for the full-duplex system. Several practical constraints are modeled in the analysis such as imperfect full-duplex radio chains, channel estimation error, pilot overhead and pilot contamination. The large scale system performance is analyzed when each BS has a large antenna array. When the number of BS antennas grows infinitely large, the $2\times$ asymptotic full-duplex spectral efficiency gain can be achieved over the half-duplex system with perfect CSI. When channel estimation error and channel training overhead are considered, the $2\times$ asymptotic full-duplex spectral efficiency gain is achieved if only full-duplex UEs are served. In addition, we numerically evaluate the finite SNR and antenna performance, which reveals that full-duplex networks can use significantly

fewer antennas to achieve spectral efficiency gain over the half-duplex counterparts. Under realistic multi-cell network settings, we demonstrate the benefits of using side-channels to significantly improve the spectral efficiency of cell-edge users.

6.2 Future Directions

In the future work, there still remains several critical challenges that need to be addressed. Firstly, the mobile energy efficiency and security problems needs to be considered for an actual implementation of ISM side-channels. The cooperative user search algorithms will be required to obtain the cooperative user set for each user to invoke the use of side-channels for interference management. Secondly, the optimal vector bin-and-cancel scheme in Chapter 3 is quite complex which involves rate splitting, superposition coding. Hence practical codeword design is required to translate the theoretical gain into practical system performance improvement. Thirdly, in addition to the ARQ design with side-channels in Chapter 4, more powerful hybrid-ARQ techniques can be considered for the cross-layer design with side-channels in the full-duplex system. Moreover, different bandwidth and power allocation strategies, and different PHY schemes for the use of side-channels can be explored in the side-channel protocol design.

Fourthly, although we provide PHY analysis for a massive MIMO full-duplex cellular networks in Chapter 5, higher layer studies are required to translate the PHY gain to an actual system. For example, different scheduling algorithms at MAC layer need to be investigated to select the best user set at each time slot who will be served by the massive MIMO full-duplex BS to maximize the network throughput. Hence user selection and scheduling problems in massive MIMO full-duplex system are important research topics in the future work.

References

- [1] T. Marzetta, “Noncooperative cellular wireless with unlimited numbers of base station antennas,” *Wireless Communications, IEEE Transactions on*, vol. 9, no. 11, pp. 3590–3600, November 2010. 1.1, 5.1, 5.3, 5.3.2.1, 5.4.1, 5.4.2
- [2] A. Sabharwal, P. Schniter, D. Guo, D. Bliss, S. Rangarajan, and R. Wichman, “In-band full-duplex wireless: Challenges and opportunities,” *Selected Areas in Communications, IEEE Journal on*, vol. 32, no. 9, pp. 1637–1652, Sept 2014. 1.1, 5.6.1
- [3] H. Q. Ngo, E. Larsson, and T. Marzetta, “Energy and spectral efficiency of very large multiuser MIMO systems,” *Communications, IEEE Transactions on*, vol. 61, no. 4, pp. 1436–1449, April 2013. 1.1, 5.1, 5.3.3, 5
- [4] C. Shepard, H. Yu, and L. Zhong, “Argosv2: A flexible many-antenna research platform,” in *Proceedings of the 19th Annual International Conference on Mobile Computing & Networking*, ser. MobiCom ’13. New York, NY, USA: ACM, 2013, pp. 163–166. 1.1, 5.1
- [5] E. G. Larsson, O. Edfors, F. Tufvesson, and T. L. Marzetta, “Massive MIMO for next generation wireless systems,” *IEEE Communications Magazine*, vol. 52, no. 2, pp. 186–195, 2014. 1.1, 2, 3.3.4, 5.1
- [6] F. Rusek, D. Persson, B. K. Lau, E. G. Larsson, T. L. Marzetta, O. Edfors, and F. Tufvesson, “Scaling up MIMO: Opportunities and challenges with very large arrays,” *Signal Processing Magazine, IEEE*, vol. 30, no. 1, pp. 40–60, 2013. 1.1, 5.1
- [7] M. Duarte, A. Sabharwal, V. Aggarwal, R. Jana, K. Ramakrishnan, C. Rice, and N. Shankaranarayanan, “Design and characterization of a full-duplex multi-antenna system for WiFi networks,” *Vehicular Technology, IEEE Transactions on*, vol. 63, no. 3, pp. 1160–1177, 2014. 1.1, 2.1

-
- [8] E. Everett, A. Sahai, and A. Sabharwal, "Passive self-interference suppression for full-duplex infrastructure nodes," *Wireless Communications, IEEE Transactions on*, vol. 13, no. 2, pp. 680–694, February 2014. 1.1, 2.1, 2.3.2.1, 5.6.1
- [9] D. Bharadia, E. McMillin, and S. Katti, "Full duplex radios," in *Proceedings of the ACM SIGCOMM 2013 Conference on SIGCOMM*, ser. SIGCOMM '13. New York, NY, USA: ACM, 2013, pp. 375–386. 1.1
- [10] E. Aryafar, M. A. Khojastepour, K. Sundaresan, S. Rangarajan, and M. Chiang, "MIDU: enabling MIMO full duplex," in *Proceedings of the 18th annual international conference on Mobile computing and networking*. ACM, 2012, pp. 257–268. 1.1
- [11] Mobile data offload for 3G networks. White Paper, IntelliNet Technologies, Inc., 2009. 1.2
- [12] K. Doppler, M. Rinne, C. Wijting, C. Ribeiro, and K. Hugl, "Device-to-device communication as an underlay to LTE-advanced networks," *Communications Magazine, IEEE*, vol. 47, no. 12, pp. 42–49, 2009. 1.2
- [13] A. Nosratinia, T. Hunter, and A. Hedayat, "Cooperative communication in wireless networks," *Communications Magazine, IEEE*, vol. 42, no. 10, pp. 74–80, 2004. 1.2
- [14] 3GPP TR 36.808 and TR 36.850. 1.2
- [15] LTE-Unlicensed. [Online]. Available: http://www.3gpp.org/news-events/3gpp-news/1603-lte_in_unlicensed 1.2
- [16] J. Bai, S. Diggavi, and A. Sabharwal, "On degrees-of-freedom of multi-user MIMO full-duplex network," in *Information Theory (ISIT), 2015 IEEE International Symposium on*, June 2015, pp. 864–868. 1.2
- [17] S. Jeon, S. H. Chae, and S. H. Lim, "Degrees of freedom of full-duplex multiantenna cellular networks," Jan 2015. [Online]. Available: <http://arxiv.org/abs/1501.02889> 1.2
- [18] A. Sahai, S. Diggavi, and A. Sabharwal, "On degrees-of-freedom of full-duplex uplink/downlink channel," in *Information Theory Workshop (ITW), 2013 IEEE*, Sept 2013, pp. 1–5. 1.2
- [19] C. Karakus and S. Diggavi, "Opportunistic scheduling for full-duplex uplink-downlink networks," in *Information Theory (ISIT), 2015 IEEE International Symposium on*, June 2015, pp. 1019–1023. 1.2
- [20] W. Ouyang, J. Bai, and A. Sabharwal, "Leveraging one-hop information in massive MIMO full-duplex wireless systems," *Submitted to IEEE/ACM*

-
- Transactions on Networking*, Sep 2015. [Online]. Available: <http://arxiv.org/abs/1509.00539> 1.2
- [21] S. Goyal, P. Liu, S. Hua, and S. Panwar, “Analyzing a full-duplex cellular system,” in *Information Sciences and Systems (CISS), 2013 47th Annual Conference on*, 2013, pp. 1–6. 1.2
- [22] Y. S. Choi and H. Shirani-Mehr, “Simultaneous transmission and reception: Algorithm, design and system level performance,” *IEEE Transactions on Wireless Communications*, vol. 12, no. 12, pp. 5992–6010, December 2013. 1.2
- [23] P. Wang, S. Yeh, F. Xue, Y. Choi, J. Bai, S. Chiu, V. Kristem, and S. Talwar, “Full-duplex in 5g small cell access: System design and performance aspects,” *submitted to IEEE Communications Magazine*, 2016. 1.2
- [24] M. Amir Khojastepour, K. Sundaresan, S. Rangarajan, and M. Farajzadeh-Tehrani, “Scaling wireless full-duplex in multi-cell networks,” in *Computer Communications (INFOCOM), 2015 IEEE Conference on*, April 2015, pp. 1751–1759. 1.2
- [25] J. Bai and A. Sabharwal, “Decode-and-cancel for interference cancellation in a three-node full-duplex network,” *Proc. IEEE Asilomar Conf. Signals, Syst., Comput.*, 2012. 1.3.1, 2.1, 2.3.2.1, 5.5
- [26] H. Kwon and J. M. Cioffi, “Multi-user MISO broadcast channel with user-cooperating decoder,” *IEEE 68th VTC Fall*, 2008. 1.3.1, 2.1, 2.3.1.2
- [27] 3GPP. Further enhancements to lte time division duplex (TDD) for downlink-uplink (DL-UL) interference management and traffic adaptation, TR 36.828, v.11.0.0. [Online]. Available: www.3gpp.org 1.3.3, 5.6.1
- [28] J. Bai, C. Liu, and A. Sabharwal, “Increasing cellular capacity using ISM band side-channels: A first study,” in *Proceedings of the 4th ACM Workshop on All Things Cellular: Operations, Applications, & Challenges*, 2014, pp. 9–14. 1.4
- [29] J. Bai, C. Dick, and A. Sabharwal, “Vector bin-and-cancel for MIMO distributed full-duplex,” <http://arxiv.org/abs/1402.0614>, 2014. 1.4, 3.3.1.1, 3.3.1.2, 3.3.2, 3.4.1, 3.4.1, 3.4.2, 3.4.3, 3.4.3, 3.4.3
- [30] J. Bai and A. Sabharwal, “Large antenna analysis of multi-cell full-duplex networks,” *Submitted to Wireless Communications, IEEE Transactions on*, 2016. 1.4
- [31] C. Shepard, H. Yu, N. Anand, E. Li, T. Marzetta, R. Yang, and L. Zhong, “Argos: Practical many-antenna base stations,” *Proc. ACM MobiCom*, 2012. 2.1

-
- [32] T. Yoo and A. Goldsmith, "On the optimality of multiantenna broadcast scheduling using zero-forcing beamforming," *Sel. Areas Commun., IEEE J.*, 2006. 2.1, 2.3.1.1
- [33] V. Kukshya and H. Krishnan, "Experimental measurements and modeling for vehicle-to-vehicle dedicated short range communication (DSRC) wireless channels," 2006. 2.2
- [34] "http://traffic-counts.dot.ca.gov/." 2.2.3
- [35] J. Jose, A. Ashikhmin, T. Marzetta, and S. Vishwanath, "Pilot contamination problem in multi-cell TDD systems," *Proc. IEEE ISIT 2009*. 2.3.1.1
- [36] N. Jindal, "MIMO broadcast channels with finite-rate feedback," *Inf. Theory, IEEE Trans.*, 2006. 2.3.1.1
- [37] S. Jafar and A. Goldsmith, "Isotropic fading vector broadcast channels: the scalar upper bound and loss in degrees of freedom," *Inf. Theory, IEEE Trans.*, 2005. 2.3.1.2
- [38] J. Bai and A. Sabharwal, "Distributed full-duplex via wireless side-channels: Bounds and protocols," *Wireless Communications, IEEE Transactions on*, vol. 12, no. 8, pp. 4162–4173, 2013. 2.3.2.1, 2.3.2.3, 3.1, 3.3, 3.3.2, 4.3.3
- [39] T. Han and K. Kobayashi, "A new achievable rate region for the interference channel," *Information Theory, IEEE Transactions on*, Jan 1981. 3.3.2
- [40] S. Karmakar and M. Varanasi, "The generalized degrees of freedom region of the MIMO interference channel and its achievability," *Information Theory, IEEE Transactions on*, vol. 58, no. 12, pp. 7188–7203, 2012. 3.3.3, 1
- [41] L. Zheng and D. Tse, "Diversity and multiplexing: a fundamental tradeoff in multiple-antenna channels," *Information Theory, IEEE Transactions on*, vol. 49, no. 5, pp. 1073–1096, 2003. 3.4, 3.4.1, 3.4.1
- [42] S. Boyd and L. Vandenberghe, *Convex optimization*. Cambridge university press, 2004. 3.4.1, 3.4.1
- [43] A. Sezgin, S. A. Jafar, and H. Jafarkhani, "The diversity multiplexing tradeoff for interference networks," *arXiv preprint arXiv:0905.2447*, 2009. 3.4.2
- [44] S. Karmakar and M. K. Varanasi, "The diversity-multiplexing tradeoff of the MIMO Z interference channel," vol. <http://arxiv.org/abs/1006.0496>, June 2012. 3.4.2
- [45] P. Wu and N. Jindal, "Coding versus ARQ in fading channels: How reliable should the phy be?" *Communications, IEEE Transactions on*, vol. 59, no. 12, pp. 3363–3374, December 2011. 4.3.1, 4.3.1.1, 4.3.1.1

-
- [46] H. Q. Ngo, M. Matthaiou, T. Q. Duong, and E. G. Larsson, "Uplink performance analysis of multicell MU-MIMO systems with ZF receivers," 2012. [Online]. Available: <http://arxiv.org/abs/1202.2875> 4.3.1.1
- [47] D. Ben Cheikh, J.-M. Kelif, M. Coupechoux, and P. Godlewski, "Multicellular zero forcing precoding performance in rayleigh and shadow fading," in *Vehicular Technology Conference (VTC Spring), 2011 IEEE 73rd*, May 2011, pp. 1–5. 4.3.1.1
- [48] X. Shao, J. Yuan, and Y. Shao, "Error performance analysis of linear zero forcing and MMSE precoders for MIMO broadcast channels," *Communications, IET*, vol. 1, no. 5, pp. 1067–1074, Oct 2007. 4.3.1.1
- [49] M. Bibinger, "Notes on the sum and maximum of independent exponentially distributed random variables with different scale parameters," 2013. [Online]. Available: <http://arxiv.org/abs/1307.3945> 4.3.1.1
- [50] I. S. Gradshteyn and I. M. Ryzhik, "Table of integrals, series, and products," *Seventh Edition, Elsevier/Academic Press*, 2007. 4.3.1.1
- [51] B. Day, A. Margetts, D. Bliss, and P. Schniter, "Full-duplex bidirectional MIMO: Achievable rates under limited dynamic range," *Signal Processing, IEEE Transactions on*, vol. 60, no. 7, pp. 3702–3713, July 2012. 5.2
- [52] —, "Full-duplex MIMO relaying: Achievable rates under limited dynamic range," *Selected Areas in Communications, IEEE Journal on*, vol. 30, no. 8, pp. 1541–1553, September 2012. 5.2
- [53] M. Vehkaperä, T. Riihonen, and R. Wichman, "Asymptotic analysis of full-duplex bidirectional MIMO link with transmitter noise," in *Personal Indoor and Mobile Radio Communications (PIMRC), 2013 IEEE 24th International Symposium on*, Sept 2013, pp. 1265–1270. 5.2
- [54] A. M. Tulino and S. Verdú, *Random matrix theory and wireless communications*. Now Publishers Inc, 2004, vol. 1. 5.3.1.3, 5.3.1.3, 5.3.2.3, 5.3.2.3
- [55] J. Hoydis, S. ten Brink, and M. Debbah, "Massive MIMO in the UL/DL of cellular networks: How many antennas do we need?" *Selected Areas in Communications, IEEE Journal on*, vol. 31, no. 2, pp. 160–171, February 2013. 5.3.2.1, 5.3.2.2
- [56] J. Jose, A. Ashikhmin, T. L. Marzetta, and S. Vishwanath, "Pilot contamination and precoding in multi-cell tdd systems," *IEEE Transactions on Wireless Communications*, vol. 10, no. 8, pp. 2640–2651, 2011. 5.3.2.3, 5.3.3
- [57] 3GPP TSG RAN Meeting RP-57. 5.4

- [58] H. Cramér, *random variables and probability distributions*. Cambridge University Press, 1970. 5.4.1, 5.4.1